Nanoscale Photofabrication on Azobenzene-Containing Polymers

Taiji Ikawa

2008

Table of Contents

Chapter 1. General Introduction

1.1. Overview and Motivation 1
1.2. Theoretical background 4
1.2.1. Azobenzene-Containing Polymers
1.2.2. Optical Near Field
1.2.3. Nanofabrication for Bioengineering Applications
1.3. Experimental Techniques 15
1.3.1. Scanning Probe Microscopy
1.3.2. Tapping-Mode Atomic Force Microscopy
1.3.3. Scanning Near-Field Optical Microscopy
1.4. Outline of This Thesis 21
References 23

Part I Nanostructure Formation on Azobenzene-Containing Polymers by Optical Near Field

Chapter 2. Topographical Nanostructure Patterning on Azobenzene-Containing Polymers by the Optical Near Field of Polystyrene Spherical Particles

2.1. Introduction 29
2.2. Experimental 30
2.3. Results and Discussions 33
2.4. Conclusion 43
2.5. Appendix I 43
References 44

Chapter 3. Dynamics of Nanostructure Formation on an Azobenzene-Containing Polymer Studied by Tapping Mode Atomic Force Microscopy

3.1. Introduction 46
3.2. Experimental 48
3.3. Results and Discussions 50
3.4. Conclusion 59

3.5. Appendix I 59
References 61

Chapter 4. Nano-fabrication on Azobenzene-Containing polymers Using Scanning Near-Field Optical Microscope
4.1. Introduction 62
4.2. Experimental 63
4.3. Results and Discussions 66
4.4. Conclusion 82
References 83

Part II Immobilization of Nano-Scale Particles on Azobenzene-Containing Polymers by Nanostructure Imprinting

Chapter 5. Molecular-shape Imprinting and Immobilization of Biomolecules on Azobenzene-Containing Polymers.
5.1. Introduction 86
5.2. Experimenta 89
5.3. Results and Discussions 92
5.4. Conclusion 103
References 104

Chapter 6. Molecular Scale Imaging of F-actin Assemblies Immobilized on an Azobenzene-Containing Polymers.
6.1. Introduction 106
6.2. Experimental 107
6.3. Results and Discussions 110
6.4. Conclusion 118
References 118

Summary 120

List of Publications 122

Acknowledgments 127

Chapter 1. General Introduction

1.1. Overview and Motivation

Azobenzene is a well-known molecule for its photochemical isomerization function.[1] The photoisomerization has been studied for more than half a century, on the other hand it continues to produce unexpected and fascinating phenomenon.[2,3] When azobenzene is incorporated into a polymer, the photoisomerization motions of azobenzene induce a wide variety of hierarchical motions from molecular level to macroscopic level, which has potential uses in various photonic applications such as optical recording, electro-optic modulations and nanostructure formation.[4] The main theme of this thesis focuses on photo-fabrication of the nanostructure on the surface of azobenzene-containing polymers and its utilization for optical recording and bioengineering applications.

Over the past two decades, with increasing interest in liquid crystals, azobenzene has been studied both as a mesogen and a disruptor of liquid crystalline phase because of its rigid-rod like shape and isomeric bent shape.[5, 6] Around the same time, photo-induced orientation of azobenzenes and accompanying dichroism and birefringence has been preferred as holographic recording materials.[7, 8] As nonlinear optical materials, the donor acceptor substituted azobenzenes have been used as the rigid dipoles to create second harmonic generation and associated effects.[8, 9] Azobenzenes are remarkable molecular switches which can cover a wide variety of roles.

One of the most intriguing topics in the past decade is fabrication of artificial surface relief structures on the azobenzene-containing polymers by exposure to an interference light pattern or a single laser beam, which was first reported independently from two research groups, Natansohn's and Tripathy's groups, in 1995 (§1.2.1).[10, 11] The size of the relief structure reaches to micron scale, which is visible with naked eye. This suggests a massive macroscopic motion of the polymer matrix and was an extremely unexpected finding and generated a huge literature since then. This phenomenon has been considered to be a photo-driven mass transport effect,[4] which is quite different from other conventional microscopic surface processing techniques such as photoresist,[12, 13] ablation[14] and stamping.[15] Various driving forces behind it have been proposed such as internal pressure,[16] light intensity gradient,[17] and intermolecular interaction.[18] However, neither the mass transport effect itself nor the nature of the driving force has been directly confirmed at the time.

Around that time there is a requirement for the dimensions of photofabrictation process and optical recording to decrease year by year. Although conventional photolithography is a useful fabrication technique, the minimum feature size possible is approximately equal to the wavelength of the light used. The same holds for the conventional optical recording. This is due to the "diffraction limit" of light. Use of "optical near field" is one of the promising ways to spatially-control matter on a nanometer-scale beyond the diffraction limit (§1.2.2). A number of research groups demonstrated the variations of the surface patterning at resolutions below the diffraction limit using either evanescent near-field optical lithography [19, 20] and or an embedded-amplitude mask.[21] Also, various optical recording techniques using the optical near field, such as the solid immersion lens,[22] the super resolution technique[23] and the optical fiber probe with small aperture[24] have been proposed. For practical use of these techniques, however, not only apparatus but also highly sensitive materials are essential because the optical near field is an extremely weak light source.

In the circumstances our research group found that a topographical change could be induced on the surface of azobenzene-containing polymers by means of photo-illumination with a monolayer of polystyrene (PS) particles of submicron diameter.[25, 26] The experimental technique to display this phenomenon is very simple; (1) a monolayer of PS particles is formed on the surface of the azobenzene-containing polymer film, (2) the polymer film is exposed to a laser beam, (3) after removing the particles, hexagonally arrayed dents, of which diameter are nearly the same as the PS particles, are formed on the surface. The dents structure with a diameter ranging from 1000 nm to 20 nm could be achieved.[27] The author explored the mechanism of the nanoscale deformation of the azopolymer based on (1) size effects of the small particles on the nanostructure formation, (2) the electric field calculated by Mie scattering theory,[28, 29, 30] and (3) the visco-elasticity analyzed by scanning probe microscopy.[31,32] The result implies that "the optical near field" of the PS particles that are smaller than the wavelength of the incident light can cause the nano-scale surface deformation of the azobenzene-containing polymer. This technique itself was considered to be an entirely new nano-structure fabrication technique, and showed the potential of the azobenzene-containing polymer for the application to near-field imaging[25] and optical data storage.[33] The works in this thesis, in part, focus on this unique nano-structure

fabrication technique based on the azobenzene-containing polymers in chapter 2 and chapter 3.

Based on the research described above, the azobenzene-containing polymers were considered to be very useful for nanoscale applications including nanofabrication and optical data storage, because it shows various photoinduced phenomena as shown in §1.2.1. Thus far, several research groups attempted to fabricate relief structures on the azobenzene-containing polymers by using the optical near field based on an optical fiber probe with subwavelength sized aperture.[34, 35, 36] Most of them were continuous process based on continuous wave oscillation system. In contrast the author examined near-field optical recording on the azobenzene-containing polymer using sub-nano second pulse using the optical fiber probe with the aperture of 100 nm in diameter.[33] Indentations of around 150 nm in diameter were achieved on the azobenzene-containing polymer by the pulse duration of 125 ns. The data suggested that the polymer is a promising medium for ultra high density optical data storage. The part of this thesis describes the application of the polymer for nanofabrication and optical data storage by using the optical fiber probe with the small aperture in chapter 4.

In the course of these studies, the author found that the small particles on the azobenzene-containing polymer could be immobilized by photo-illumination.[37] Of particular interest was that not only PS particles but biologically-derived macromolecules including globular proteins, filamentous proteins and deoxyribonucleic acids (DNA) could be immobilized on the polymer. The author confirmed that the polymer surface deformed along the shapes of the small particles, suggesting that the small particles were physically immobilized on the surface because of the increase in the contact area between the small particles and the polymer. The immunological and enzymatic studies showed that the immobilized proteins kept their vital activities. This novel concept for the immobilization of the biological macromolecules has the distinct potential for biological applications including protein chip application and biological imaging.[38] Moreover, it provides a new concept of the fabrication of two-dimensional array of spherical particles.[39] The last part of this thesis shows the immobilization of the small particle including biological macromolecules on the polymer surface, and the application of the phenomenon for biological imaging in chapter 5 and chapter 6.

1.2. Theoretical Background

1.2.1. Azobenzene-Containing Polymers

Photoisomerization of Azobenzenes

Azobenzene and its derivatives can exist in two forms that differ in the isomerization state of the azo group (-N=N-, Figure 1. 1).[1] One is the trans-form, which has the stable rod-like form in shape. The other is the cis-form, which has the relatively unstable bent form. The stable trans-form isomerizes into the unstable cis-form when the azobenezenes absorb light at a certain wavelength. Cis to trans back isomerization can also take place thermally and/or photochemically. These photoisomerization motions of the azobenzenes induce a drastic change in physical and optical properties, and thus, the azobenzenes are very useful as a molecular-scale switching device.

Classification of Azobenzens

Azobenzenes have been classified into three groups by spectroscopic analysis: azobenzene-type molecules, aminoazobenzene-type molecules and pseudo-stilbene-type molecules (Figure 1. 2).[1, 4]

Azobenzene-type molecules have two absorption bands due to π-π^* and n-π^* transition with relatively poor overlap between the two bands. The lifetime of the cis isomer is relatively long up to hours and more.

Aminoazobenzene-type molecules, where 4-position of azobenzene ring is substituted with amino group, show significant overlap of the two absorption bands and the lifetime of the cis isomer is shorter than azobenzene-type molecules.

Pseudo-stilbene-type molecules, where 4- and 4'-positions of two azobenzene rings are substituted with electron-donating and electron-withdrawing groups, has the two bands overlapped on around the same energy level and the lifetime of the cis isomer is shortest up to second range. Since the π-π^* and n-π^* bands are practically superimposed, light for photoactivation of the trans-cis isomerization will also photoactivate the cis-trans isomerization, which will significantly speed up the whole process. The process can be repeated under illumination, and thus, pseudo-stilbene-type molecules are the best molecules for inducing drastic changes to their surrounding matrix.

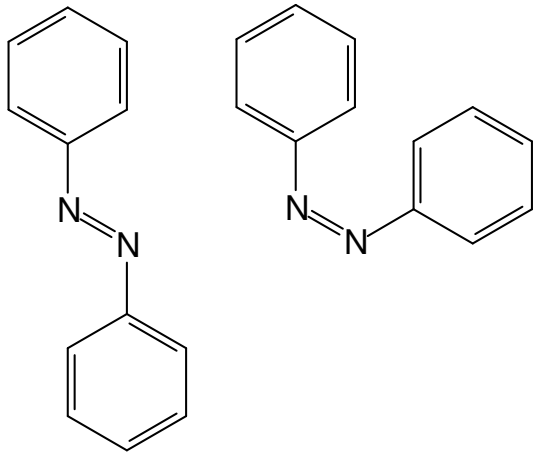

Figure 1. 1. Isomers of azobenzene.

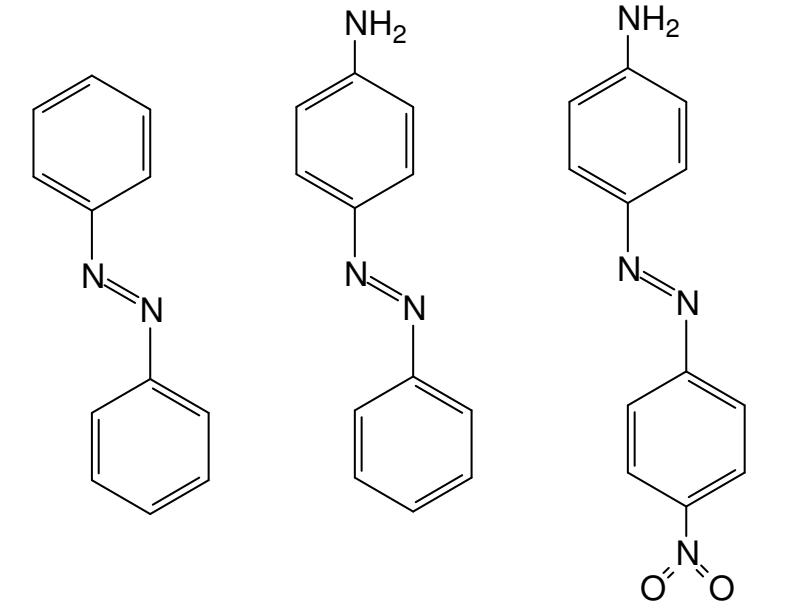

Figure 1. 2. Three groups of azobenzene derivatives.

Photoinduced Motions in Azobenzene-Containing Polymers

Under photoillumination, azobenzenes undergo repeated photoisomerization even in a glassy-state polymer. Even nonbound azobenzenes affect their environment if they are dissolved in a polymer matrix. The molecular motions of azobenzenes induce the multi level motions in the polymer. The motions can be roughly classified into the following three types.[4]

First type of the motions is the photo-induced orientation of chromophores in a polymer matrix. This phenomenon was firstly reported in 1957 by Teite[40] and then, Todorov et al. demonstrated a first optical application in holography in 1984.[7] With linearly polarized light, the photoisomerization is only activated when the chromophore's transition dipolemoment axis has a component parallel to the light polarization. The direction perpendicular to the light polarization is excluded from optical activation and become enriched in chromophores. The concentration of the chromophores aligned perpendicular to the light polarization steadily increases under illumination with polarized light, until a saturation level is attained (Figure 1. 3). This motion produces dichroism and birefringence in polymers. If the light is circularly polarized, there will be no preferred orientation within the film plane, but about the same amount of chromophores will probably align in the homeotropic direction. Pseudo-stilbene-type azobenzenes is the best molecule for inducing photo-induced orientation because of their fast isomerization process. Aminoazobenzenes are good candidates for the motion, but "normal" azobenzenes shows little photoinduced orientation due to their slow back isomerization process.[41]

Second type is the "domain" level motions in conjunction with chromophore motions. To induce this type of the motions, the azobenzenes should be part of ordered and/or constrained matrix, for example, liquid crystalline, semi crystalline, Langmuir-Brodgett or monolayer films. The azobenzenes show photo-isomerization and alignment even in the constrained matrix and thus whole liquid crystals or crystal's domains reorient to a direction perpendicular to the light polarization. The order parameter within the domain does not change, but an overall orientation of whole domains occurs, thus creating a very strong overall orientation. The most initial reports on photoinduced orientation were done in liquid crystalline polymers by Todorov and Wendroff. The liquid crystal alignment takes place even on a monolayer of azobenzenes, which is known as "command surface

conception" demonstrated by Ichimura et al.[5, 6] Also, the photoisomerization can act as a trigger to disrupt an ordered phase of liquid crystals, which is the most common case found in the literature. The difference in shape between the E (trans) azobenzene isomer and the Z (cis) provides a powerful mesogen (E) and an effective liquid crystalline phase disruptor (Z, with some exceptions). These kinds of "domain" motions are ranging from the nanometer to submicron level. For inducing these motions, any types of azobenzenes are useful.

Third type of the motions is massive macroscopic motion at an even larger scale. The photo-illumination with interference pattern of the laser beams produces relief patterns on the polymer surface that is visible with the naked eye (Figure 1. 4). Direct exposure to the laser beam also forms a dent structure on the polymer surface.[42] For this kind of motion, it also requires that the azobenzenes should be connected to polymers. This motion has been considered to be a photo-driven mass transport effect because total volume of the polymer is almost the same after photo-illumination, which is quite different from other conventional microscopic surface processing. Various driving forces behind it have been proposed such as internal pressure,[10] light intensity gradient[42] and intermolecular interaction. However, neither the mass transport effect itself nor the nature of the driving force has been directly confirmed.

Recently, Karageorgiev et al. reported the observation of light-induced isothermal transition of the polymer film from a solid phase to a fluid phase by atomic force microscopy.[43] In their report, the polymer behaves like a viscoelatic fluid during photo-illumination, whereas the fluidity is affected by the light field vector. The result suggests that the photoisomerization motion of the azobenzene plasticizes the polymer matrix during photo-illumination, which is considered to be the first step of the massive macroscopic motion of the polymer.

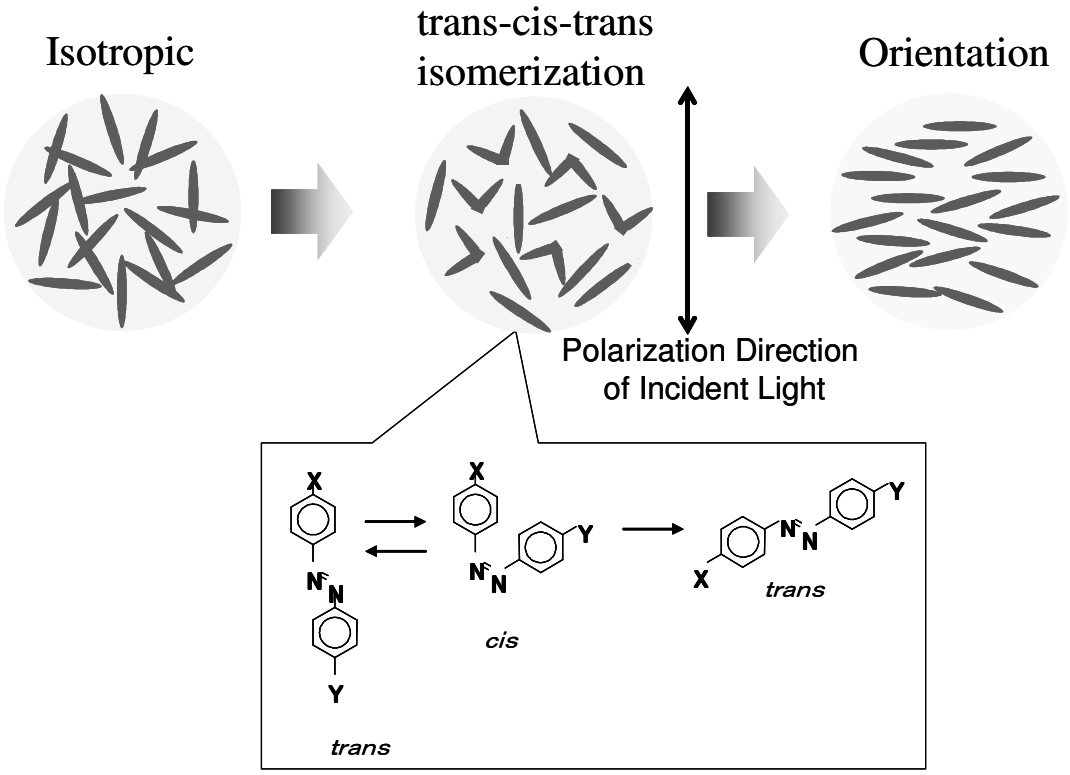

Figure 1. 3. Photoinduced orientation of azobenzene derivatives.

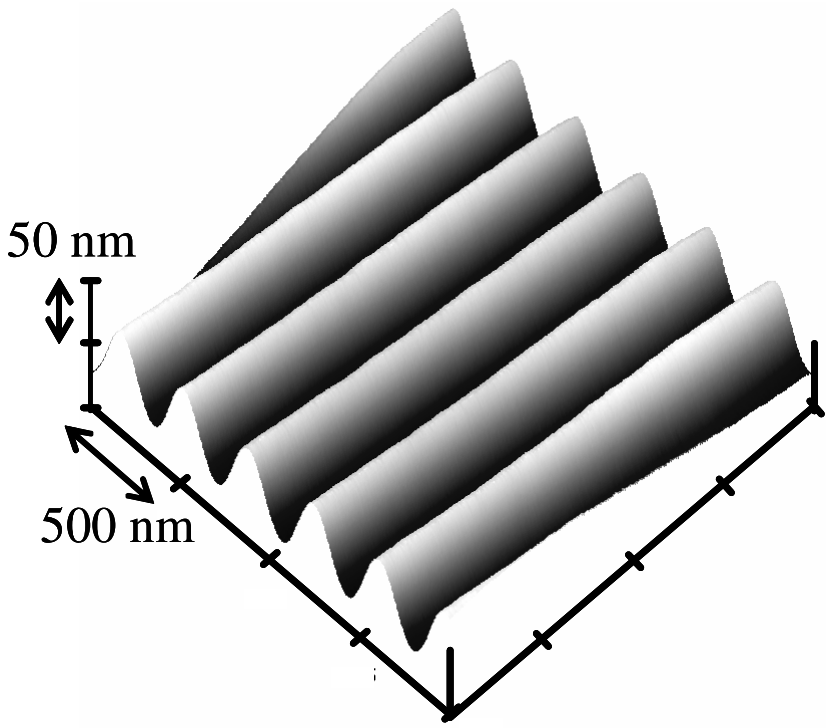

Figure 1. 4. A relief pattern formed on an azobenzene-containing polymer surface by exposure to an interference pattern of light, imaged by atomic force microscopy.

1.2.2. Optical Near Field

Optical Near field of Small Aperture

The concept of optical near field has derived from the effort aimed at achieving optical microscopy beyond the diffraction limit.[44] The diffraction limit in conventional microscopy arises from the size of the spot that a light beam can be focused to with normal lens elements. At the focal point, the beam forms a symmetric pattern of concentric rings known as Airly disk pattern.[45] Based on Abbe's calculation, the distance, d, from the highest intensity point located in a middle of the center spot to the first node in the intensity (i.e. d is the resolution limit) is given by the following formula,

$$d=0.61\ (\lambda_0 / n \sin\theta) \qquad (1)$$

where λ_0 is a vacuum wavelength, n is the refractive index of the medium in which the light travels and θ is the light convergence angle for the focusing element. The denominator in eq. 1, $n \sin\theta$ is also known as the numerical aperture (NA) for the objective and can be as high as 1.3-1.4 for modern objectives working in oil or water. Eq. 1 is, therefore, usually simplified to $d= \lambda_0 / 2$. The maximal resolution is approximately equals to half the wavelength of the radiation used, which for visible light results in a spatial resolution 250-300 nm.

The limitation in conventional optical microscopy has been well-known for a long time. Early in the 20th century, Synge published a series of papers in which he proposed a new type of optical microscope designed to circumvent the limitation imposed by diffraction limit.[46, 47, 48] He proposed forming a microscopic aperture with dimensions much smaller than the optical wavelength in an opaque screen. By illuminating the backside of the screen with a high intensity light source, light passing through the aperture would be confined by the dimensions of the hole. When the aperture is positioned in close proximity of the sample surface, the light emerging from the aperture could be used to image a specimen (Figure 1. 5).

The practicability of Synge's idea was first confirmed in the work of Bethe who treated the passage of light through subwavelength diameter hole formed in an infinitely thin and perfectly conductive screen (Figure 1. 5).[49] The work was later corrected by Bouwkamp.[50,51] These works were key in describing the fields near the small aperture and led to an accurate picture of the electric field of the small aperture. The expression for the field components in the near-field region just beyond the aperture was described

here; [52]

$$A(f,z) \approx A_0(f)\exp(-\frac{\pi z}{a}) \quad (2)$$

where a is the aperture radius, z is vertical distance from the aperture, A(*f, z*) is Fourier transform of the complex amplitude distribution as a function of z and $A_0(f)$ is angular spectrum of Fraunhofer diffraction. The equation 2 shows that there exist the field components in the region close to the aperture and the field components exponentially attenuate with distance from the aperture. The field component is defined as optical near field. When the aperture is positioned in close proximity of the sample surface, the sample surface scatters the optical near field as the propagating light. The experimental demonstration, however, could not be preformed in those days because of the difficulties in the nanometer-sized aperture fabrication, high intensity light source for the illumination, and precise position control for sample manipulations.

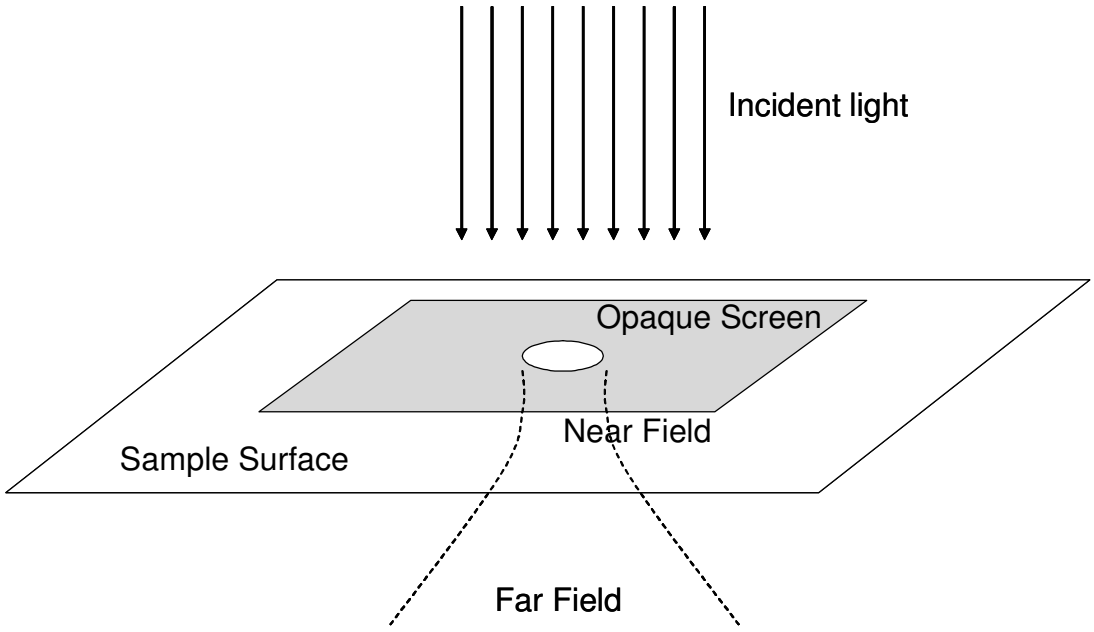

Figure 1. 5. Schematic representation of Synge's Idea for achieving sub-diffraction limit spatial resolution.

The experimental feasibility of high-resolution imaging using a subwavelength aperture was first reported by Ash and Nicolles in 1972.[53] With 3 cm microwaves passing through a small aperture, periodic features in a metal grating sample were measured with λ/60 spatial resolutions. In mid 1980s, Pohl's laboratory at IBM first reported subdiffraction-limited optical measurements using Synge's concept.[54,55] His group overcame the significant technical problems associated with subdiffraction-limited optical measurements and demonstrated modern day instrument for scanning near-field optical microscopy or near-field scanning optical microscopy (SNOM or NSOM). In their system, small nanometric aperture used as an excitation source and it had a mechanism for positioning and holding the small aperture within nanometer of the sample surface. The most successful design for the small aperture was introduced by Betzig et al. at AT&T Bell Labs.[56, 57] They demonstrated a tapered fiber optic waveguide coated with a refractive metal coating, which is known as an optical fiber probe. The technique of modern SNOM is described in §1.3.3.

Optical Near Field of Spherical Particles

An alternative idea of the optical near field is described here. A spherical particle in space is considered. When the particle is illuminated by light, there arises not only a propagating (scattering) field, but an electromagnetic field restricted around the sphere (Figure 1. 6).[32] The restricted component is an optical near field. German physicist Gustav Mie first showed a complete analytical solution of Maxwell's equations for the scattering of electromagnetic radiation by the spherical particles, including optical near field of the particles.[28-30] In its original formulation it assumed a homogeneous, isotropic and optically linear material, including metals and dielectrics, irradiated by an infinitely extending plane wave. However, solutions for layered spheres are also possible. Some computer software developed to perform electromagnetic scattering simulations mainly based on classical Mie theory can be found on some web sites.[58]

Since the near field component does not propagate, it cannot directly observed by a detector at a distance much larger than a wavelength of incident light. The near field component can be scattered by a very small object, e.g. a very sharp metallic tip. Thus, the non-propagating optical near field can be measured with a detector in the distance as a propagating light scattered by the very small object. The resolution depends on the size of

the very small object. This type of the near field imaging is known as scattering (apertureless) SNOM.[59, 60]

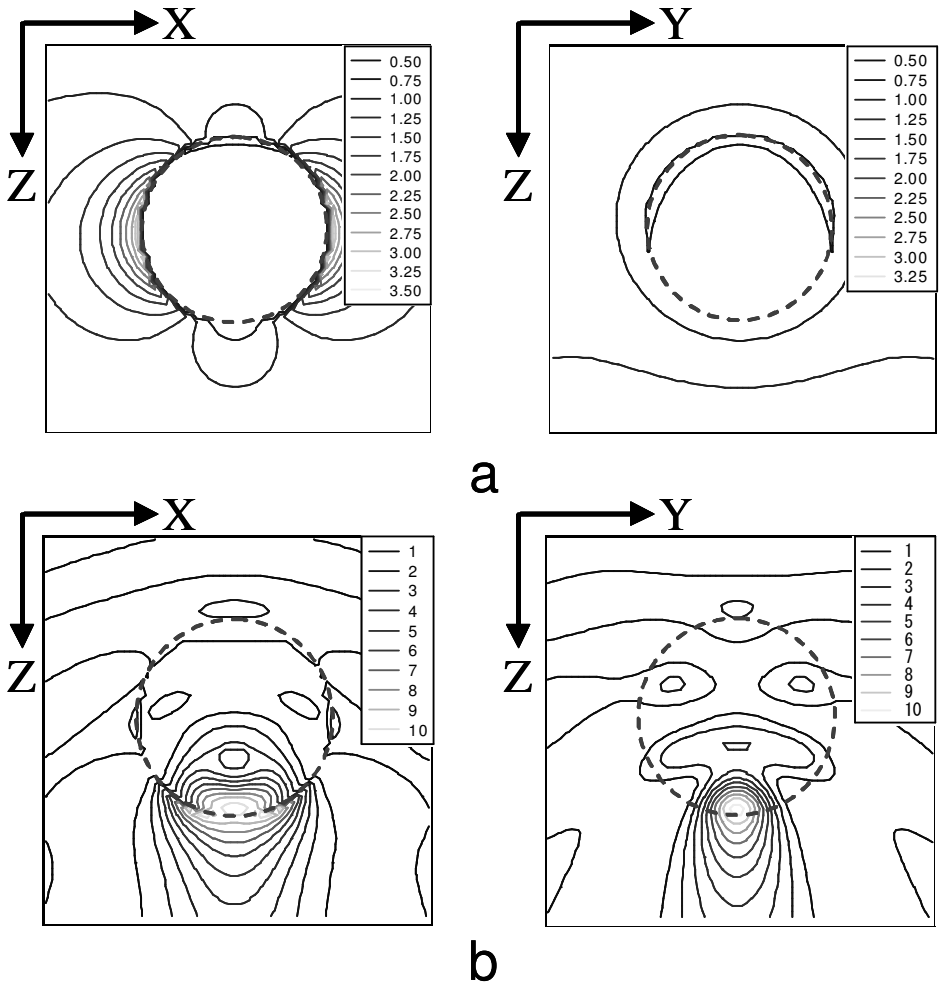

Figure 1. 6. Calculated intensity distributions of the electric fields around the PS particles. **a**, the particle of 100 nm in diameter. **b**, the particle of 500 nm in diameter. The left and right images show the X-Z and Y-Z planes. The direction of light propagation is along the Z-direction, and is displayed from the top to the bottom of the images. The polarization directions are parallel to the X-axis. The dotted circles represent the size of the spheres. The colored lines indicate the contour lines denoting the relative intensities to the incident light. The intensities are displayed in the legends. The wavelength of the incident light is 488 nm.

Nanofabrication by Optical Near field

Fabrication technology on the nanometer scale will become more and more important in the future from the view point of industrial applications, such as high-resolution lithography for the manufacture of quantum devices or extremely high density recording media. Several technologies, such as nanoimprinting,[61, 62] electron beam lithography,[63,64] and field ion beam patterning[65] have been investigated for nanofabrication. On the other hand, photolithography has remained a useful nanofabrication technology because of its ease of repetition and capability for large area fabrication. Its diffraction limit, however, restricts the fabrication scale of conventional photolithography; equation 1 is applicable to the limit of fabrication. Recently, near-field optical lithography has been developed as a new technology to overcome the diffraction limit.[66] A number of research groups have demonstrated the patterning surfaces at resolution below the diffraction limit using conformal mask lithography. This has been realized by the use of light-coupling masks,[67] an evanescent field optical lithography method,[19, 20] or an embedded-amplitude mask.[21] Nanofabrication using near-field optical lithography was also attained with an optical fiber probe (§1. 3. 3) using SNOM.[68, 69, 70]

Near-Field Optical Recording

The use of an optical near field is one of the promising procedures for ultra high-density optical recordings in the near future, because it goes beyond the diffraction limit. Various optical recording techniques using the optical near field as light source have been proposed. Thus far Betzig et al. recorded marks of 60 nm in diameter on magnet-optic materials using an optical fiber probe with a subwavelength-sized aperture.[24] Likewise, Hosaka et al. demonstrated the formation and observation of phase-changed domains of 60 nm in diameter in a thin Ge-Sb-Te film using an optical fiber probe.[23] In these cases, the recording speed was limited to sub-milliseconds (about 10 KHz), because the throughput of the fiber probes, fabricated by a heating-and-pulling process, was very low and the apertures of the probes were heated and damaged by coupling with the high power light (about 10 mW). Besides, the heat conduction from the probes to the recording mediums plays an important role in the mark formation.[23] Recently, Yatsui et al. demonstrated a recording and reading system using both the contact slider with a pyramidal silicone probe array and the phase-change medium.[71]

Even in their system, a light power of 200 mW was required for recording the marks at the frequency of 2 MHz. For achieving an actual recording and reading system using the optical near field, not only high throughput probes but also sensitive recording mediums are important.

As an alternative promising method for high-density optical-recording, a near-field optical head using solid immersion lens (SIL) was proposed.[22] In SIL system, the combination of 1.5 Numerical-Aperture (NA) optical head, GaN laser diode and air-gap servo system in the range of 50 nm were used as a light source. The recording density of 50 Gbit/inch^2 is expected based on SIL method.

1.2.3. Nanofabrication for Bioengineering Applications

Biologically-derived macromolecules (biomolecules; e.g. deoxyribonucleic acids, ribonucleic acid and proteins) are extremely diverse in their physical sizes, chemical and structural properties. Efficient immobilization of various biomolecules is a key aspect of many applications including microarray technologies,[72, 73] cell adhesion[74, 75] and biotechnology in general.[76,77,] Functions of the biomolecules are susceptible to physical and chemical surface properties and nanotopography of the substrate, as such interfacial forces effect a nanoscale change in molecular shape and structure,[78, 79, 80] therefore, the first problem to be overcome is the tendency for biomolecules to denature on contact with the substrate surfaces.

Extensive approaches have been developed, using either covalent attachment or noncovalent affinity binding.[81] The covalent coupling process can achieve stable coupling, but it needs complexity and cost of derivation steps, and limited sites for attachment leads to shorter lifetime. In the conventional chemical process, for example, three steps are required for the immobilization of the biomolecules; activation, binding and deactivation. These complicated steps each have the potential to denature the biomolecules. Furthermore, protein stabilization agents such as sodium azide inhibit many chemical reactions. On the other hand, the noncovalent affinity binding process is the simplest approach to the immobilization but it tends not to be stable, and activity of biomolecule is often lost in time-dependent structural changes.[82] Recent study for the noncovalent affinity binding process has been directed toward the selective adsorption of

biomolecules using nanopatterned surfaces [83, 84, 85] and/or molecularly imprinted polymers[86,87] so as to hold the 3-dimensional structure of the biomolecules.

Moreover, materials and fabrication technologies are critically important for tissue engineering in designing temporary, artificial extracellular matrices as scaffolds, which support three-dimensional tissue formation. [88] Nano-structured scaffolds by using electrospinning technique, [89, 90] self-assembly, [91] and nanocomposites [92] has been proposed.

1.3. Experimental Techniques

1.3.1. Scanning Probe Microscopy

Scanning probe microscopy (SPM), chiefly scanning tunneling microscopy (STM) and atomic force microscopy (AFM), has become a powerful tool for investigating the structure and dynamic behavior of surfaces and interfaces since invention of STM in 1981 by Binnig and Rohrer from the IBM Research Laboratory. [93, 94] AFM was developed soon after STM in 1985.[95] Since then a variety of imaging techniques based on SPM has been proposed. [96] SPM can image the surfaces of materials with unparalleled magnification. The magnification is so extreme that individual atoms become visible. SPM is, therefore, one of the foremost tools for imaging, measuring and manipulating matter at the nanoscale.

The principle of SPM is remarkably simple, like an old-fashioned record player.[96] The instrument uses an extremely sharp needle, referred to as the 'tip', to interrogate the shape of the surface. In STM, the tip is made by an electrochemically-etched tungsten wire or platinum iridium. The STM tip does not touch the surface by keeping the tunneling currents between the tip and the surface at a few pico Amperes (pA) and a few nano Amperes (nA); the distances between the tip and the surface of only 0.5 to 1.0 nm, i.e. 2 to 4 atomic diameters. On the other hand, the AFM tip gently touches the surface. The AFM tip is made of silicon nitrite or silicon. The tip radius of curvature is typically around 10 nm. The AFM tip is attached to a tiny leaf spring, the cantilever, which has a low spring constant. The deflection of this cantilever is detected, often with the use of a laser beam, which is reflected from the cantilever. Thus, the AFM measures contours of constant attractive or repulsive forces between the tip and the surface, at as small as a few pico newton level. Depending on the situation, the forces that are measured in AFM

include mechanical contact force, Van der Waals forces, capillary forces, chemical bonding, electrostatic forces, magnetic forces. Because the AFM does not rely on the presence of a tunneling current, it can also be used on non-conductive materials.

The SPM tips are attached to a piezo-electric element. This is a piece of material with the useful property that it changes its length a little bit, when it is put under an electrical voltage. By adjusting the voltage on the piezo element, the distance between the tip and the surface can be regulated. In most SPMs, the voltage on the piezo element is adjusted such that the tunneling current or atomic force always has the same value, for example 1 nA for STM and 1 nN for AFM. In this way, the distance between the last atom on the tip and the nearest atoms in the surface is being kept constant. This distance regulation is performed automatically, by so-called feedback electronics, which continually measure the deviation of the tunneling current or the atomic force. While this feedback system is active, two other parts of the piezo element are used to move the tip in the X- and Y-directions, parallel to the surface, to scan over the surface, line by line, similar to the way a television or computer screen image is built up. The combination of small displacements in the X-, Y-, and Z-directions, parallel and perpendicular to the surface, is obtained with suitable combinations or geometries of piezo-electric elements.

In the XY-scan, every time that the last atom of the tip is precisely above a surface atom, the tip needs to be retracted a little bit, while it has to be brought slightly closer when the tip atom is between the surface atoms. Thus, the tip automatically follows a bumpy trajectory, which mimics the atomic corrugation of the surface. The information about this trajectory is available in the form of the voltages that have been applied by the feedback electronics to the piezo element during the XY-scan.

1.3.2. Tapping-Mode (Dynamic-Mode) Atomic Force Microscopy

The problem in AFM using static tip deflection as feed back signal, the technique is so-called contact- or static- mode AFM, is that the tip sometimes exerts considerable forces to the sample surface, thereby causing sample deformation and/or damage, so that the height images may not present the true topographic information in the case of the soft samples. To avoid the surface deformation and damage, tapping-mode (dynamic-mode) AFM has been developed soon after the introduction of contact-mode AFM.[96, 97, 98, 99]

In tapping-mode AFM a tip is oscillated vertically at the resonance frequency of a

cantilever. At approaching the tip to a sample surface, the vibrational characteristics of the cantilever oscillation (e.g., the amplitude, resonance frequency, and phase angle of vibration) will change due to the tip-sample interactions. Usually, the regulation of the tip-sample interactions is performed by the amplitude of the oscillation as feed back signal. When the amplitude of the free oscillation is A_0, the observed amplitude of oscillation is maintained at A_{sp} as feedback signal by adjusting the vertical position of the sample during scanning. Since the fast oscillation of the tip can reduces the duration of tip-sample contact, one can avoid the sample deformation and damage. In addition, new imaging modes have been developed by detecting changes in the vibrational characteristics. Use of oscillating probes and new imaging modes has lead to significant progress especially on soft samples like polymers and biological specimens.

During tapping-mode AFM operation, the phase angle of the cantilever oscillation changes with surface properties of samples.[97-99] The change in the phase angle can be mapped simultaneous with topographic imaging, which is called a phase image (Figure 1. 7). The phase image provides a map of stiffness variations on the surface such that a stiffer region displays a more positive phase shift in case of a relatively harder sample, Young's modulus of which is larger than approximately 1 GPa, because the phase shift $\Delta\Phi_0$ is approximately described as:

$$\Delta\Phi_0 \propto \langle S \rangle (Q/k) = \sqrt{\langle A \rangle} E^* (Q/k), \quad (3)$$

where $\langle S \rangle$ and $\langle A \rangle$ is the time-averaged value of the stiffness and the contact area, respectively. E^* is the effective modulus, Q is the quality factor of a cantilever, and k is the spring constant of the cantilever. E^* is proportional to the stiffness when the tip is much harder than the sample and the contact area $\langle A \rangle$ is regarded as a constant value. As an example, for the low- and high-density parts of a microlayered polyethylene sample, the phase shifts are substantially larger on the high-density part (young's modulus 1 GPa) than on the low-density part (0.3 GPa).[97]

Note that a very softer material, young's modulus of which is smaller than few tenth of GPa, leads to a larger contact area $\langle A \rangle$. A change in stiffness can be dominated by a change in the contact area $\langle A \rangle$, which makes the phase shift greater on a softer material than on a harder material. As an example, polydiethylsiloxane elastomer (PDES, young's modulus less than 0.1 GPa) on a Si substrate shows larger phase shift on PDES than on the Si substrate.[97] Thus, it is very important to interpret the phase image carefully.

The phase imaging technique is a powerful technique for distinguishing different surface features of both multi-component compounds and one-component systems with different density distributions. A number of studies on polymer blends and composites, block copolymers and patterned surfaces based on the phase imaging technique have been presented.[100]

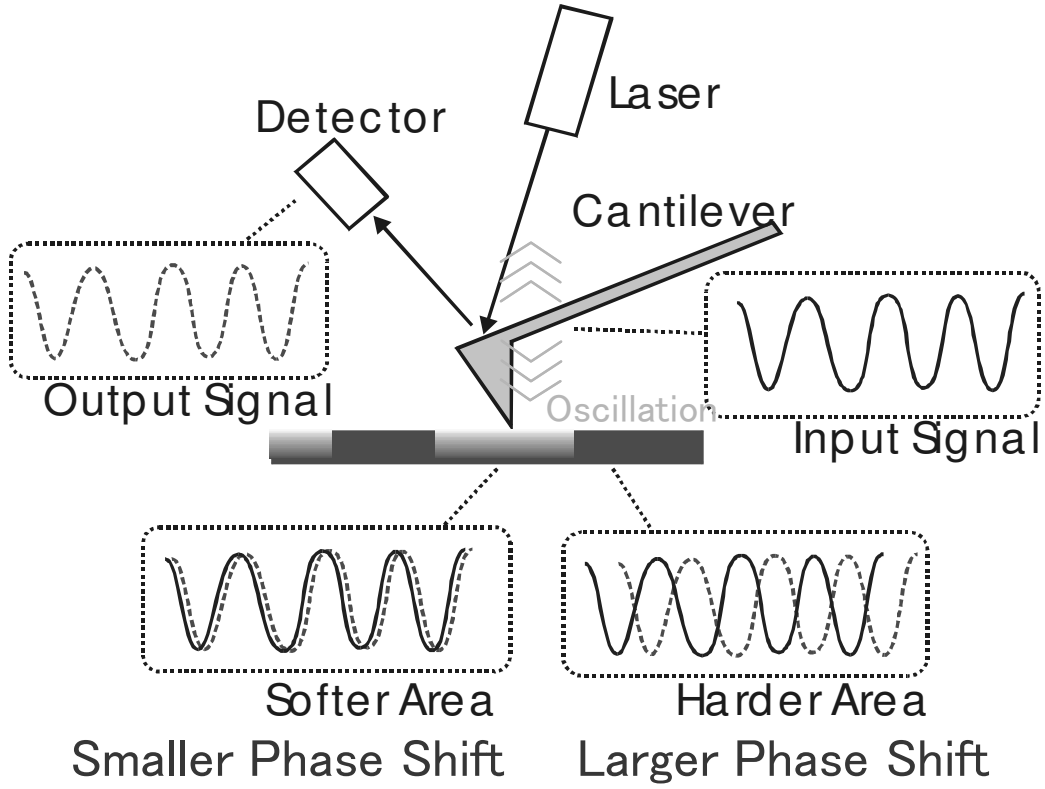

Figure 1. 7. Phase imaging by tapping-mode AFM.

1.3.3. Scanning Near-Field Optical Microscopy

For the most part, AFM reveals topographical information but yields little chemical information. Ideally, one would like to combine the high resolution of these techniques with sensitivity, specificity and flexibility afforded by optical techniques. This goal has driven the development of scanning near-field optical microscopy or near-field scanning optical microscopy (SNOM or NSOM) which can be used to conduct optical measurement with spatial resolution beyond the classical diffraction limit of light. [44, 66]

One of the common microscope designs utilized for SNOM measurements is shown in Figure 1. 8. In this set up an optical fiber with a small aperture is used as a probe. The other side of the optical fiber is coupled with light from a laser and the optical fiber delivers light to the aperture of which dimensions smaller than the optical wavelength. The optical fiber probe is attached to z-piezo tube and quartz crystal and is oscillated laterally at its resonance frequency like tapping-mode AFM. The distance between the probe and a sample was controlled by shear-force as a feed back signal and z-piezo tube.[101] In the shear-force method, the amplitude of the oscillation of the optical fiber probe is kept low, usually <10 nm, to avoid diminishing the resolution in the optical image. As the tip approaches the sample surface, shear forces acting between the tip and the sample dampen the amplitude of the tip oscillation. This drop of in amplitude normally occurs over a range of tens of nanometers from the sample surface. The amplitude can be monitored by several methods and used to generate feed back signal.

The heart of any near-field microscope lies in the quality of the aperture (Figure 1. 9). Early optical fiber probe designs included etched quart crystals and pulled micropipets,[102] but these probes generally suffered from low throughput and poor reproducibility. By far, the most successful probe was introduced by Betzig et al. and make use of a tapered fiber optic waveguide coated with a reflactive metal coating.[103] Ohtsu and co-workers have been developing etching techniques that can be used to create a variety of novel probe structures.[66, 104] They have shown that etching techniques can be utilized to fabricate SNOM probes with large cone angles, which is at least 1 order of magnitude more efficient than the probe fabricated by heating and pulling a single mode optical fiber. In their techniques, a single mode optical fiber is etched in a 40% HF solution and tapered edge is formed at the end of the optical fiber, and then, the edge was coated with aluminum by a vacuum evaporated technique (Figure 1. 9). The power output and

throughput efficiency of the probes is dependent on the particular parameters of the probe. Typically, however, probes with 100 nm diameter apertures can deliver tens of nanowatts of light with hundreds of microwatts coupled into the fiber. The power density existing at the aperture is on the order of 100 W/cm^2.

The SNOM technique is still evolving but what is equally true is that it has already evolved to a point where unique and useful measurements can be made on a wide range of samples, single molecule studies, thin film analysis, and biological applications.[44]

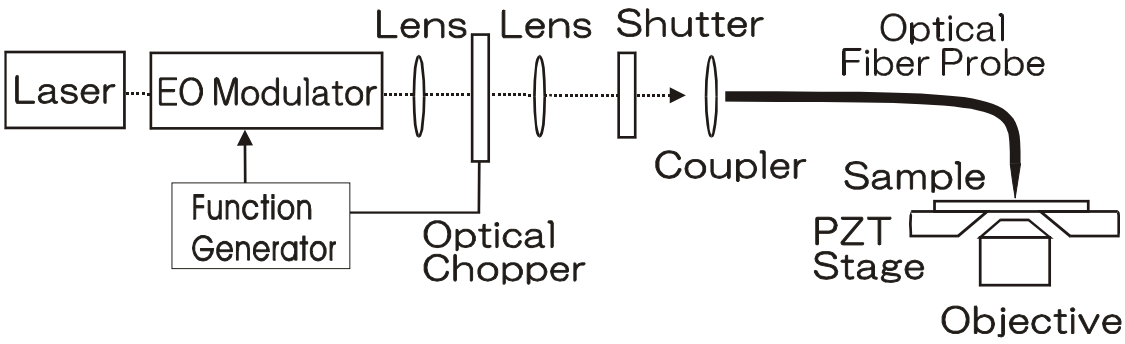

Figure 1. 8. Schematic of a scanning near-field optical microscope (SNOM).

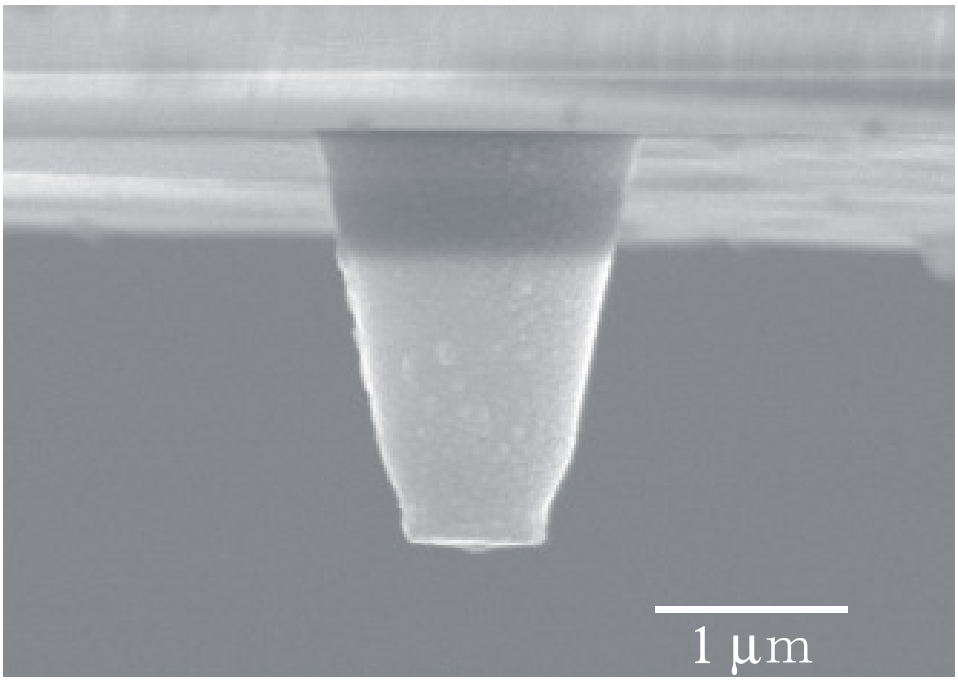

Figure 1. 9. A SEM image of a probe-pointed optical fiber. The aperture size is around 100 nm.

1.4. Outline of This Thesis

This thesis consists of six chapters. In the first chapter the author introduces the background and the motivation of this thesis. The principles of the dynamics of azobenzene-containing polymers, optical near field, atomic force microscopy and scanning near-field optical microscopy are presented. The following chapters divided into two parts.

In Part I, the author demonstrates two kinds of photofabrication methods of the nanometric structure on the surface of the azobenzene-containing polymer. One is photofabrication by the optical near field of dielectric spherical particles, which is shown in chapter 2. The dynamics of nanostructure formation on the azobenzene-containing polymer surface studied by tapping-mode atomic force microscopy is described in chapter 3. The other is photofabrication by SNOM, which is shown in chapter 4.

Chapter 2 comprises fabrication of a hexagonally arrayed indented nanostructure on the surface of azobenzene-containing polyurethane film by the optical near field generated around dielectric spherical particles. The size effect of the polystyrene particles ranging from 98 nm to 990 nm in diameters and the influence of polarization of light were examined. The indentation shapes were dependent on the size of particles and the polarization of the incident light, which strongly suggests that the indentations are induced by the electromagnetic field around the particles.

Chapter 3 discusses the surface deformation mechanism of the azobenzene-containing polyurethane by the optical near field generated around the dielectric particles. The deformation pattern on the film surface was compared with the calculated intensity distribution around the particles, and the polymer migration on the film surface was analyzed by tapping mode atomic force microscopy. These analyses strongly suggest that the near-field gradient force induces the surface deformation.

Chapter 4 focuses on photofabrication on the surface of the azobenzene-containing polymer film by SNOM equipped with optical fiber probes with the subwavelength-sized apertures, and the feasibility of near-field optical recording on the polymer surface are discussed. The formation of the pit structure of 150 nm in diameter was achieved by the optical fiber probe coupled with a sub-microsecond light pulse of 10 mW in optical power and 488 nm in wavelength.

In Part II, the author presents a novel and simple concept for photo-immobilization of

small particles based on the nanoscale surface deformation on the azobenzene-containing polymer. The principle of the immobilization and its application including biological detection and imaging are described in chapter 5 and chapter 6.

Chapter 5 gives a detailed description of the photo-immobilization method for nano-scale particles including biologically derived macromolecules. In short, the surface of an azobenzene-containing polymer deforms along the contour of the small particles and physically holds them upon photo-irradiation. The method offers a highly effective way for protein immobilization, because various proteins are held on the azopolymer surface, keeping their shapes as they are, in a simple process. Immunological and enzymatic studies showed that proteins immobilized on the polymer surface retained their original functionality. The method is, therefore, promising for a variety of biological applications.

Chapter 6 contains an application of the photo-immobilization based process for direct imaging of hierarchical assemblies of biologically derived macromolecules, filamentous (F-) actin. F-actin is among the most abundant proteins in the eukaryotic cell cytoskeleton.[105] In the cell, F-actin is found in many structures including 2D and 3D networks, which impart mechanical stability to the cell, and thick bundles known as stress fibers, which traverse the cell and lead to adhesion of cells to the extra-cellular matrix. It is very important to elucidate the structures of biologically relevant filamentous actin on which mechanical and rheological properties of cells are ultimately dependant.[106] The imaging technique was used to investigate the phase behavior of F-actin assemblies as a function of concentration of the divalent cation Mg^{2+}. The data provided direct experimental evidence of a coil-on-coil (braided) bundle structure at high Mg^{2+} concentrations and a two-dimensional nematic raft structure at medium Mg^{2+} concentrations. This new technique is expected to be broadly applicable to the direct imaging of the large class of biological filamentous systems.

References

[1] H. Rau, In *Photochemistry and Photophysics*, J. K. Rabek, ED, CRC Press: Boca Raton, FL, 1990; vol. 2, p119.

[2] G. S. Kumar and D. C. Neckers, *Chem. Rev.* **89**, 1915 (1989).

[3] S. Xie, A. Natansohn and P. Rochon, Chem. Mater. **5**, 403 (1989).

[4] A. Natansohn and P. Rochon, *Chem. Rev.,* **102**, 4139 (2002).

[5] K. Ichimura, Chem. Rev., **100**, 1847 (2000)

[6] K. Ichimura, Y. Suzuki, T. Seki, A. Hosoki, and K. Aoki, *Langmur*, 4, 1214 (1988).

[7] T. Todorov, L. Nikolova, N. Tomova, *Appl. Opt*. **23**, 4309 (1984).

[8] J. A. Delaire, K. Nakatani, *Chem. Rev*. ,**100**, 1817 (2000)

[9] D. M. Burland, R. D. Miller and C. A. Walsh, *Chem. Rev.* **94**, 31 (1994).

[10] P. Rochon, E. Batalla, A. Natansohn, *Appl. Phys. Lett.,* **66**, 136 (1995).

[11] D. Y. Kim, S. K. Tripathy, L. Li, J. Kumar, *Appl. Phys. Lett.* **66**, 1166 (1995).

[12] R.R. Dammel, In Diazonaphthoquinone-based Resists, Bellingham, WA: SPIE Optical Engineering Press, Vol. TT-11, 1993.

[13] D. van Steenwinckel et al., *J. Vac. Sci. Tech. B,* **24**, 316 (2006).

[14] R.J. Lade, I.W. Morley, P.W. May, K.N. Rosser and M.N.R. Ashfold, *Diamond Rel. Mater.* **8**, 1654 (1999).

[15] S.Y. Chou, P. R. Krauss and P. J. Renstrom**.**, *Science* **272**, 85 (1996).

[16] C. J. Barrett, A. L. Natansohn, P. L. Rochon, *J. Phys. Chem.*, 100, 8836 (1996).

[17] N. K. Viswanathan, S. Balasubramanian, L. Li, J. Kumar, S. K. Tripathy, *J. Phys. Chem. B.,* **102**, 6064 (1998).

[18] T. Pedersen, P. M. Johansen, C. R. Holme, P. S. Rmanujam, S. Hvilsted, *Phys. Rev. Lett.,* **80**, 89 (1998).

[19] M. M. Alkaisi, R. J. Blaikie, S. J. McNab, R. Cheung, and D. R. S. Cumming, *Appl. Phys. Lett.,***75**, 3560 (1999).

[20] R. J. Blaikie, M. M. Alkaisi, S. J. McNab, D. R. S. Cumming, R. Cheung and D. G. Hasko, *Miroelectron. Eng.* **46**, 85 (1999).

[21] J. G. Goodberlet, *Appl. Phys. Lett.* **76**, 667 (2000).

[22] K. Kishima, I. Ichimura, K. Saito, K. Yamamoto, Y. Kuroda, A. Iida, S. Masuhara, K. Osato, *IEICE technical report. Magnetic recording*. **101**, 25 (2002).

[23] S. Hosaka, T. Shintani, M. Miyamoto, A. Hirotsune, M. Hirotsune, M. Terao, M.Yoshida, K. Fujita, and S. Kammer, *Jpn. J. Appl. Phys.,* **35**, 443 (1996).

[24] E. Betzig, J.K. Trautman, R. Wolfe, E.M. Gyorgy, and P.L. Finn, *Appl. Phys. Lett.,* **61**,142 (1992).

[25] Y. Kawata, C. Egami, O. Nakamura, O. Sugihara, N. Okamoto, M. Tsuchimori and O. Watanabe, *Optics Comm.*, **161**, 6 (1999).

[26] O. Watanabe, T. Ikawa, M. Hasegawa, M. Tsuchimori, Y. Kawata, C. Egami, O. Sugihara and N. Okamoto, *Mol. Cryst. Liq. Cryst.,* **345**, 305 (2000).

[27] M. Hasegawa, T. Ikawa, M. Tsuchimori, O. Watanabe, Y. Kawata, *Macromolecules,* **34**, 7471 (2001).

[28] G. Mie, *Ann. D. Physik* , **30**, 57 (1908).

[29] H. C. van de Hulst, in *Light scattering by small particles*, New York, Dover, 1981.

[30] M. Born and E. Wolf, In *Principles of optics,* fifth ed.,Oxford, Pergamon Press, 1975.

[31] T. Ikawa, T. Mitsuoka, M. Hasegawa, M. Tsuchimori, O. Watanabe, Y. Kawata, C. Egami, O. Sugihara, N. Okamoto, *J. Phys. Chem., B*. **104**, 9055 (2000).

[32] T. Ikawa, T. Mitsuoka, M. Hasegawa, M. Tsuchimori, O. Watanabe and Y. Kawata, *Phys. Rev. B,* **64**, 195408 (2001).

[33] T. Ikawa, C.-D. Keum, H. Takagi, M. Tsuchimori, O. Watanabe, W. Mori, M. Harada, M. Tawada and H. Shimoyama, *IEICE Transactions on Electronics,* **E85-C**, 1287(2002).

[34] S. Davy and M. Spajer, *Appl. Phys. Lett.,* **69**, 3306 (1996).

[35] B. Vohnsen and S. I. Bozhevolnyi, *Appl. Opt.,* **38**, 1792 (1999).

[36] T. Fukuda, K. Sumaru, T. Kimura, H. Matsuda, Y. Narita, T. Inoue, and F. Sato, *Jpn. J. Appl. Phys.*, **40**, L900 (2001).

[37] T. Ikawa, F. Hoshino, T. Matsuyama, H. Takahashi and O. Watanabe, *Langmuir,* 22, 2747 (2006).

[38] T. Ikawa, F. Hoshino, O. Watanabe, Y. Li, P. Pincus and Cyrus R. Safinya, *Physical Review Letters,* **98**, 018101 (2007)

[39] O. Watanabe, T. Ikawa, T. Kato, M. Tawata and H. Shimoyama, *Applied Physics Letters,* **88**, 204107 (2006)

[40] A. Teitel, *Naturwissenschaften,* **44**, 370 (1957).

[41] M. S. Ho, A. Natansohn, P. Rochon, *Can. J. Chem.,* **73**,1773 (1995).

[42] J. Kumar, L. Li, X. L. Jiang,D.-Y. Kim, T. S. Lee, and S. Tripathy, *Appl. Phys. Lett.,* **72**, 2096 (1998)

[43] P. Karageorgiev, D. Neher, B. Schulz, B. Stiller, U. Pietsch, M. Giersig and L. Brehmer, *Nature Materials,* **4**, 699 (2005).

[44] R. C. Dunn, *Chem. Rev.,* 99, 2891 (1999).

[45] E. Abbe*, Arch. Mikrosk. Anat.,* **9**, 413, (1873).

[46] E. H. Synge, *Philos. Mag.,* **6**, 356 (1928).

[47] E. H. Synge, *Philos. Mag.,* **11**, 65 (1931).

[48] E. H. Synge, *Philos. Mag.,* **13**, 297 (1932).

[49] H. A. Bethe, *Phys. Rev.* **66**, 163-182 (1944).

[50] C. J. Bouwkamp, *Philips Res.Rep.,* **5**, 401 (1950).

[51] C. J. Bouwkamp, *Philips Res. Rep.,* **5**, 321 (1950).

[52] K. Tsuruta, *O plus E,* **20**, 1418 (1998).

[53] E. A. Ash, G. Nicholls, *Nature,* **237**, 510 (1972).

[54] D. W. Pohl, W. Denk, M. Lanz, *Appl. Phys. Lett.* **44**, 651 (1984).

[55] U. During, D. W. Pohl, F. J. Rohner, *J. Appl. Phys.,* **59**, 3318 (1986).

[56] E. Betzig, A. Lewis, A. Harootunian, M. Isaacson, E. Kratschmer, *Biophs. J.,* **49**, 269 (1986).

[57] E. Betzig, R. J. Chichester, *Science,* **262**, 1422 (1993).

[58] http://www.scatlab.com/, http://www.t-matrix.de/

[59] E. Zenhausern, Y. Martin and H. K. Wickramasinghe, *Science,* **269**, 1083 (1995).

[60] A. Downes, D. Salter, and A. Elfick, *Opt. Express* **14**, 5216-5222 (2006)

[61] S. Y. Chou, P. R. Kraus, and P. J. Renstrom, *J. Vac. Sci. Technol. B* **14**, 4129 (1996).

[62] I. Martini, D. Eisert, M. Kamp, L. Worschech, A. Forchel, and J. Koeth, *Appl. Phys. Lett.,* **77**, 2237 (2000).

[63] J. R. Wendt, G. A. Vawter, R. E. Smith, and M. E. Warren, J. *Vac. Sci. Technol. B* **13**, 2705 (1995).

[64] T. Yoshimura, H. Shiraishi, J. Yamamoto, T. Terasawa, and S. Okazaki, *Appl. Phys. Lett.,* **68**, 1799 (1996).

[65] B. D. Terris, D. Weller, L. Folks, J. E. E. Baglin, and A. J. Kellock, *J. Appl. Phys.,* **87**,

7004 (2000).

[66] *Near-Field Nano/Atom Optics and technology*, edited by M. Ohtsu (Springer, New York, 1998).

[67] H. Schmid, H. Biebuyck, and B. Michel, *Appl. Phys. Lett.,* **72**, 2379 (1998).

[68] S. Davy and M. Spager, *Appl. Phys. Lett.,* **69**, 3306 (2000).

[69] M. K. Hendon, R. T. Collins, R. E. Hollingsworth, P. R. Larson, and M. B. Johnson, *Appl. Phys. Lett.,* **74**, 141 (1999).

[70] I. I. Smolyaninov, D. L. Mazzoni, and C. C. Davis. *Appl. Phys. Lett.,* **67**, 3859 (1995)

[71] T. Yatsui, M. Kourogi, K. Tsutsui, M. Ohtsu, and J. Takahashi, *Opt. Lett.,* **25**, 1279 (2000).

[72] *Protein Microarray Technology,* D. Kambhampati, Ed. Wiley-VCH, Weinheim, 2003.

[73] *Protein Microarray,* M. Schena, Ed., Jones and Bartlett Publishers, Sudbury, 2004.

[74] S. P. Palecek, J. C. Loftus, M. H. Ginsberg, D. A. Lauffenburger, A. F. Horwitz, *Nature,* **385**, 537 (1997).

[75] G. L. Griffith, G. Naughton, *Science,* **295**, 1009 (2002).

[76] A. G. Mayers, *Biomolecular Sensors*; E. Gizeli, R. C. Lowe, Eds, Taylor and Francis, London, 2002

[77] G. M. Whitesides, E. Ostuni, S. Takayama, X. Jiang, D. E. Ingber, *Annu. Rev. Biomed. Eng.* **3**, 335 (2001).

[78] J. J. Ramsden, *Quarterly Reviews of Biophysics*, **27**, 41, (1993).

[79] M. Wahlgren, T. Arnebrant, *TIBTECH,* **9**, 201 (1991).

[80] E. Ostuni, R. G. Chapman, R. E. Holmlin, S. Takayama, Whitesides, G. M. *Langmuir*, **17**, 5605 (2001)**.**

[81] A. G. Mayers, *Biomolecular Sensors*; E. Gizeli, R. C. Lowe, Eds, Taylor and Francis, London, 2002.

[82] J. J. Ramsden, *Quarterly Reviews of Biophysics*, **27**, 41, (1993).

[83] A. Curtis, C. Wilkinson, *Trends in biotechnology,* **19**, 97 (2001).

[84] F. Cunin, T. A. Schmedake, J. R. Link, Y. Y. Li, J. Koh, S. N. Bhatia, M. J. Sailor, *Nature Materials,* **1**, 39 (2002).

[85] H. Shi, W-B. Tsai, M. D. Garrison, S. Ferrari, B. D. Ratner, *Nature,* **398**, 593 (1999).

[86] K. Haupt, *Chem. Comm.* 171 (2003).

[87] C. Alexander, L. Davidson, W. Hayes, *Tetrahedron* **59**, 2025 (2003).

[88] P. X. Ma*, Matericals Today*, (5) 30 (2004)

[89] E. D. Boland., et al., *J. Macromol.Sce.-Pure Appl. Chem.*, **38**, 1231 (2001)

[90] J. A. Matthews, et al., *Biomacromolecules,* **3**, 232 (2002).

[91] L. A. Smith and P. X. Ma, *Colloids Surf. B,* **39**, 125 (2004).

[92] K. M. Woo, J. Seo, R. Y. Zhang, P. X. Ma, *Biomaterials,* **28**, 2622 (2007).

[93] G. Binnig, H. Rohrer, Ch. Gerber, and E. Weibel, *Phys. Rev. Lett.*, **49**, 57 - 61 (1982).

[94] G. Binnig, H. Rohrer, Ch. Gerber, and E. Weibel, *Appl. Phys. Lett.,* **40**, 178-180 (1982).

[95] G.. Binnig, C. F. Quate, and Ch. Geber, *Phys. Rev. Lett.*, **56**, 930 (1986).

[96] E. Meyer, R. Bennewitz, H. J. Hug, In *scanning probe microscopy*, Springer, Berlin (2004).

[97] S.N. Magonov, V. Elings, M.-H. Whangbo, *Surf. Sci*., **375**, L385 (1997)

[98] G. Bar, Y. Thomann, R. Brandisch, H.-J. Cantow, *Langmuir*, **13**, 3807 (1997)

[99] Ph. Leclère, R. Lazzaroni, J. L.Brédas, J. M. Yu, Ph. Dubois, R. Jérôme, *Langumuir*, **12**, 4317 (1996)

[100] S. N. Magonov, In *Applied Scanning Probe Methods* (Nanoscience and Technology), Springer, Berlin 2004.

[101] E. Betzig, P. L. Finn, J. S. Weiner, *Appl. Phys. Lett*., **60**, 2484 (1992).

[102] E. Betzig, M. Isaacson, A. Lewis, *Appl. Phys. Lett.*, **51**, 2088 (1987)

[103] E. Betzig, J. K. Trautman, T. D. Harris, J. S. Weiner, R. L. Kostelak, *Science,* 251, 1468 (1991).

[104] S. Mononobe, M. Naya, T. Saiki, M. Ohtsu, *Appl. Opt.* 36, 1496 (1997).

[105] B. Alberts et al., *Molecular biology of the cell* (Garland Science, New York, 2002), 4th ed.

[106] G.C.L. Wong, A. Lin, J.X. Tang, Y. Li, P.A. Janmey, and C.R. Safinya, *Phys. Rev. Lett.* **91**, 018103 (2003).

Part I Nanostructure Formation on Azobenzene-Containing Polymers by Optical Near Field

Chapter 2. Topographical Nanostructure Patterning on Azobenzene-Containing Polymers by the Optical Near Field of Polystyrene Spherical Particles

2. 1. Introduction

In chapter 2, the author demonstrates a topographical nanostructure patterning on the surface of azobenzene-containing polymer films by the optical near field generated around polystyrene (PS) spherical particles of sub-micron diameter.[1, 2] The experimental procedure for the nanostructure formation is simple and easy as followings: first, the monolayer of the PS particles is formed on the surface of the polymer film, second, the monolayer and the polymer film are irradiated with a laser beam of a wavelength coinciding with the absorption band of the azobenzene group, third, hexagonally arrayed dents are formed on the polymer surface after removing the monolayer by sonication. By using the particle of 19 nm in diameter, the dent structure of around 20 nm in diameter was achieved (2. 5. Appendix I).[1] The size of the structure is beyond the diffraction limit of light, thus, the technique is promising for non-optically probing near-field microscopy[3] and the nanostructure photofabrication. As described in chapter 1, the polymer containing azobenzene group (pseudostilbene-type) shows surface deformation by intensity distribution of light. In the above procedure, the polymer surface is also considered to deform with reflecting the intensity distribution of the optical near field around the particles during the photoirradiation. However, the mechanism and the driving force of this phenomenon have not been clarified.

In this chapter, the effect of the size of the PS particle on the dent structure is presented by using the urethane-urea copolymer with pseudostilbene-type azobenzene group (disperse red 19-type).[1] The effects of the polarization of the irradiated light, film thickness and the substitutents of the azobenzene group are examined, and then a possible mechanism and the role of the azobenzene group are discussed.

2. 2. Experimental

Figure 2. 1 shows the chemical structures of the urethane-urea copolymer (**polymer 1**) and polyurethane polymers (**polymers 2-4)**, which were used in this chapter. The synthetic route to manufacturing **polymer 1** had been described elsewhere[4], and the other polymers were also prepared according to the same method as used for **polymer 1**. The number- and weight-average molecular weights (M_n and M_w) of the polymers were measured by gel permeation chromatography (GPC; Tosoh SC-8010; column, Shodex OhpakSB-G + SB-806M HQ × 2; eluent, *N, N'*-dimethylformamide) calibrated with standard polyethylene glycol. The glass transition temperature (T_g) was determined by differential scanning calorimetry (DSC; Perkin Elmer DSC-7 and TAC 7/DX thermal controller; heating rate, 10 °C/min). The measurement of the inherent viscosity of the polymers was performed at 30ºC in 1-methyl-2-pylorridone (Ubbelohde viscometer). The general properties of these polymers are summarised in Table 2. 1.

Sample films were prepared by spin-coating from ~8 wt% pyridine solutions of each polymer. These solutions were passed through a 0.20 μm filter (Millipore) to remove impurities before spin-coating. Optically clear films were formed on the glass substrates. The films that we obtained were placed in a vacuum oven at 130°C for over 24 hours to obtain solvent-free-samples. The thickness of the polymer films was measured by using a surface profiler (a subsidiary of veeco instruments, inc. Dektak3 ST)

Photoinduced surface modification of the polymer films was performed by the following procedure (Figure 2. 2). An aqueous solution including the PS spherical particles (Moritex Co.) was dropped on the surface of the polymer films, and then the spheres were allowed to arrange themselves by a self-organization process. After drying the samples at room temperature overnight, they were irradiated with linearly polarized light of 488 nm in wavelength from Ar^+ laser (Lexel Model 95 Ion Laser). The light beam was irradiated at normal incidence to the surface of the polymer films, and the sample films were held vertically to avoid the effects of gravity. The sample films were then washed with benzene for three days in order to remove the spheres from the surface, and then subsequently they were dried in vacuo at 25°C for two days.

The surface structure of the polymer films was investigated by scanning electron microscopy (SEM; JEOL JSM -890) in vacuo and atomic force microscopy (AFM;

Digital Instruments Inc. Nanoscope E) under ambient conditions. For all measurements, a 15-μm scanner was used in contact mode, with a microlever force constant of 0.38 N/m. A scan rate of 5 Hz was employed.

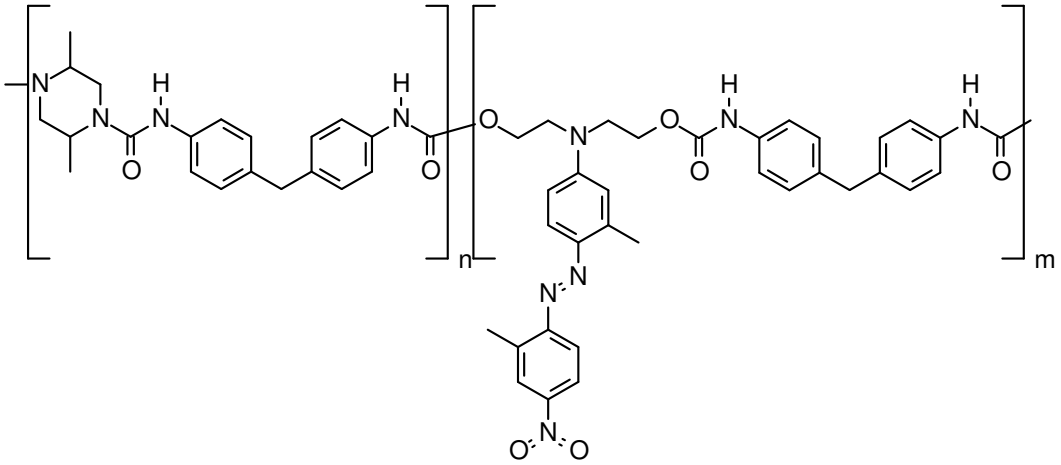

Polymer 1

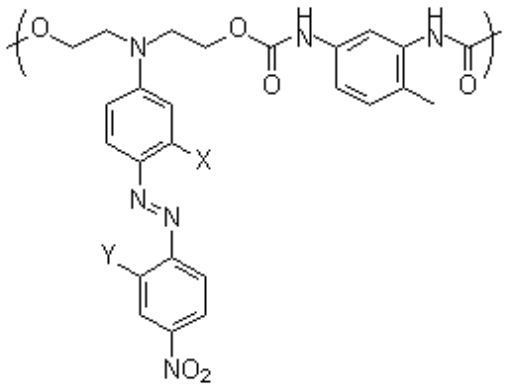

Polymer 2, 3, 4

Figure 2. 1. Chemical structures of the azobenzene-containing polymers used in this study.

Table 2. 1. Composition, molecular weight, glass transition temperature and viscosity of the polyurethanes used in this study**.**

polymer	X	Y	M_n[a]	M_w[a]	M_w/M_n[a]	T_g (°C)[b]	η (dL/g)[c]
Polymer 1	**-**	**-**		170,000		145	
polymer 2	H	H	4,440	8,137	1.83	128	0.11
polymer 3	H	CH_3	3,488	5,585	1.60	120	0.10
polymer 4	CH_3	CH_3	3,388	6,239	1.84	124	0.09

[a] Determined by GPC using a polyethylene glycol-calibrated column set.

[b] Determined from DSC measurements.

[C] Determined from viscosity measurement using 1-methyl-2-pyrrolidone at 30ºC.

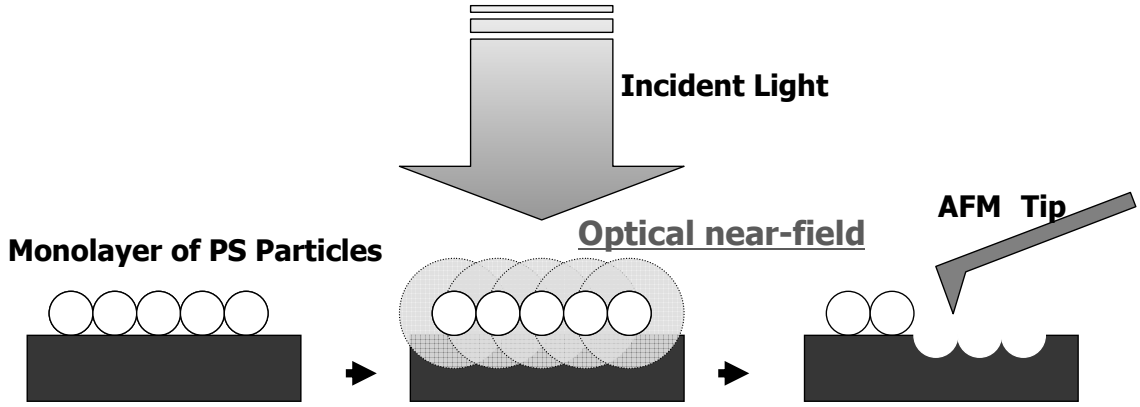

Figure 2. 2. Schematic representation of the nanostructure patterning by spherical particles.

2. 3. Results and Discussion

SEM Analysis

The surface profiles of the azobenzene-containing polymer films after photo-irradiation were investigated by SEM. Figure 2. 3 shows typical examples of three-dimensional views of the film surface of **polymer 1**. The PS particles used in Figure 2. 3 a and b were 241 nm and 98 nm in diameter, respectively, and the particles were partially removed from the surface by sonication. In both images, hexagonally arrayed particles and corresponding dents were observed on the polymer surface. The remained particles on the polymer surface were partly buried on the polymer surface, indicating that the dents had been formed directly below the particles during photoirradiation. The dent structures on the polymer films reflect the arrangement and the shape of the particles.

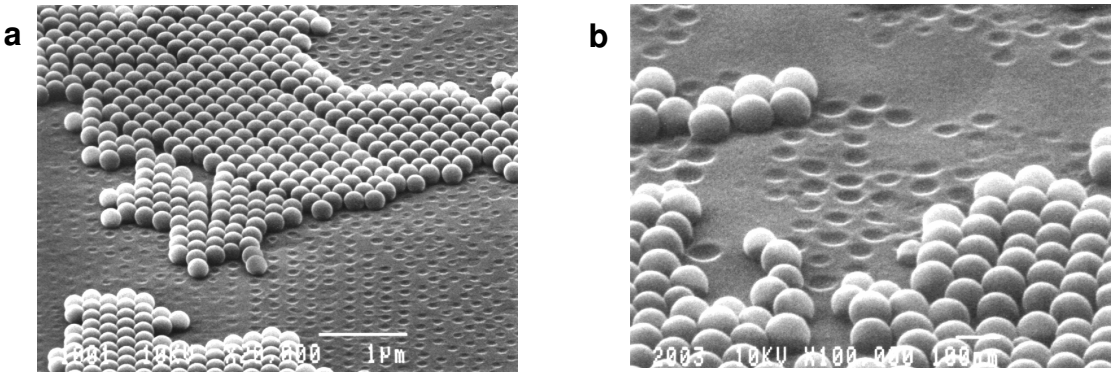

Figure 2. 3. SEM images of the azobenzene-containing polymer surfaces treated by the PS particles. **a**, the particles of 241 nm in diameter. **b**, the particles of 98 nm in diameter. The particles were partially removed from the surface by sonication. The sample films were irradiated for 5 min with linearly polarized light of 488 nm in wavelength and 500 mW/cm^2 in optical power density.

AFM Analysis

Effects of the Size of the Particle and the Polarization of the Incident light

The precise structures formed by the PS particles were analyzed by AFM. Figure 2. 4 shows AFM images of the surfaces of **polymer 1** treated by the PS particles of 98 nm, 241 nm, 505 nm and 990 nm in diameter. The influence of the polarization of the incident light, circularly and linearly polarized light, on the dent shape is displayed in Figure 2. 4 a and b, respectively. The interesting point is the large difference in the shapes of the dents, depending both on the particle size and the polarization of light.

For the polymer surface treated by the particles of 505 nm and 990 nm in diameters, the dent shapes were influenced by the polarization of the incident light. The dents formed by circularly polarized light were in circular symmetry (Figure 2. 4 e and f), whereas the dents formed by linearly polarized light were anisotropic in shape (Figure 2. 4 g and h). The cross section of the dents showed that the periphery of the dent formed a large hump in the polarization direction of the incident light (Figure 2. 5). For the polymer surface treated by the particles of 98 nm and 241 nm in diameters, on the other hand, the dent shapes were less affected by the polarization of the incident light. Nearly symmetric hump was observed on the dents formed by the linearly polarized light (Figure 2. 4. b and d). These results indicate that the polarization of the incident light influences the dent shape, and the influence is more efficient for the particles larger than 500 nm in diameter.

Changes in the dent shapes as functions of the particle size and the irradiated time are summarized in Figure 2. 6. As increasing the size of the PS particle, the depth of the formed dent increased (Figure 2. 6. a), however, the diameter of the dent changed little in all cases (Figure 2. 6. b). The diameters of the dents and the particles were nearly equal for the particles of 98 nm and 241 nm in diameter, whereas the diameters of the dents were smaller than that of the particles lager than 505 nm in diameter (Figure 2. 6. b). These results show that the shapes of the particle and the formed dents are not proportional and suggest that the formation of the dent is caused not only by the contact of the polymer surface with the particles.

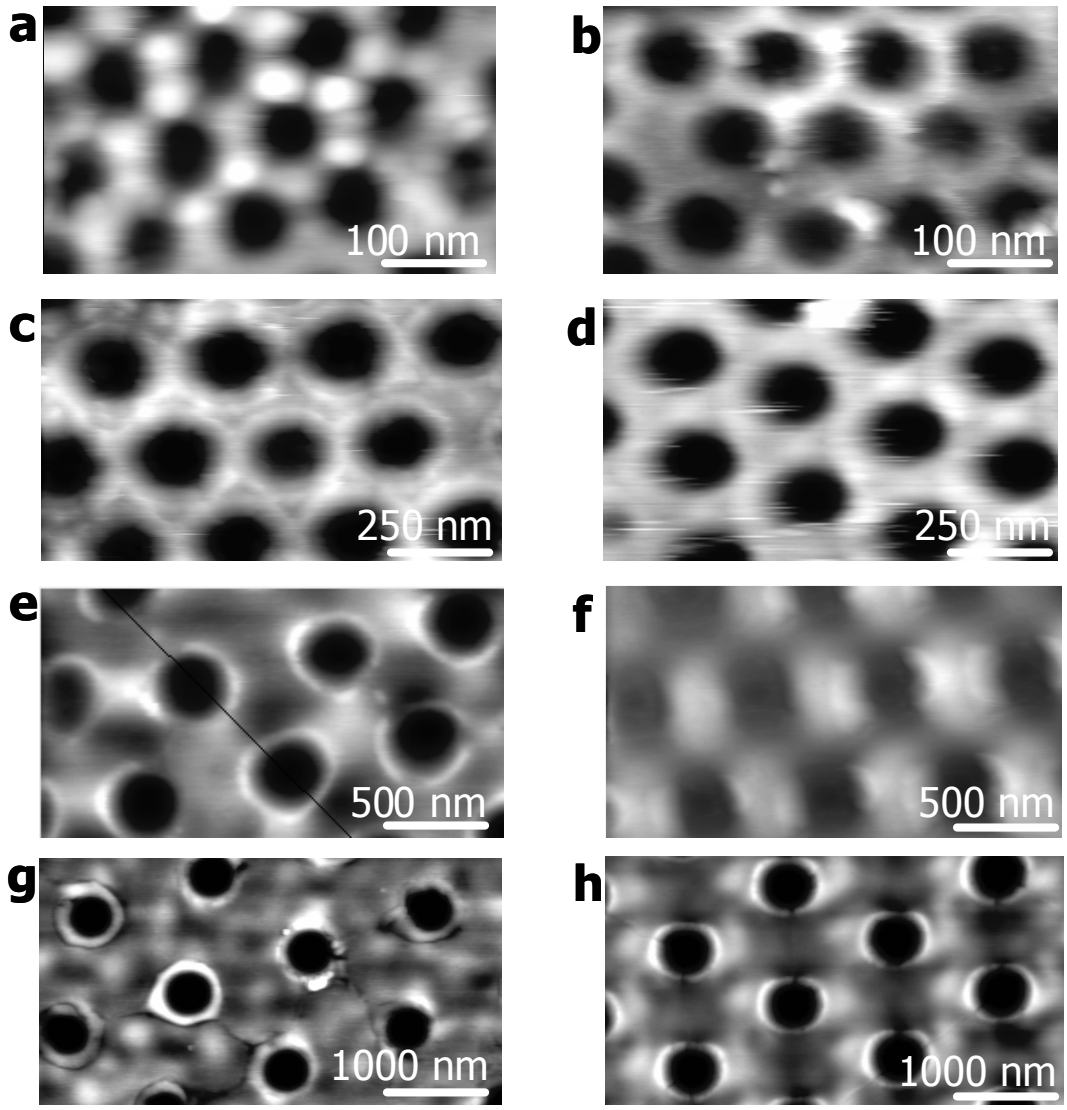

Figure 2. 4. 2D AFM images on the surface of **polymer 1** treated by the particles of 98 nm in diameter (**a** and **b**), 241 nm in diameter (**c** and **d**), 505 nm in diameter, (**e** and **f**) and 990 nm in diameter (**g** and **h**). In **a, c, e** and **g,** the polymer surfaces were irradiated with circularly polarized light. In **b, d, f** and **h**, the polymer surfaces were irradiated with linearly polarized light; the polarization direction is parallel to the horizontal axis.

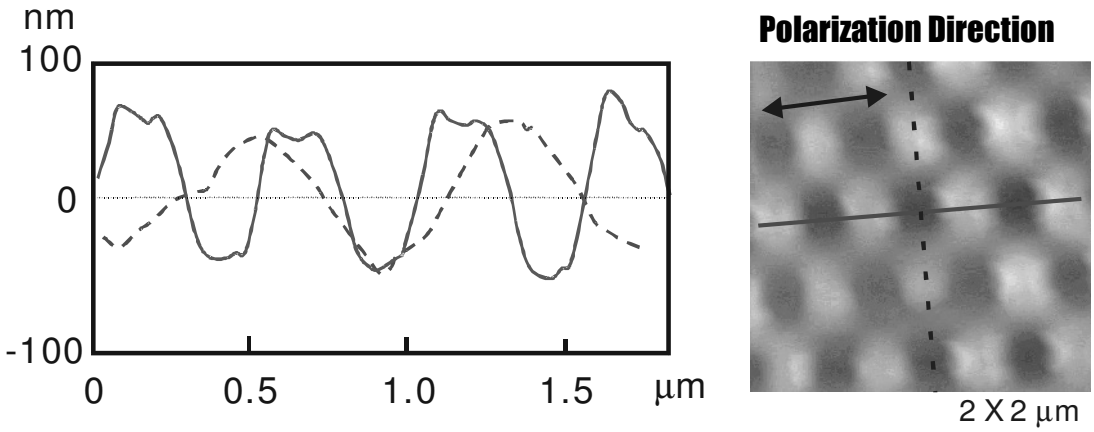

Figure 2. 5. Cross sections of the surface of **polymer 1** treated by the particles of 505 nm in diameter and irradiated with linearly polarized light. The cross sections indicated in the solid and dotted lines are parallel and perpendicular to the polarization direction of the incident light, respectively.

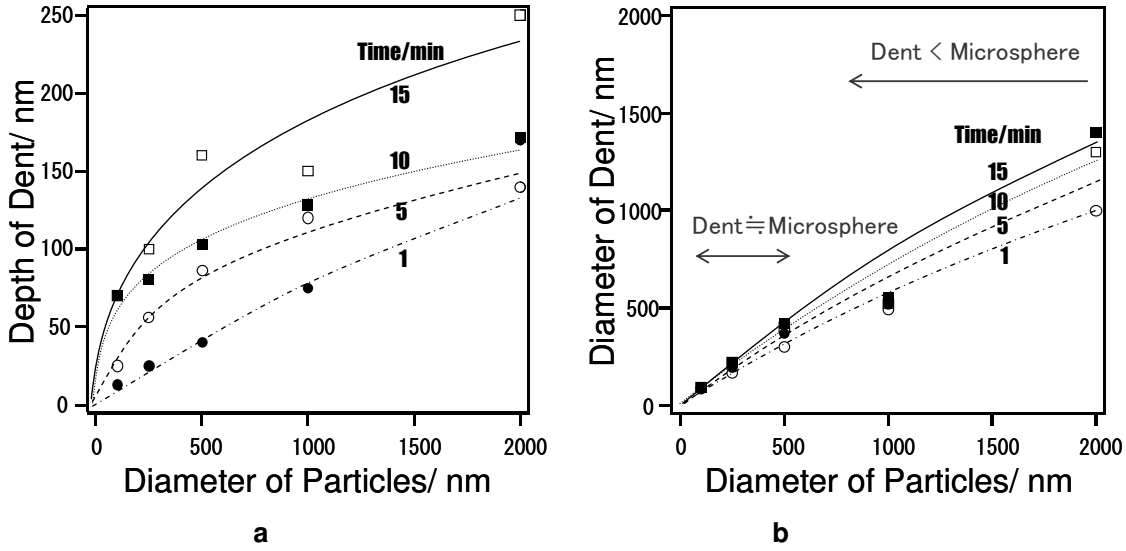

Figure 2. 6. Changes in the dent shape as functions of the particle size and the irradiation time. **a,** depth of dents. **b**, diameter of the dents. The irradiation times are 1 min (solid circle), 5 min (open circle), 10 min (solid square), 15 min (open square).

These phenomena shown in above could be ascribed to the difference in the scattering behaviour of light by the difference in the size of the PS particles. In the above experiments, the wavelength of the irradiated light was 488 nm. In this condition, the scattering behaviour changes drastically between the particle sizes of 250 nm and 500 nm in diameter.

When the particles of 505 nm and 990 nm in diameter are irradiated, the irradiated light would be focused beneath each particle because of the traditional diffraction effect. In other words, each particle acts as an optical lens. In fact, from calculations based on Mie scattering theory, it had been found that the optical field just under the particles larger than 500 nm was enhanced by several tens of times more than the irradiated light (§1.2.2).[5] Moreover, the higher intensity optical field would penetrate more deeply into the inner film. Consequently, the depth of the dent formed by the particles of 505 nm and 990 nm in diameter will be deeper than that formed by the particles of 241 nm and 98 nm in diameter. The shapes of the dents formed by linearly polarized light (Figure 2. 4. f and h, and Figure 2. 5) were similar to the shape of the dent induced by the direct irradiation with Gaussian beam, which is demonstrated by Tripathy and co-workes.[6] The polarization dependence of the dent shape strongly suggests that the surface deformation is associated with the electromagnetic field around the particles.

On the other hand, when the particles of 241 nm and 98 nm in diameter are irradiated, the particles would not diffract light and only the electromagnetic fields around the particles (the optical near field) would be enhanced (§1.2.2),[5] because the particle size is smaller than the wavelength of light. The intensity of the optical near field decays exponentially with increasing distance from the particle surface.[7] Therefore, the interaction between the optical near field of the particles and the polymer is restricted around the near-surface of the polymer, resulting in the formation of shallower dent.

Effect of the Thickness of the Polymer Film

To clarify the effect of the optical near field around the particle, the influence of the film thickness on the dent formation were examined (Figure 2. 7). In the experiment, the PS particle of 241 nm in diameter was used to avoid the optical lens effect of the particles, as described above. The film thicknesses were 90, 160, 360, 730 and 1500 nm; the

thickness was controlled by varying the rotational speed of the spin coater. Although the diameter of the dents was nearly constant for all film thicknesses, the modification depth was increased as increasing the thickness of the sample film, and the modification depth became saturated around 75 nm at the film of 360 nm in thickness. For the films of 90 nm and 160 nm in thickness, on the other hand, the modification depth was restricted to 36 nm and 45 nm, respectively. These dent structures were stable when maintained at below T_g of the polymer but could be erased by heating the polymer film above its $T_{g,.}$

The saturation value of 75 nm for the modification depth of the thick polymer film suggests that the deformation is restricted at certain extent. This might be related to the optical near field of the particles, because the effect of the electromagnetic filed around the particles is restricted around the particle surface. Meanwhile, the deformation of the thin polymer film is restricted around 40 nm. This strongly suggests that the polymer deformation is depressed at the near-interface between the glass substrate and the polymer film. A similar film thickness dependence was also reported during the formation of the surface relief grating on a thin azobenzene-functionalised polymer film by using the exposure to the interference pattern of light.[8, 9]

From these results, a mass transport process (chapter 1)[10] would be the most probable explanation for the formation of the dent structure on the surface of the polymer films. If the formation of the dent is ascribed to the ablation or chemical process, the modification depth will not be dependent on the film thickness and the dent structure could not be erased by heating. In addition, a difference in stiffness between the inside and the periphery of the formed dents were observed in the following study (chapter 3). [11] The stiffness of the inside of the dents was lower than that of the periphery of the dents. This would be strong evidence for the movement of the polymer chains from just below the PS particles to the periphery. Thus, the formation of the dent in the region of the optical near field of the particle could be ascribed to a mass transport process involving the polymer chains, and such a large-scale molecular motion would be highly restricted at the near-surface of the glass substrate.

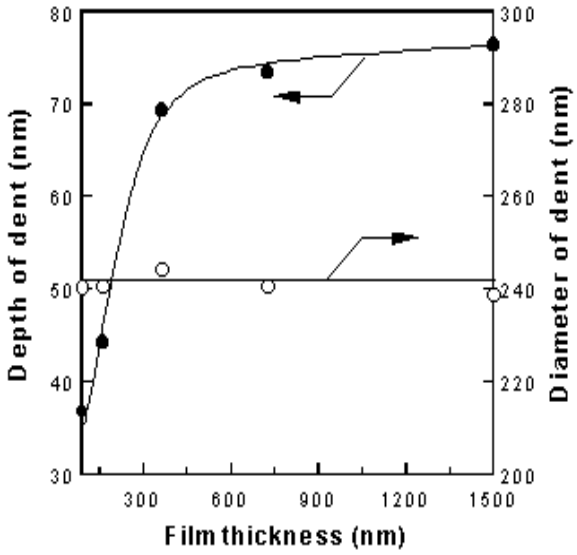

Figure 2. 7. Effect of film thickness on the achievable depth and diameter of the dent on the films of **polymer 1** irradiated with an intensity of 150 mW/cm^2 for 5 min.

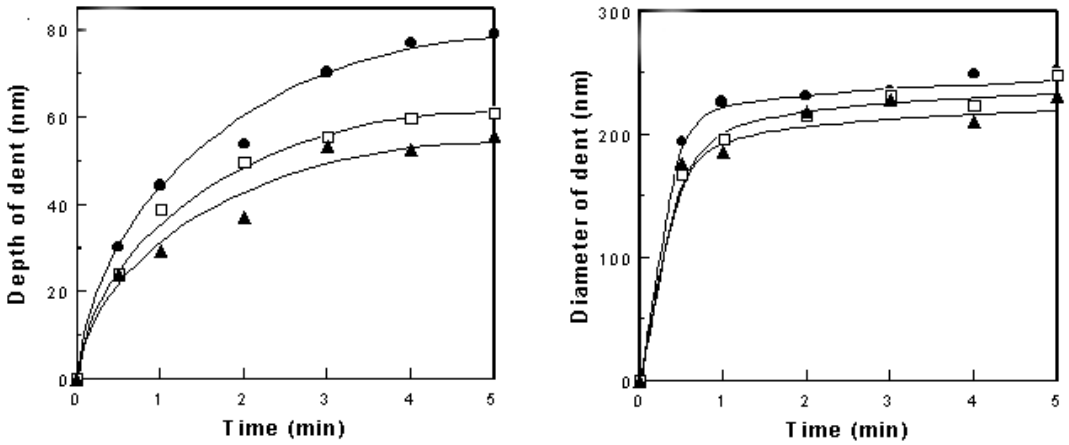

Figure 2. 8. a, Modification depth and **b**, diameter as a function of the irradiation time for polymer 2 (solid circles), polymer 3 (open squares) and polymer 4 (solid triangles).

Function of the Azobenzene Group

In the followings, the role of the azobenzene group to the dent formation is examined. It is clear that the azobenzene contributes to the formation of the dent structure on the surface of the polymer film because the dent structure could only be obtained in the azobenzene-containing polymers. For the experiment, three kinds of photo-responsive polyurethane, **polymers 2**, **polymer 3** and **polymer 4** were prepared. **Polymer 2** included the disperse red 19-type azobenzene group in the side chain, whereas **polymer 3** and **polymer 4** included azobenzene group that introduced methyl groups at their 2- and 2-, 2'- positions, respectively. The main difference between these polymers was the bulkiness of the position close to the azo group, but these polymers showed little difference in M_n, M_w, T_g and viscosity (Table 2. 1). **Polymer 2, polymer 3** and **polymer 4** exhibited similar shapes on the absorption spectra, and their maximum absorbances were at 460 nm, 460 nm and 465 nm, respectively. The absorption of these polymers at the wavelength of the irradiated light showed nearly the same values, which were $5.73\times10^4 cm^{-1}$, $5.35\times10^4 cm^{-1}$ and $5.51\times10^4 cm^{-1}$ respectively. In the following experiment, the thermal effects due to light absorption on the surface deformation behaviour could be negligible, because the absorption of these polymers at the wavelength of the irradiated light was nearly the same, and there was little difference in T_g and the viscosity of the polymers as shown in Table 1.

The irradiation time dependence on the depth and the diameter of the formed dents of **polymers 2, polymer 3 and polymer 4** are shown in Figure 2. 8. The polymer films were of similar thickness (~600 nm), which was irradiated with linearly polarized light of 150 mW/cm^2 by using the PS particles of 241 nm in diameter. The modification depth and diameter of the dent increased with increasing irradiation time, and saturated after about 5 min for all of the polymers, but there were differences in both the depth achievable and diameter of the dent between the polymers. Both values for the dents in **polymer 2** were large compared to that of the other polymers.

These results may be closely related to the difference in the photoisomerization behaviour of the azobenzene groups of each polymer. It is well known that the substitutents of azobenzene which do not influence the spectroscopic type of the azobenzene (chapter 1) do not change the isomerization yield in the solution.[12] However,

in the condensed phase, the introduction of bulky substituents onto positions close to the azo- group depresses the photochemical trans-cis isomerization cycle of the azobenzene group as a result of the decrease in the free volume around the azobenzenes.[13, 14] Specifically, the amount to which the azobenzene group undergo the photo-isomerization cycle for **polymers 3** and **4** would be less than that for **polymer 2**, which leads to the formation of a shallower dent structure.

In addition, the effect of the irradiated light energy on the behaviour of the optical surface-modification was explored by using **polymer 2** (Figure 2. 9). The sample films were irradiated with light of 488 nm in wavelength at different intensities (70 mW/cm^2 and 280 mW/cm^2) by using the PS particles of 241 nm in diameter, whilst maintaining the same overall influence of the total irradiated energy by varying the irradiation time. In spite of the fact that the irradiated energy was kept constant, the degree of modification of the depth and diameter of the dents on the sample films exposed to a higher light intensity was larger than that in the sample film exposed to lower intensity light (Figure 2. 9. a and b). A similar tendency also could be observed in **polymer 3** and **polymer 4**.

It is expected that differences in the intensity of the irradiated light would have an effect on the efficiency of the photoisomerization cycles of the azobenzene group because the amount of cis-azobenzene photochemically produced in a unit time depends on the intensity of the irradiated light. When a high intensity light was used for the exposure, a large amount of the cis-azobenzene would be produced in a unit time, leading to the establishment of effective isomerization cycles. On the contrary, irradiation with a lower intensity light would generate a lower amount of the cis-azobenzene, resulting in a decrease in the amount of the azobenzene performing the isomerization cycles. The photoisomerization cycle of the azobenzene derivatives causes a softening of the polymer films (the azobenzene group acts as a plasticiser that is activated upon photo-irradiation, chapter 1).[10] Such softening of the polymer films would allow the effective migration of the polymer chains. Therefore, such a difference in the surface modification behaviour would be due to differences in the amount of the azobenzene group undergoing the isomerization cycles.

The results shown in Figure 2. 8 and Figure 2. 9 strongly suggest that the photoisomerisation motion of the azobenzene group included in the polymer induces the

dent formation. Namely, in the initial stage, the photoisomerization cycles of the azobenzene groups must induce the softening of the polymer film. In the second stage, the polymer chains move around the PS particles. Finally, when the photoirradiation ceases, the dent structure is fixed by the cessation of the photoisomerization cycles of the azobenzene groups.

Although the photoisomerization motion of the azobenzene group and subsequent softening of the polymer matrix is believed to be the origin of the deformation, the driving force for the dent formation on the azobenzene-containing polymers is not fully understood at the present stage. Not only the contact between the particles and the polymer surface, but the electromagnetic field around the particle is considered to be one of the driving forces for the deformation of the polymer surface, because the shape of the dent is closely related to the polarization direction of the irradiated light, and it is not proportional to the shape of the particle (Figure 2. 4 and Figure 2. 5). Tripathy and co-workers proposed that the gradient of the optical electric field is the main driving force for the migration of the polymer chain.[15,16,17,18,19,20] This is one of the leading candidate for the driving force. The mechanism of the dent formation is discussed in chapter 3.

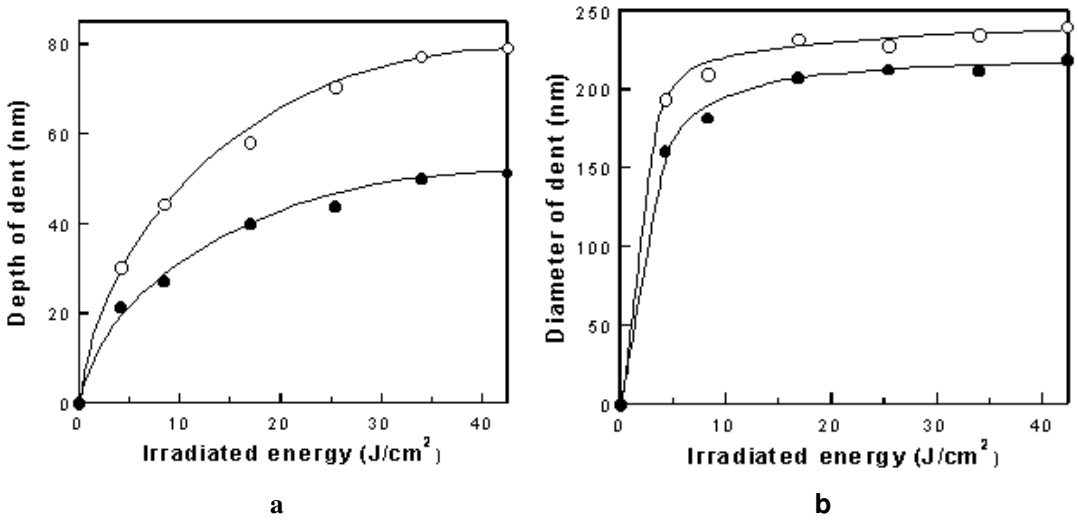

Figure 2. 9. Effect of the intensity of the irradiated light on (**a**) modification depth and (**b**) diameter of the dent on the film surface of polymer 2: solid circle = 70 mW/cm^2; open circle = 280 mW/cm^2.

2. 4. Conclusion

In chapter 2, the author studied the formation of the dent structure on the surface of azobenzene-containing polymer films by photoirradiation with the PS spherical particles ranging from 98 to 990 nm in diameter. By using this method, the dent structures with a resolution ranging from several hundreds down to tens of nanometers could be formed on the polymer surface. The size and shape of the formed dent were not proportional to that of the particles, and changed with the polarization of the irradiated light. This is considered to be due to the difference in the light scattering behaviour of the particles. The dent structure could be erased by heating the polymer above its glass transition temperature, and the modification depth was restricted for the thin polymer film. These results strongly suggests that the surface deformation of the polymer film was the migration of polymer chains induced by the optical near field around the PS spheres. The photoisomerization of the azobenzene group is considered to cause the surface deformation because the efficiency of the isomerization affected the modification depth.

2.5. Appendix I

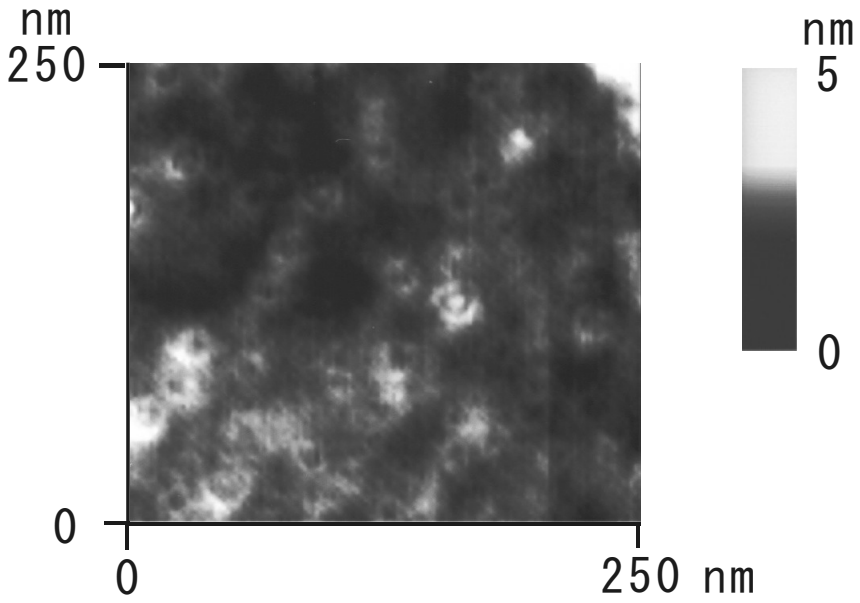

Figure 2. 10. Tapping-Mode AFM Image of **polymer 1** surface treated by the PS particles of 19 nm in diameter. The dents of around 20 nm in diameter and 2 nm in depth were observed on the polymer surface.

References

[1] O. Watanabe, T. Ikawa, M. Hasegawa, M. Tsuchimori, Y. Kawata, C. Egami, O. Sugihara, N. Okamoto. *Mol. Cryst. Liq. Cryst.*, **345**, 305 (2000).

[2] M. Hasegawa, T. Ikawa, M. Tsuchimori, O. Watanabe, Y. Kawata, *Macromolecules*, **34**, 7471 (2001).

[3] Y. Kawata, C. Egami, O. Nakamura, O. Sugihara, N. Okamoto, M. Tsuchimori, O. Watanabe, *Opt. Commun.* **6**, 161 (1999).

[4] O. Watanabe, M. Tsuchimori, A. Okada, *J. Mater. Chem.,* **6**, 1487, (1996).

[5] T. Ikawa, T. Mitsuoka, M. Hasegawa, M. Tsuchimori, O. Watanabe, and Y. Kawata, *Physical Review B*, **64**, 195408 (2001)

[6] S. Bian, L. Li, J. Kumar, D.-Y. Kim, J. M. Williams, and S. K. Tripathy, *Appl. Phys. Lett.*, **73**, 1817 (1998).

[7] M. Ohtsu, *Near-Field Nano/Atom Optics and Technology*; Springer-Verlag: Tokyo, 1998.

[8] K. Sumaru, T. Yamanaka, T. Fukuda, H. Matsuda, *Appl. Phys. Lett.* **75**, 1878 (1999).

[9] T. Fukuda, H. Matsuda, T. Shiraga, T. Kimura, M. Kato, N. K. Viswanathan, J. Kumar, S. K. Tripathy, *Macromolecules,* **33**, 4220 (2000).

[10] A. Natansohn, and P. Rochon, *Chem. Rev.*, **102**, 4139 (2002).

[11] T. Ikawa, T. Mitsuoka, M. Hasegawa, M. Tsuchimori, O. Watanabe, Y. Kawata, C. Egami, O. Sugihara, N. Okamoto, *J. Phys. Chem., B*. **104**, 9055 (2000).

[12] H. Rau, In *Photochemistry and Photophysics* ; J. F. Rabek, Ed.; CRC Press, Inc.: Boca Ruton, 1990; Vol. 2, p 119.

[13] A. Natansohn, S. Xie, P. Rochon, *Macromolecules,* **25**, 5531 (1992).

[14] M. S. Ho, A. Natansohn, P. Rochon, *Macromolecules,* **28**, 6124 (1995).

[15] Kim, D. Y.; Tripathy, S. K.; Li, L.; Kumar, J. *Appl. Phys. Lett.* **1995**, *66*, 1166.

[16] D. Y. Kim, L. Li, X. L. Jiang, V. Shivshankar, J. Kumar, S. K. Tripathy, *Macromolecules,* **28**, 8835 (1995).

[17] X. L. Jiang, L. Li, J. Kumar, D.-Y. Kim, V. Shivshankar, S. K. Tripathy, *Appl. Phys. Lett.* ***68***, 2618 (1996).

[18] J. Kumar, L. Li, X. Jiang, D.-Y. Kim, T. S. Lee, S. K. Tripathy, *Appl. Phys. Lett.* **72**,

2096 (1998).

[19] N. K. Viswanathan, S. Balasubramanian, L. Li, J. Kumar, S. K. Tripathy, *J. Phys. Chem. B.* **102**, 6064 (1998).

[20] S. Bian, J. M. Williams, D.-Y. Kim, L. Li, S. Balasubramanian, J. Kumar, S. K. Tripathy, *J. Appl. Phys.* **86**, 4498 (1999).

Chapter 3. Dynamics of Nanostructure Formation on an Azobenzene-Containing Polymer Studied by Tapping-Mode Atomic Force Microscopy

3. 1. Introduction

In chapter 3, the author explores the mechanism of the nanostructure formation on the surface of an azobenzene-containing polymer by light irradiation with a monolayer of polystyrene (PS) spherical particles. As shown in chapter 2, the nanostructure of the monolayer of the PS particles ranging from 19 nm to 990 nm in diameter can be transcribed into a topographic image on the polymer surface.[1,2,3] Based on the analysis of the surface deformation behaviour, the phenomenon is considered to be related to followings: the electromagnetic field (the optical near field) around the particles, the subsequent photoisomerization motion of azobenzene group and the mass transport of the polymer matrix. However, the overall mechanism of the phenomenon has not been clear up still now.

Regarding the surface deformation of the azobenzene-containing polymers, it is well known that a topographic relief structure on the polymer can be generated by exposure to an interference pattern from the coherent superposition of laser beams (§1.2.1).[4,5,6] In this process, the topographic changes on the polymer surface follow the intensity distribution of the electromagnetic field in the surface plane. This phenomenon has been considered to be a photo-driven mass transport effect, and various driving forces behind it have been proposed, such as internal pressure,[4] light intensity gradients[5] and intermolecular interaction.[6] However, neither the mass transport effect itself nor the nature of the driving force have been directly confirmed.

To clarify the mechanism of the nanostructure formation on the surface of the azobenzene-containing polymer, the electromagnetic fields (the optical near field) around the particles were calculated based on Mie theory (§1.2.2), and then, tapping-mode atomic force microscopy (tapping-mode AFM, §1.3.2)[3,7] was employed for analysing the mass transport on the polymer surface. In tapping-mode AFM, the cantilever oscillates vertically near its resonance frequency. As the tip is brought close to the sample's surface,

the vibrational characteristics of the cantilever (e.g., the amplitude, resonance frequency, and phase angle of oscillation) vary due to the tip-sample interaction. The factors influencing the shift in phase angle (hereafter referred to as phase shift) are capillary force, van der Waals force, and viscoelasticity. With the tip sufficiently in contact with the sample, the phase shift mainly occurs due to the viscoelasticity of the surface, and the phase image provides a map of the variation in the viscoelastic property (§1.3.2). The map of the viscoelasticity on the nanostructure should reflect the mass transport on the polymer surface.

In this chapter, the author compares the calculated intensity distributions of the electromagnetic fields around the particles ranging from 100 nm to 2000 nm in diameter for the incident light of 488 nm in wavelength to the phase images of the nanostructure formed by the particles of 98 nm and 505 nm in diameter on the polymer surface by using tapping-mode AFM. The intensity distributions of the electromagnetic fields around the particles are shown to change drastically with the sizes of the particles and the wavelength of the incident light. For the particles smaller than the wavelength of the incident light (the particles ranging from 100 nm to 250 nm in diameter), the intensity of the electromagnetic field is enhanced at the sides of the particles along the polarisation directions of the incident light. For the particles larger than the wavelength of the incident light (the particles ranging from 500 nm and over in diameter), on the other hand, the intensity is enhanced towards the forward area of the particles. (Hereafter the author refers to the particles smaller than the wavelength of the light as Rayleigh particles and particles larger than the wavelength of the light as Mie particles.) The intensity distribution does not fully correspond with the surface deformation, but suggests that the gradient force of the optical near-field deforms the surface three-dimensionally. The phase image supports the mechanism of the surface deformation on the basis of the gradient force model.

3. 2. Experimental

A urethane-urea copolymer containing pseudstilbene-type azobenzene (disperse red 19 type) was synthesised and used as the substrate (§2.2).[8] After dropping an aqueous solution of mono-dispersed PS particles onto the substrate, the water was evaporated from the solution. The particles rearranged themselves via a self-organisation process, and the sample was then irradiated with coherent light of 488 nm in wavelength from the Ar^+ laser. To rule out the influence of gravity on the deformation, all of the substrate surfaces were set aligned vertically during the exposures. Next the particles were removed from the surface by immersing in water and/or by eluting in benzene, and then finally the surface was observed by scanning electron microscopy (SEM, JEOL, JSM-890) and tapping -mode AFM (Digital Instruments, Nanoscope IIIa).[3] A commercial silicon cantilever (Nanosensor, SSS NCH8, the tip radius of curvature was about 5 nm, the cantilever length was 125 μm, the force constant was 50 N/m, and the free resonant frequency was 298 kHz) was used for tapping-mode AFM. The scan speed was 500 nm/s in tapping-mode AFM. When the sample has steep and deep dents, imaging artifacts might arise from tip convolution effects.[9,10,11] To prevent the artifacts, SEM images of the new tips chosen by random sampling were observed. Besides, the tip which could obtain the sharper images were selected and used for the AFM analysis.

The intensity distributions of the electromagnetic fields were calculated in a vacuum around PS particles ranging from 20 nm and 2000 nm in diameter using Mie's equation.[12,13] In the calculation, the refractive index of the polystyrene was taken to be 1.59, and the wavelength of incident light was 488 nm. The coordinates for the calculation is shown in Figure 3. 1. In addition, the electromagnetic field around these isolated particles on the polymer surface were calculated by using the complex refractive index of the polymer taken into account for the calculation, which is based on the interactive calculations of the extended Mie scattering theory and of plane-wave decomposition in order to include the multi-scattering between the particles and the polymer surface.[14, 15] The calculated results are shown as the intensity distribution of the electric fields.

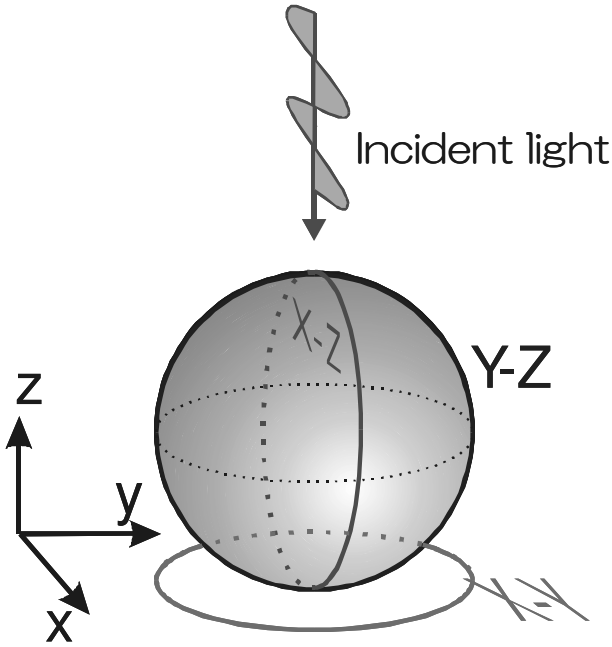

Figure 3. 1. The coordinates for the calculation of the electromagnetic field around the PS particles by using Mie's equation.

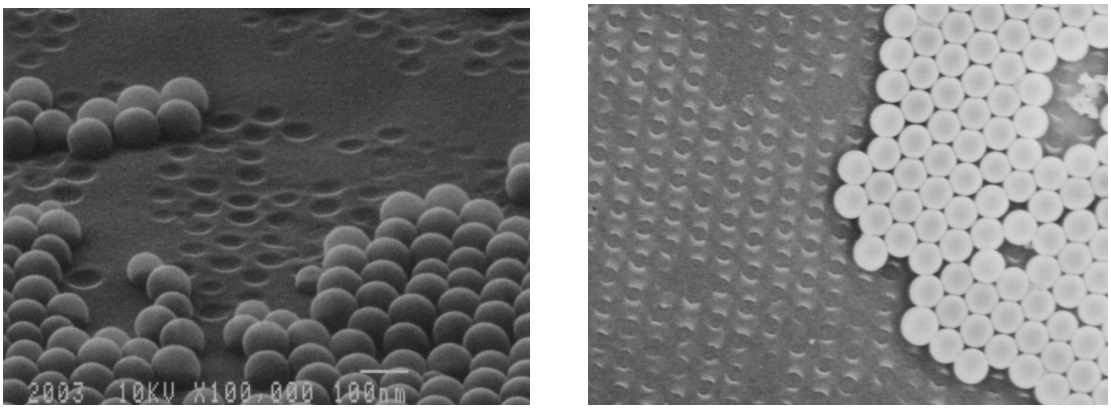

Figure 3. 2. SEM images of the azobenzene-containing polymer surface with the PS particles. **a**, particles of 98 nm in diameter (bird's eye view). **b**, particles of 505 nm in diameter (2D view). These samples were exposed to coherent light of 488 nm in wavelength and 0.5 W/cm^2 in optical power density, and then washed by sonication.

3. 3. Results and Discussions

Surface Shape Analyzed by SEM

The SEM images of the azobenzene-containing polymer surface with the 98 nm and 505 nm residual particles are shown in Figure 3. 2 a and b, respectively. These images show that the dents were formed just under the particles, regardless of the actual size of the particles. In Figure 3. 2a, the image clearly shows how the areas just under the particles were depressed while the surrounding area were raised up. In addition, the particles were embedded in the dents. In Figure 3. 2b the image shows that the dents and the residual particles were arranged hexagonally. The particles at the monolayer edge and the adjacent dents were aligned in a hexagonal arrangement; and therefore the particles located themselves on the dent.

Surface Shape Analyzed by AFM

Then, AFM was carried out for analyzing the surface shapes in detail (chapter 2). The analysis accounts for the dent formation processes practically. The sizes of the dents as a function of the exposed times are summarized in Figure 3. 3. For the particle of 98 nm in diameter, the diameter of the dent was as large as that of the corresponding particle, and was almost unchanged during the exposure (Figure 3. 3a, solid circle). For the particle of 505 nm in diameter, on the other hand, the diameter of the dent was smaller than that of the corresponding particles, and was slightly increased with the exposed time (Figure 3. 3a, open circle). The depths of the dents induced by the both particles were increased with the exposed times, and were inclined to saturate (Figure 3. 3b). The saturated depths were about 50 nm and 150 nm for the particles of 98 nm and 505 nm in diameter, respectively. It should be emphasized that the diameters of the particle and the corresponding dent were about the same even in the early stage of the dent formation (The contribution of the imaging artifacts originated from the tip convolution effect should be little because of the shallow dents.) The result represents that the surface deformation did not follow the shape of particle, the shapes of the dent and the corresponding particle were distinct from each other. The same phenomenon was observed in chapter 2 (Figure 2.6 and Figure 2.7). The facts strongly suggest that some factors other than interfacial forces such as van der Waals forces play an important role

for the surface deformation.

In these experiments, the surface deformation was believed to be essentially temperature independent. When the azobenzne-containing polymer with the particles of 98 nm and 505 nm in diameter were exposed to light with an optical power density ranging from 0.01 W/cm^2 to 0.5 W/cm^2, light of 0.01 W/cm^2 caused a dent in the same manner as the 0.5 W/cm^2 laser light with the total optical energies being the same, although the depths of the formed dents were different (chapter 2, Figure 2. 9). The PS particles, which had a glass transition temperature (T_g) of 105°C, remained unchanged during these experiment, therefore, the temperature on the surface of the substrates should be at least lower than 105°C, which is well below T_g of the azobenzene-containing polymer (145°C). By using the infrared thermometer, increasing in temperature on the polymer surface during photoirradiation of 0.5 W/cm^2 was confirmed to be at least less than 10°C from the room temperature. These results indicate that the contribution of the thermal effects to the surface deformation is low, therefore, the surface deformation of the polymer is considered to be photo-chemically induced.

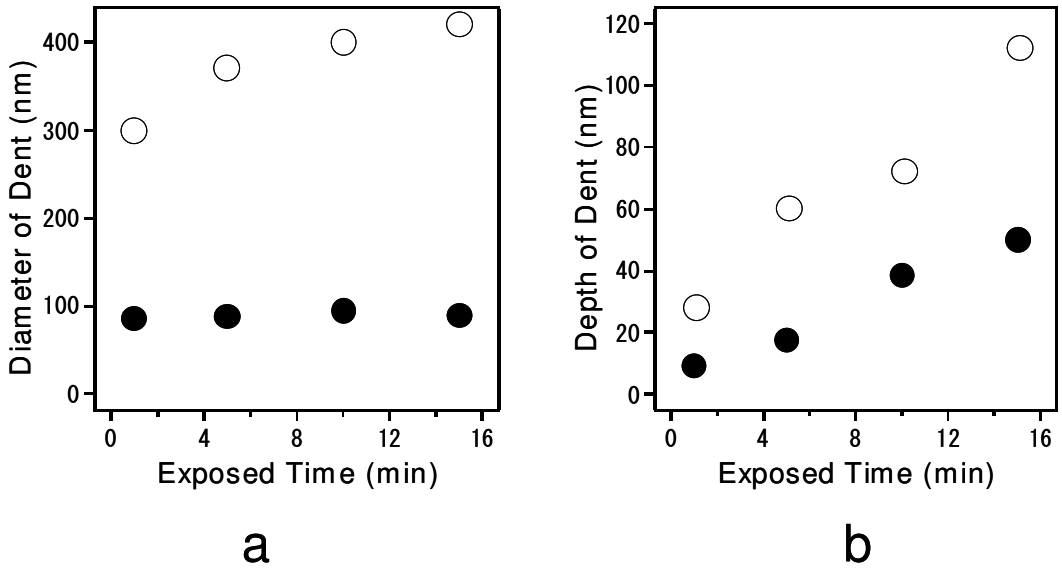

Figure 3. 3. Changes in the sizes of the dents during the exposure. **a**, diameter. **b**, depth. These samples were treated by the particles of 98 nm in diameter (solid circle) and the particles of 505 nm in diameter (open circle). The samples were exposed to light of 488 nm in wavelength and 5 W/cm^2 in optical power density.

Intenisty Distributions of the Electromagnetic Fields Around the Particles

Next, the calculated intensity distributions of the electromagnetic fields around the particles of 100 nm and 500 nm in diameter are shown as the contour lines in Figure 3. 4, with the X-Z and Y-Z planes that contain the centres of the particles. (The distributions around the particles ranging from 2000 nm to 100 nm in diameter are shown in §3.5. Appendix I). The intensity distributions change drastically with the sizes of the particles. The electromagneticl fields around the particle of 100 nm in diameter are enhanced at the sides of the particles along the polarisation directions of the incident light (Figure 3. 4a). The Rayleigh particle hardly has any focussing effect on the incident light because of the diffraction limit, but works like an electric dipole. In contrast, the electromagneticl field around the particles of 500 nm in diameter are enhanced towards the forward area of the particle (Figure 3. 4b). The Mie particle focuses the incident light because the particle works as a lens. These calculations reveal that the intensity distributions of the electromagneticl fields around the Rayleigh and Mie particles are different.

The above calculated intensity distributions around the particles in the vacuum are almost identical with that around the particles on the polymer surface; the latter is more close to the actual experimental system. The electromagneticl field around these isolated particles on the polymer surface were calculated by using the complex refractive index of the polymer taken into account for the calculation (Figure 3. 5). The calculated distributions are qualitatively equivalent to those seen in the images in Figure 3. 4. In addition, a solitary dent isolated from the rest of the arrangement was sometimes found to be formed on the surface (Figure 3. 2a). The shapes of the isolated dents are about the same as those in the regular arrangement. This suggests that it does not make much difference between the electromagnetic fields around the particles in the arrangement and the solitary particles.

Comparing the experiments with the calculations, it is found that the dent formation does not follow the intensity distribution of the electromagnetic field for the Rayleigh particles, but it does for the Mie particles. The Rayleigh particle forms dents just below the particle itself, while the intensity distribution in the surface plane is almost homogeneous. Therefore, it is necessary to take account of some factor acting on the surface besides the intensity distribution. In contrast, a Mie particle causes a dent just

below the particle, which does obey the intensity distribution in the surface plane. In the cases where there is direct exposure to the interference pattern (SRG formation)[5] and to the focused Gaussian beam,[16] the deformation follows the intensity distribution of the electromagnetic fields in the surface plane. As shown in Figure 3. 4b, the dent induced by a Mie particle is identical with one induced by direct exposure to a focused Gaussian laser beam[16], because the Mie particle acts like lens. These comparisons tell us that the surface deformation phenomenon originating from a Rayleigh particle is a special case in that there is disagreement between the surface deformation and the intensity distribution in the surface plane. Some factor beyond the intensity distribution in the surface plane must be introduced in order to elucidate the phenomenon.

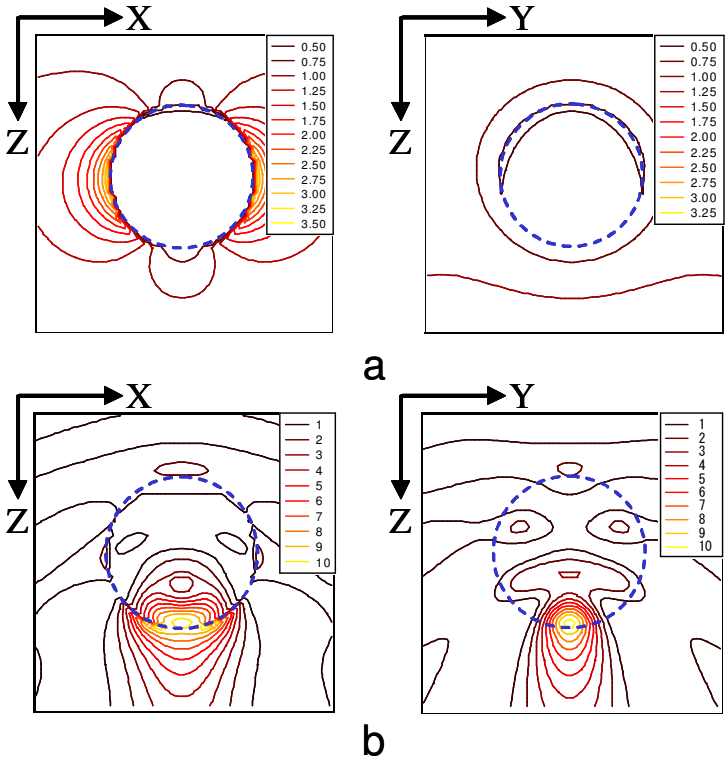

Figure 3. 4. Calculated intensity distributions of the electric fields around the particles. **a**, the particle of 100 nm in diameter. **b**, the particles of 500 nm in diameter. The left and right images show the X-Z and Y-Z planes. The direction of light propagation is along the Z-direction, and is displayed from the top to the bottom of the images. The polarization directions are parallel to the X-axis. The dotted circles represent the size of the particles. The coloured lines indicate the contour lines denoting the relative intensities to the incident light. The intensities are displayed in the legends.

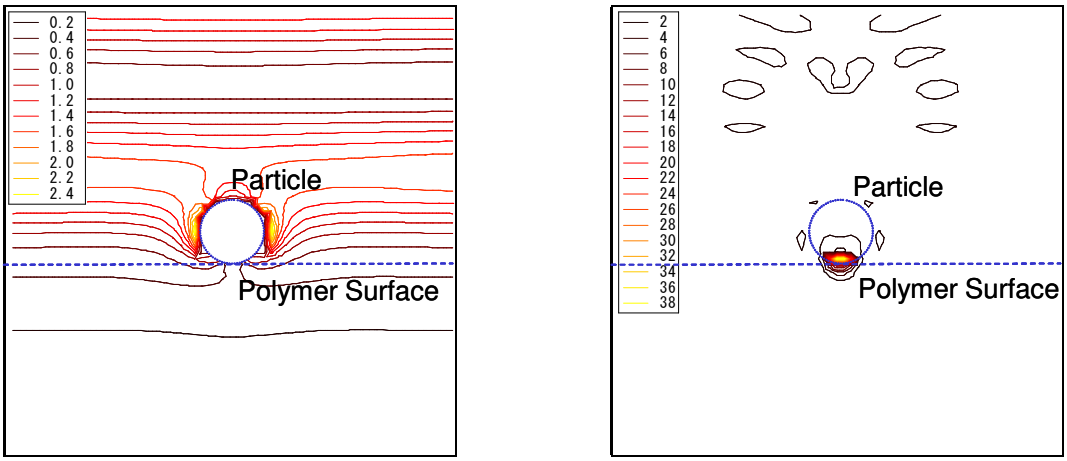

Figure 3. 5. Calculated intensity distributions of the electric fields around the particles on the azobenzene-containing polymer surface. **a**, the particle of 100 nm in diameter. **b**, the particles of 500 nm in diameter. The images show the X-Z plane. The direction of light propagation is along the Z-direction, and is displayed from the top to the bottom of the images. The polarization directions are parallel to the X-axis. The dotted circles and lines represent the size of the particles and the polymer surface. The coloured lines indicate the contour lines denoting the relative intensities to the incident light. The intensities are displayed in the legends.

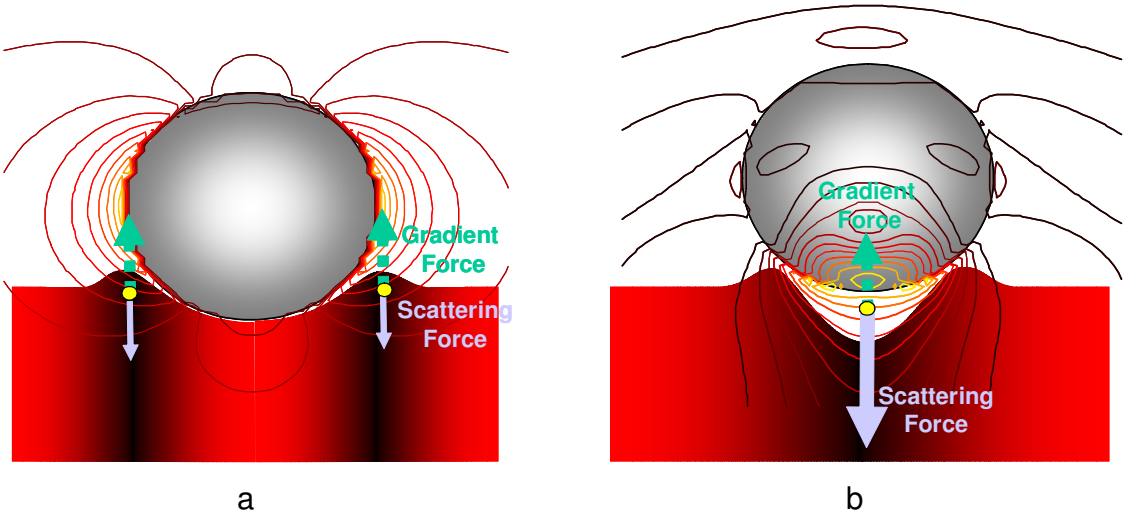

Figure 3. 6. Superposition of a cross-section of the polymer surface and the calculated intensity distribution of the PS particles. **a**, the particle of 100 nm in diameter. **b**, the particle of 500 nm in diameter. The directions of the forces are represented in the images by the arrows.

Gradient and Scattering Force around the Particles

Regarding the surface deformation induced by the Rayleigh particle, the author proposes that the mechanism originates from the three-dimensional near-field's gradient force. The proposed mechanism is outlined as follows. Firstly, the azobenzene derivatives absorb the incident light, which induces trans-cis-trans isomerisation.[17] Secondly, the isomerisation plasticises the azobenzene-containing polymer.[4,5,6] Thirdly, the gradient force of the electromagnetic field around the Rayleigh particle attracts and draws up the azobenzene-containing polymer. The direction of the gradient force is shown in Figure 3. 6 a. Concerning the gradient force, Ashkin first demonstrated the existence of the gradient force by conventional optics.[18] For the azobenzene-containing polymer surface deformation, Kumar and co-workers presented a gradient force model that originated from the intensity distribution of the electromagnetic field in the surface plane.[5, 16]

The principle of the gradient force is described as follows. Dielectric materials in a vacuum are affected by the optical electromagnetic field $\mathbf{E}=\mathbf{E_0}\exp(i\omega t)$ and $\mathbf{H}$, so that the dielectric materials receive a dynamic force $\mathbf{f}_d$:

$$\mathbf{f}_d = \varepsilon_0 \chi\left\{\nabla(\frac{1}{2}\mathbf{E}^2) + \frac{1}{\varepsilon_0}\frac{\partial \mathbf{p}_e}{\partial t}\right\} \qquad (3.\ 1)$$

where ε_0 is the electric permittivity, χ is the electric susceptibility of the dielectric material and $\mathbf{p_e} = \varepsilon_0 \mathbf{E}\times\mathbf{B}$ is the momentum of light. Dielectric materials that absorb light are often represented phenomenologically by a complex susceptibility,

$$\chi = \chi' - i\chi'' \qquad (3.\ 2)$$

corresponding to a complex permittivity $\varepsilon=\varepsilon_0(1+\chi)$. Substituting equation 3. 2 into equation 3. 1 and extracting only the real part of equation 3. 1, an equation relating to the dynamic force is obtained,

$$\mathbf{f}_d = \varepsilon_0 \chi'\left\{\nabla(\frac{1}{2}\mathbf{E}^2)\right\} + 2\pi f\chi''\mathbf{p}_e \qquad (3.\ 3)$$

where $2\pi f = \omega$. In equation 3. 3, the first and second terms are related to the gradient of the intensity of the electric field and the absorption of the dielectric material respectively.

The directions of these forces are dependent on χ. We obtain $\chi' = 1.87$ and $\chi'' = 1.10$ for the isotropic azobenzene-containing polymer at 488 nm in wavelength.

These data were calculated from the refractive index and the extinction coefficients measured by spectro-ellipsometry.[19] From the experimental data, equation 3.3 indicates that the gradient force (the first term in equation 3. 3) attracts the azobenzene-containing polymer from the region with the weaker electric field towards the stronger field, whereas the force induced by absorption (the scattering force, the second term in equation 3.3) acts parallel with the momentum of the photon.

The gradient forces and the scattering force around the particles estimated from equation 3. 3 are shown in Figure 3. 6. For the Rayleigh particle, the gradient force was found to be larger than the scattering force (380 N/m^3 and 290 N/m^3 for the gradient force and the scattering force, respectively. The calculated points and directions are indicated as arrows in Figure 3. 6 a). Thus, the gradient force around the Rayleigh particle is considered to draw up the azobenzene-containing polymer around the sides of the particles, such that a dent is formed on the surface (Figure 3. 6a). Oppositely, for the Mie paticles, the scattering force was found to be dominant (1300 N/m^3 and 1900 N/m^3 for the gradient force and the scattering force, respectively. The calculated points and directions are indicated as arrows in Figure 3. 6 b). Hence, the scattering force is considered to push the azobenzene-containing polymer into the substrate (Figure 3. 6b). In addition to these optically induced forces, the interfacial forces such as the van der Waals forces might play some part for the surface deformation. However, the surface deformation does not follow the shape of the dent as shown in Figure 3. 3 and Figure 3. 6 (chapter 2). From these results, the contribution of the optically induced forces is believed to be dominant for the surface deformation.

Change in Viscoelastic Properties Analyzed by Tapping-Mode AFM

The direction of the polymer migration was confirmed by using tapping-mode AFM (§1.3.2). The phase image during tapping-mode AFM provides a map of stiffness variations on the surface such that a stiffer region displays a more positive phase shift.[3, 7] The reason for this is that the phase shift $\Delta\Phi_0$ is approximately described as:

$$\Delta\Phi_0 \propto \sqrt{\langle A \rangle} E^* (Q/k), \qquad (3.4)$$

where <A> is the time-averaged value of the contact area, E* is the effective modulus, Q is the quality factor of a cantilever, and k is the spring constant of the cantilever. E^* is

proportional to the stiffness when the tip is much harder than the sample. In our experiments, <A> is a constant, because tapping-mode AFM was operated at room temperature and at moderate tapping setting (large A_0 and somewhat small r_{sp}). Accordingly, the phase shift is determined to be dominated by the stiffness on the surface, such that a stiffer region has a greater phase shift. The stiffness variation on the surface represents polymer migration because the area condensed by the migration becomes harder.

The tapping-mode AFM images of the surface treated by the particles of 98 nm in diameter are shown in Figure 3. 7a. The phase image shows that the insides of the dents became relatively softer (smaller phase shift) and the vicinal area became harder (larger phase shift). This result accounts for the polymer migration induced by the gradient force. If the gradient force of the optical near-field draws up and gathers the azobenzene-containing polymer chain to the sides of the particle (Figure 3. 6a), the margin and the inside of the dent become harder and softer respectively. The stiffness variation on the surfaces analyzed by tapping-mode AFM supports the proposed mechanism on the basis of the optical near-field's gradient force.

The tapping-mode AFM images of the surface treated by the particles of 505 nm in diameter are shown in Figure 3. 7b. In contrast to Figure 3. 7a the phase image shows that the insides of the dents become relatively harder (larger phase shift). This result is consistent with our proposed theory that the polymer chain is pushed into the inside of the substrate due to the scattering force. Furthermore, if the refractive index of the azobenzene-containing polymer changes with the intensity distribution of the electric field during the exposure, the χ' component in the plane of the surface might become apparently negative, as Kumar and co-workers pointed out. The azobenzene-containing polymer chains move from stronger electric field areas to the weaker areas in the surface plane due to the gradient force in the surface plane. Thus, the inside of the dent is considered to become harder.

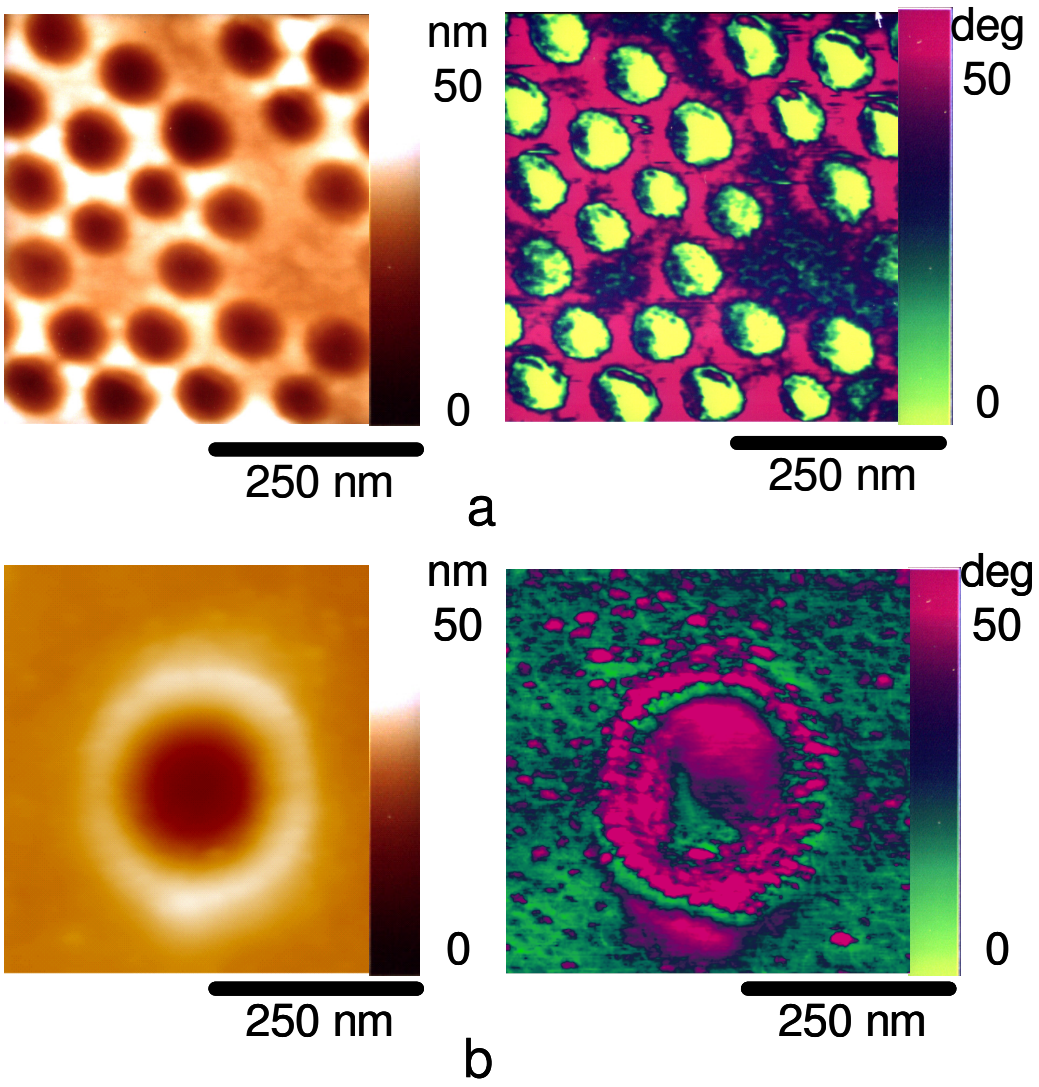

Figure 3. 7. Tapping-mode AFM images of the dent structure on the azobenzene-containing polymer surface. **a**, the dent formed by the particles of 98 nm in diameter. **b**, the dent formed by the particles of 505 nm in diameter. The left-hand and right-hand images show the topographic and phase images respectively. All of the samples were irradiated with laser light of 488 nm in wavelength and 0.01 W/cm^2 for 250 min.

3. 4. Conclusion

To explain the surface deformation of an azobenzene-containing polymer induced by light irradiation with the PS particles, the intensity distributions of the electromagnetic fields around the particles were calculated, and the distributions were compared with the viscoelastic properties of the polymer surface analyzed by tapping-mode AFM. The calculated intensity distributions around the particles of 100 nm and 500 nm in diameter were distinct from one another, and disagree with the observed deformation for the particles of 98 nm in diameter. To resolve the discrepancy, a mechanism based on the optical near-field's gradient force is proposed. Analysis of the polymer migration on the polymer surface by using tapping-mode AFM supports the proposed mechanism.

3. 5. Appendix I

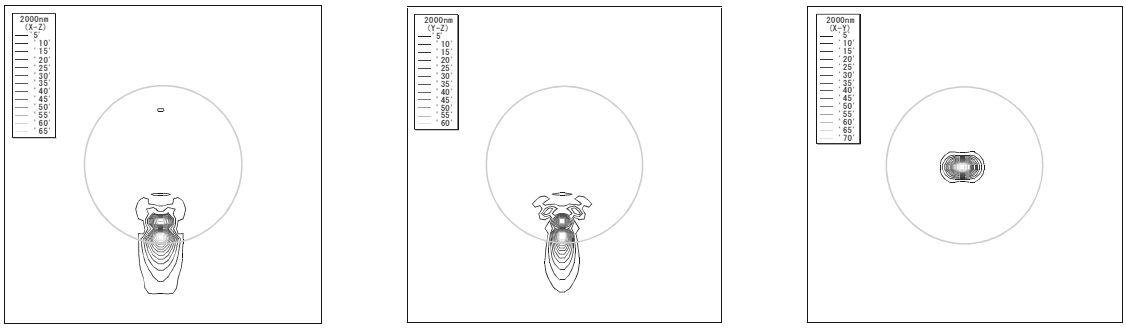

a. the PS particle of 2000 nm in diameter

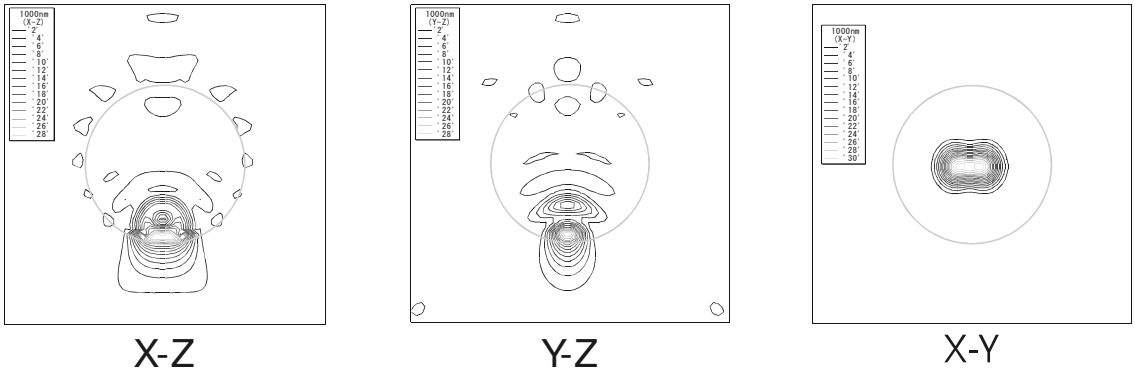

b. the PS particle of 1000 nm in diameter

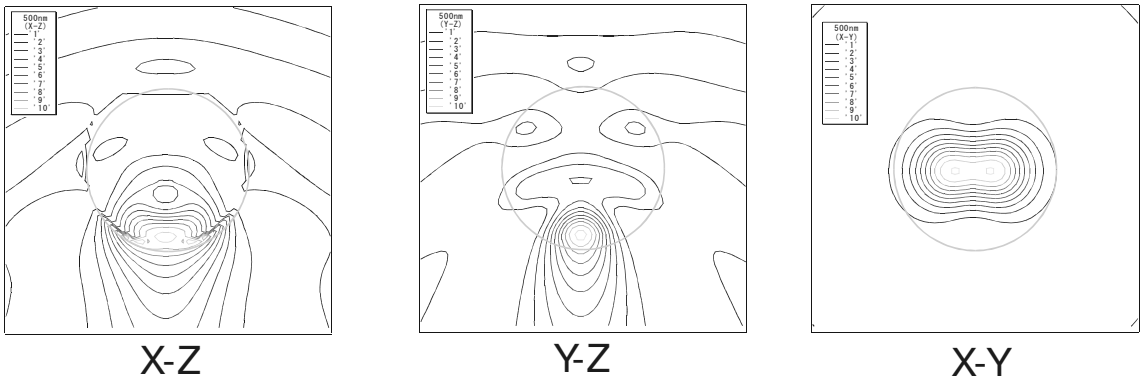

c. the PS particle of 500 nm in diameter

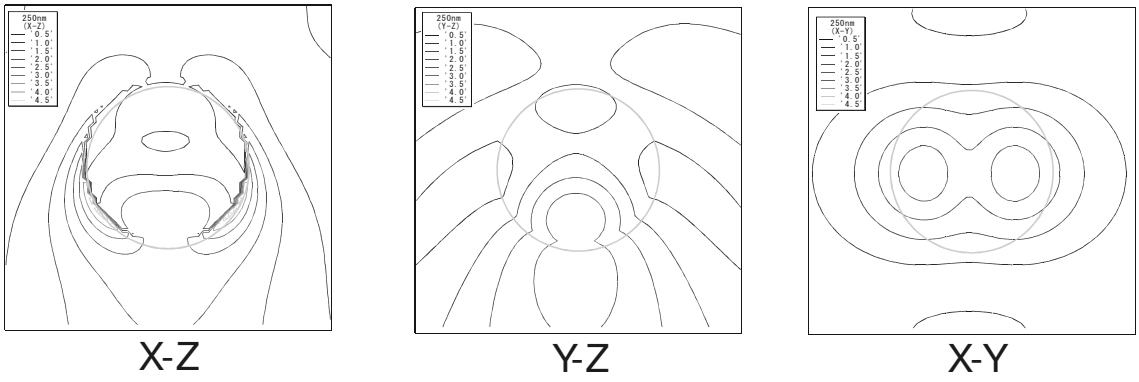

d. the PS particle of 250 nm in diameter

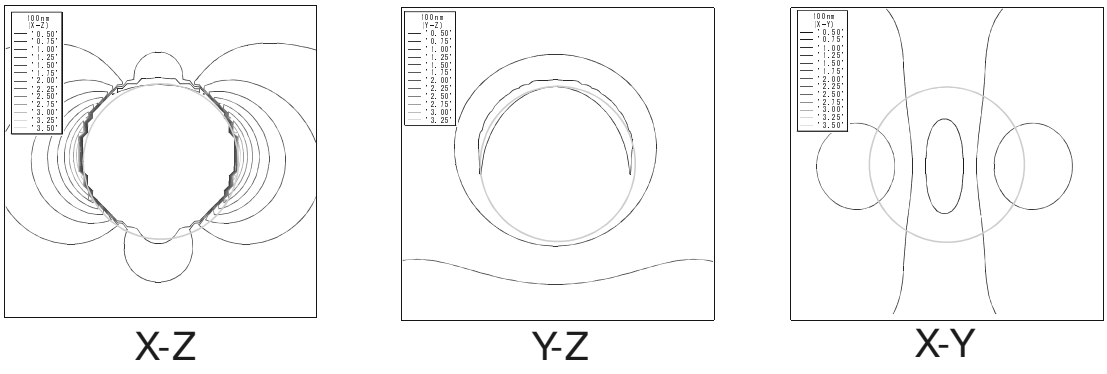

e. the PS particle of 100 nm in diameter

Figure 3. 8. The intensity distributions of the electric fields around the PS particles ranging from 2000 nm to 100 nm in diameter. The wavelength of the incident light is 488 nm. **a**, 2000 nm. **b**, 1000 nm. **c**, 500 nm. **d**, 250 nm. **e**, 100 nm. The coordinates are indicated in Figure 3. 1.

References

[1] Y. Kawata, C. Egami, O. Nakamura, O. Sugihara, N. Okamoto, M. Tsuchimori, O. Watanabe, *Optics Comm.,* **161**, 6 (1999).

[2] O. Watanabe, T. Ikawa, M. Hasegawa, M. Tsuchimori, Y. Kawata, C. Egami, O. Sugihara, N. Okamoto, *Mol. Cryst. Liq. Cryst.*, **345**, 305 (2000).

[3] T. Ikawa, T. Mitsuoka, M. Hasegawa, M. Tsuchimori, O. Watanabe, Y. Kawata, C. Egami, O. Sugihara, N. Okamoto, *J. Phys. Chem. B,* **104**, 9055 (2000).

[4] P. Rochon, E. Batalla, A. Natansohn, *Appl. Phys. Lett.*, **66**, 9 (1995).

[5] J. Kumar, L. Li, X.L. Jiang, D.Y. Kim, T. S. Lee, S. Tripathy, *Appl. Phys. Lett.*, **72**, 2096 (1998).

[6] T. G. Pedersen, P. M. Johansen, N.C.R. Holme, P.S. Ramanujam, S. Hvilsted, *Phys. Rev. Lett.,* **80**, 89 (1998)**.**

[7] S.N. Magonov, V. Elings, M.-H. Whangbo, *Surf. Sci.*, **375**, L385 (1997)

[8] O. Watanabe, M. Tsuchimori, A. Okada, *J. Mater. Chem.*, **6**, 1487 (1997)

[9] D. J. Keller, F. S. Franke, *Surf. Sci.*, **294**, 409 (1993)

[10] D. Keller, *Surf. Sci.*, **253**, 353 (1991)

[11] L. Montelius, J.O. Tegenfeldt, *Appl. Phys. Lett.*, **62**, 2628 (1993)

[12] G. Mie, *Ann. D. Physik.*, **25**, 377 (1908).

[13] M. Born, E. Wolf, *Principles of Optics*, 5th ed. (Pergamon Press, Oxford, UK, 1975), Chapter 13.

[14] W. Inami, and Y. Kawata, *J. Appl. Phys.*, **89**, 5876 (2001)

[15] W. Inami, and Y. Kawata, *J. Appl. Phys.*, **94**, 2183 (2003)

[16] S. Bian, L. Li, J. Kumar, D.Y. Kim, J. Williams, S. K. Tripathy, *J. Appl. Phys.*, **86**, 4498 (1999)**.**

[17] H. Rau, *Photochemistry and Photophysics*, *Vol. II* (CRC Press, 1990), pp. 119-142.

[18] A. Ashkin, J.M. Dziedzic, J.E. Bjorkholm, S. Chu, *Opt. Lett.* **11**, 288 (1986).

[19] O. Watanabe, M. Tsuchimori, *Polymer,* **42**, 6447 (2001).

Chapter 4. Nano-fabrication on Azobenzene-Containing Polymers Using Scanning Near-Field Optical Microscope

4. 1. Introduction

In chapter 4, the author demonstrates the nano-fabrication on an azobenzene-containing polymer by a scanning near field optical microscope (SNOM) equipped with an optical fiber probe with the submicron-sized aperture, and examines the feasibility of the ultra high-density optical recording on the polymer as a recording medium. As shown in chapter 1, the polymer has been probed to be of a progressive nature as the optical recording medium because of its dipole orientation and subsequent dichroic absorption and birefringence.[1] In chapter 2 and chapter 3, the polymer was confirmed to be capable of the nano-scale patterning on its surface using the optical near field of the submicron-sized particles.[2, 3, 4] In addition, the marks of 100 nm in diameter were achieved on the azobenzene-containing polymer by a 6 ns laser pulse.[5] The polymer is, therefore, promising for ultra high-density optical recording medium based on the optical near field beyond the diffraction limit of light.

So far, various optical recording techniques based on the optical near field, e.g., a submicron-sized aperture,[6] a solid immersion lens,[7] super-resolution technique,[8] have been proposed. In these techniques the submicron-sized aperture was shown to be capable of delivering a dramatic increase in data storage density. For example, Betzig et al. recorded the marks of 60 nm in diameter on magnet-optic materials using an optical fiber probe with a submicron-sized aperture.[6] Likewise, Hosaka et al. demonstrated the formation and observation of phase changed domains of 60 nm in diameter on a thin Ge-Sb-Te film by using the same kind of the probe.[9] In both cases, however, the recording speeds were limited to sub-milliseconds (about 10 kHz) due to the very low throughput (10^{-5}) of the optical fiber probes that were fabricated by a heating-and-pulling process. Generally, the optical fiber probe fabricated by the heating-and-pulling process has a low-tapered shape. When the probe is coupled with light, most of optical energy changes to thermal energy during the propagation in the low-tapered waveguide of the optical fiber probe. When coupled with high intensity light (more than 10 mW), the aperture will be damaged by the thermal energy. Furthermore, the heat conduction from

the probes to the recording mediums affects the mark formation.[9] Recently, Yatsui et al. demonstrated a recording and reading system using both the contact slider with a pyramidal silicone probe array and the phase-change medium.[10] Even in their system, an optical power of 200 mW was required for recording the marks at the frequency of 2 MHz. To increase the recording speed, the improvement of the throughput of the aperture is indispensable.

To achieve an actual recording and reading system using the optical near field, not only high throughput probes but also sensitive recording mediums are essential. Organic photoreactive materials including the azobenzene-containing polymer are considered to be useful memory mediums because of their high sensitivity.[11] Some groups attempted to write relief structures on the azobenzene-containing polymer surface using optical fiber probes,[12,13,14] however, the feasibility as the substrate for nanofabrication and the optical recording medium is still unclear. In this chapter, the author examines the mark formation on the azobenzene-containing polymer using the optical fiber probes with the submicron-sized apertures, and discusses the feasibility of the nanofabrication and the high-speed near-field recordings on the polymer surface

4. 2. Experimental

A urethane-urea copolymer containing pseudostilbene-type azobenzene (disperse red 19 type) was synthesized and used for the experiments (§2.2). The polymer had a molecular weight of 170,000 (relative to polystyrene), a glass transition temperature (T_g) of 145ºC and an absorption maximum of 475 nm.

The experimental setup for the nano-fabrication is illustrated in Figure 4. 1 a. An optical fiber probe with an aperture ranging from 40 nm to 100 nm in diameter (JASCO, the optical fiber probe was fabricated by selective etching techniques,[15] and the throughput of the optical power was typically 0.002 for the aperture of 100 nm in diameter) was attached to a scanning near-field optical microscope (Omicron, Twin-SNOM). All of the shape at the aperture of the optical fiber probe was checked by using scanning electron microscopy (SEM) before the experiment (Figure 4. 1 b). The distance between the probe and the polymer surface was controlled by the shear-force technique. The distance was typically around 2 nm. For controlling the distance between

the polymer surface and the optical fiber probe ranging from 10 nm to 100 nm, Z-direction of the sample stage was directly controlled without the shear-force feed back.

For the mark formation and the optical imaging, the optical fiber probe was coupled with coherent light of 488 nm or 647 nm in wavelength and 20 mW of optical power from an argon-krypton laser. The pulse duration was controlled by a combination of an optical chopper and an electro-optic modulator with a function generator. The polarization direction of the optical near field at the aperture was estimated by the far field light generated by coupling the optical near field of the aperture with glass substrate. The degree of the polarization of the far field light was around 0.7. For obtaining the optical image, light of 647 nm in wavelength was coupled with the optical fiber probe, and the intensity of light from the aperture was detected through the sample by using a x100 objective and a photon-counting system (transmittance-mode SNOM). An analyzer was inserted in front of the photon-counting system. In the experiment, the reflection-mode optical image could not be observed because the aperture was hiding by the large shoulder around the aperture (Figure 4. 1 b).

The nanofabrication on the polymer was performed as follows. First, the optical fiber probe was approached onto the polymer surface. Second, the probe was coupled with the pulsed laser light. At last, the topographic and optical image was obtained by using the corresponding optical fiber probe using the shear-force technique.

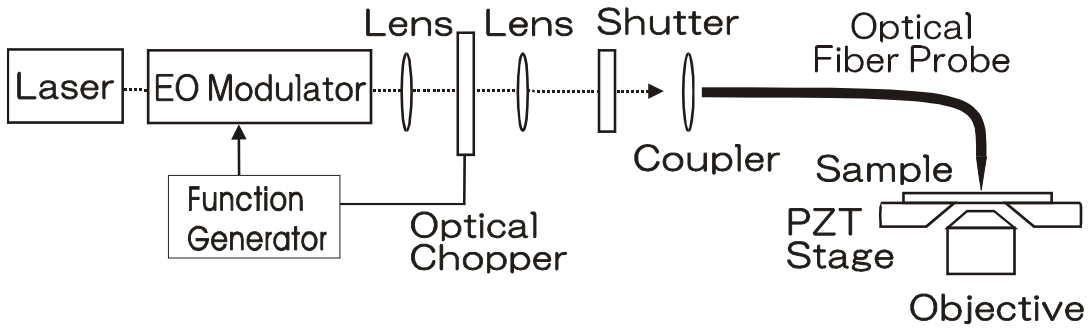

a

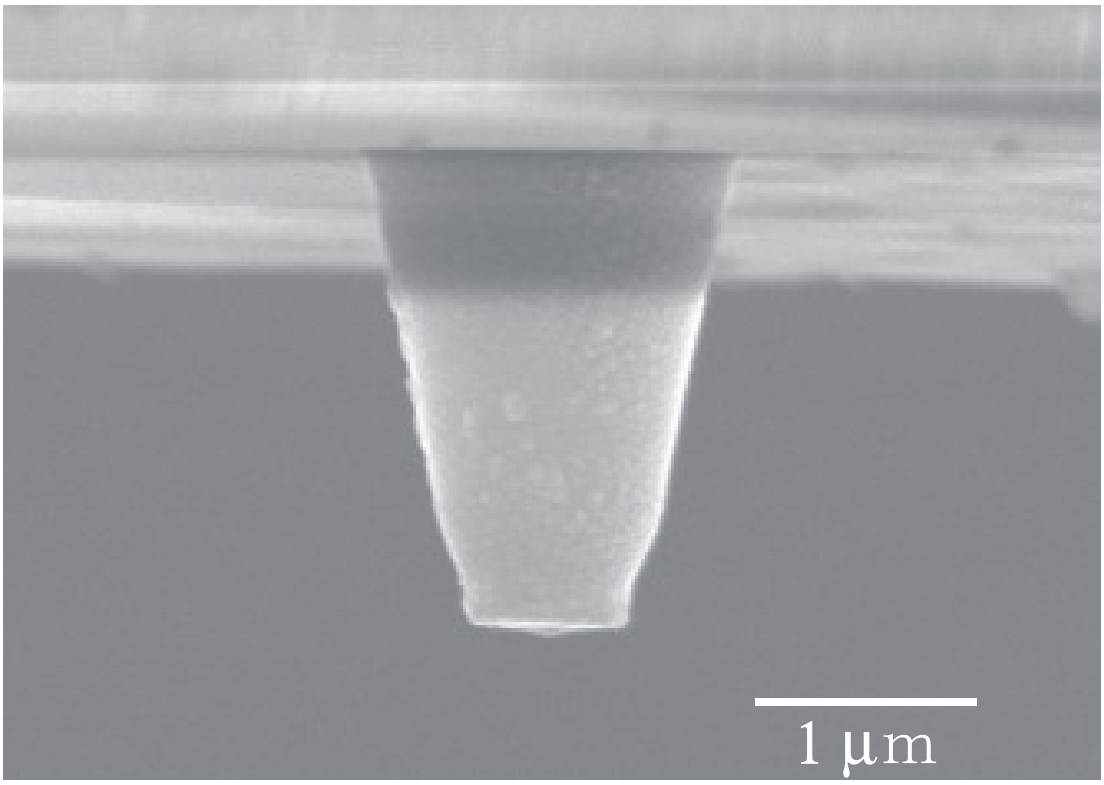

b

Figure 4. 1. a, an experimental setup for the nano-fabrication by SNOM. **b**, a SEM image of the optical fiber probe.

4.3. Results and Discussions

Polarization Dependence of the Mark on Azobenzene-Containing Polymer

Typical examples of the response of the azobenzene-containing polymer to the optical fiber probe are shown in Figure 4. 2. The experimental condition was as follows: linearly or circularly polarized light was coupled with the optical fiber probe with the aperture of 110 nm in diameter, the distance between the polymer surface and the aperture was 2 nm, the estimated optical power intensity at the aperture was 3 kW/cm^2, and the pulse duration was 250 ms. When the linearly polarized light was coupled with the optical fiber probe, a two-humped mark was formed on the polymer surface (Figure 4. 2 a). The humps were lined along the polarization direction at the aperture. The distance between the two humps were 200 nm, and the total size of the mark was 400 nm in diameter and 15 nm in height. When the polarization plane of the coupled light was rotated by 45 degrees to the left, the resulting marks was also rotated by 45 degrees to the left (Figure 4. 2 b). When circularly polarized light was coupled to the optical fiber probe, the doughnut-shaped mark was formed (Figure 4. 2 c). These results clearly show that the shape of the mark was different from the shape of the aperture of the optical fiber probe, reflecting the polarization of light coupled to the optical fiber probe.

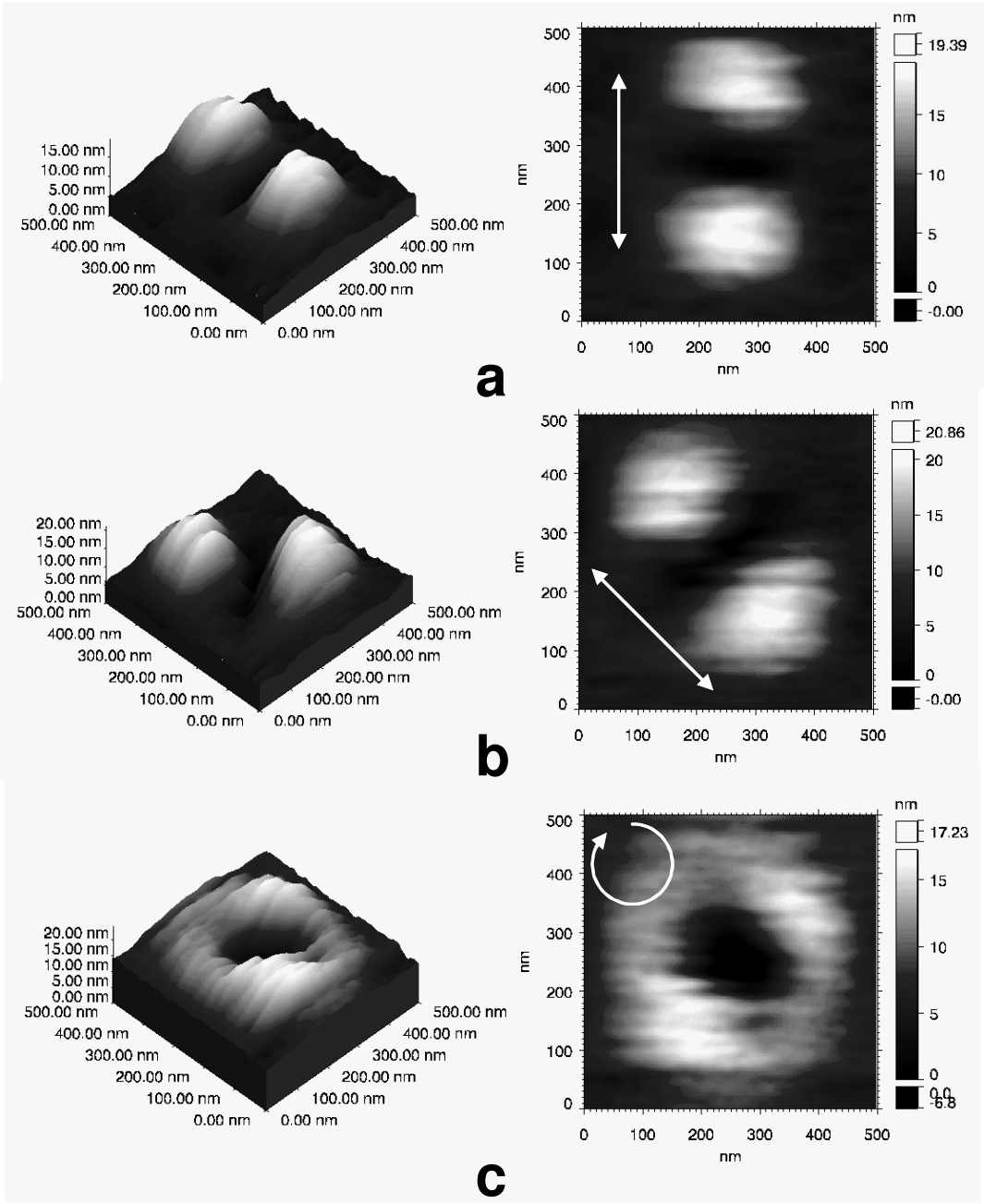

Figure 4. 2. Topographic images of the marks formed on the azobenzene-containing polymer surface by using the optical fiber probe with the aperture of 110 nm in diameter. The estimated optical power density at the aperture was 3 kW/cm^2 and the exposed time was 250 ms. **a** and **b**, linearly polarized light were coupled with the optical fiber probe. **c**, circularly polarized light was coupled with the optical fiber probe. The polarization directions were indicated by arrows.

Effect of the Optical Power Density on the Mark Formation

In the mark formation on the azobenzene-containing polymer surface, there is a close relationship between the light intensity and the pulse duration. To achieve the mark formation by a short second light pulse, high optical power is essential. In this section, the influence of the optical power on the mark formation was examined. Changes in the mark shape with the pulse duration are shown in Figure 4. 3, Figure 4. 4, and Figure 4. 5. These images represents the pit formation process.

For the light pulse of 250 kW/cm^2 in optical power density at the aperture (the optical fiber probe was coupled with 20 mW light), the doughnut-shaped mark was formed by the coupled light with any polarization. The mark of 150 nm in diameter and 2 nm in height was formed by a pulse duration of 50 ns (Figure 4. 3 a). No pit was observed for the pulse duration of less than 50 ns. With increasing the pulse duration to 250 ns, the size of the mark increased to 300 nm in diameter and 10 nm in height (Figure 4. 3 b). The cross-sections of the marks show that the height of the rim of the mark increased with increasing the pulse duration whereas the distances between the rims remained almost unchanged (Figure 4. 3 b). The distances between the rims were corresponded to the aperture of 100 nm in diameter.

Then, the nanostructure was constructed on the polymer surface by using the optical fiber probe. Figure 4. 3 d shows the two-dimensional topographic image of the polymer surface irradiated by the optical fiber probe with the light pulse of 250 kW/cm^2 and 125 ns. The marks of about 200 nm in diameters were generated on the polymer surface. The shape of each mark was about the same. This indicates that the aperture of the optical fiber probe was not damaged in this experimental condition.

For the light pulses of 112 kW/cm^2 and 1.5 W/cm^2 in optical power density, on the other hand, two-humped marks were formed on the polymer surface and the humps were lined along the polarization direction (Figure 4. 4 and Figure 4. 5). The diameters of the marks were 100 nm for the pulse of 112 kW/cm^2 and 5 μs, and 400 nm for the pulse of 1.5 W/cm^2 and 2 s. From these experiments, it is confirmed that the mark size was decreasing with increasing optical power density at the aperture.

From the above experiments, the formation of the mark was found to be strongly influenced by the optical power density. Figure 4. 6 summarizes the result of the mark

formation. As increasing the optical power density of the light pulse to 250 kW/cm^2, the marks could be formed by the hundredth lower energy (Figure 4. 6 a), and the formed mark became smaller (Figure 4. 6 b) and become polarization-independent shape. This nonlinearity for the mark formation strongly suggests that the mechanisms of the mark formation are not the same ones, and that thermal deformation plays an important role for the mark formation in the case of 250 kW/cm^2.

In the above experimental condition, especially the light pulse of 250 kW/cm^2, it seems possible that the pits were formed by heat conduction from the optical fiber probe to the polymer surface due to the increased temperature at the probe during coupling with the high power light.[9] However, this possibility is negligible because no pit was formed by the light pulse of 25 μs, 647 nm in wavelength, and 250 kW/cm^2 in optical power density; light of 647 nm in wavelength is not absorbed by the polymer. In these experiments, the aperture of the probe was not damaged by the high optical power light pulse, and the temperature at the tip should be kept below the glass transition temperature (114°C) of the polymer. From these experiments, the mark formations in Figure 4. 3, Figure 4. 4 and Figure 4. 5 are considered to be the photoinduced phenomena.

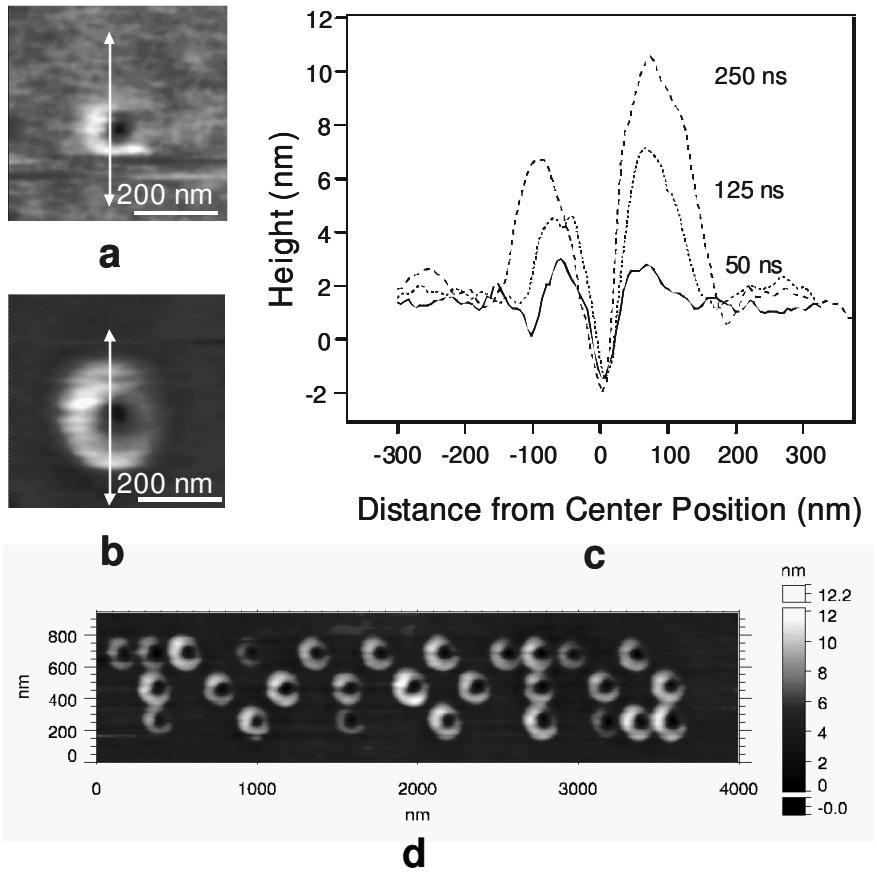

Figure 4. 3. Topographic images of the marks formed on the azobenzene-containing polymer surface by using the optical fiber probe with the aperture of 110 nm in diameter. The estimated optical power density at the aperture was 250 kW/cm^2. **a** and **b**, the marks formed by the light pulses of 50 ns and 250 ns, respectively. Arrows show the polarization direction, which is measured by far field light. **c**, the cross sections of the marks formed by the light pulses of 50 ns, 125 ns, and 250 ns. **d**, the marks formed on the polymer surface by the light pulses of 125 ns.

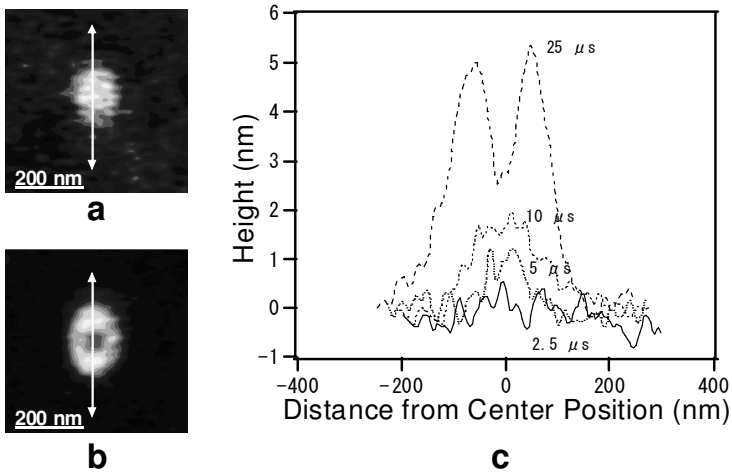

Figure 4. 4. Topographic images of the marks formed on the azobenzene-containing polymer surface by using the optical fiber probe with the aperture of 110 nm in diameter. The estimated optical power density at the aperture was 112 kW/cm^2. **a** and **b**, the mark formed by the light pulses of 10 μs and 25 μs, respectively. Arrows show the polarization direction, which is measured by far field light. **c**, cross sections of the marks formed by the light pulses of 2.5 μs, 5 μs, 10 μs and 25 μs. The cross sections are along the polarization direction, as shown in **a** and **b** as arrows.

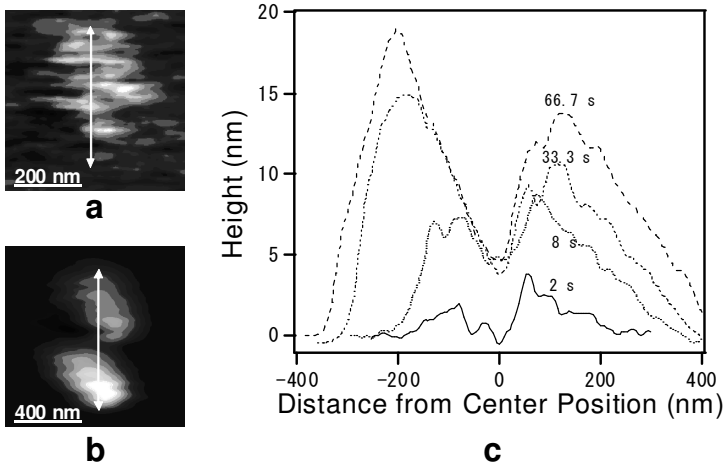

Figure 4. 5. Topographic images of the marks formed on the azobenzene-containing polymer surface by using the optical fiber probe with the aperture of 110 nm in diameter. The estimated optical power density at the aperture was 1.5 W/cm^2. **a** and **b**, the mark formed by the light pulses of 2 s and 66.7 s, respectively. Arrows show the polarization direction, which is measured by far field light. **c**, cross sections of the marks formed by the light pulses of 2 s, 8 s, 33.3 s, and 66.7 s. The cross sections are along the polarization direction, as shown in **a** and **b** as arrows.

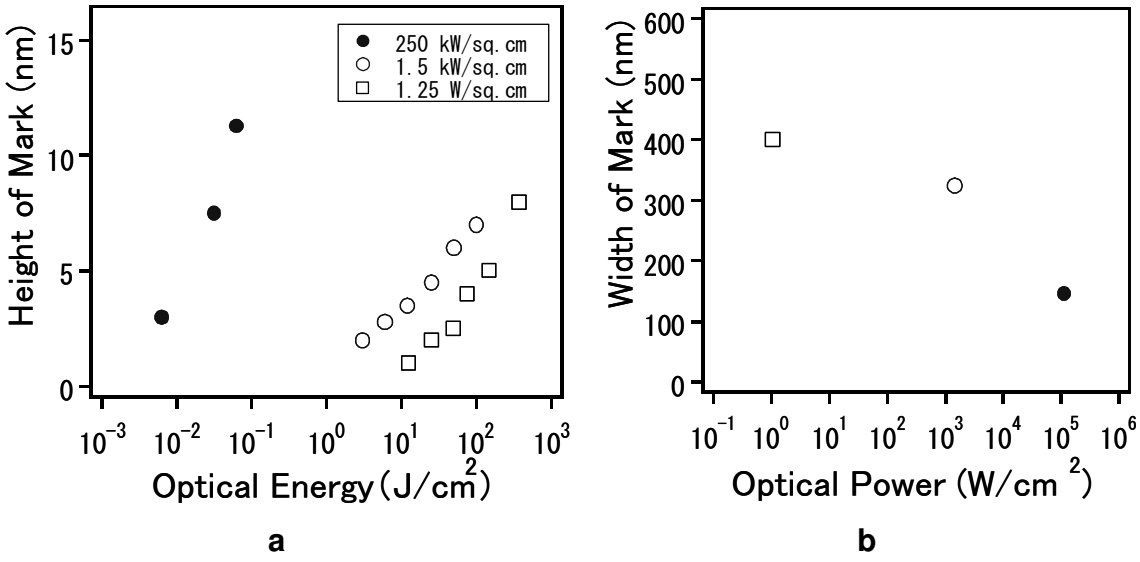

Figure 4. 6. Change in the mark size as a function of the optical power density at the aperture of the optical fiber probe (110 nm in diameter). **a**, the heights of the marks. **b**. the diameters of the smallest marks with the pulses of 1.25 W/cm^2, 1.5 kW/cm^2 and 250 kW/cm^2.

Influence of the Aperture Size on the Mark Formation

An important objective in nanofabrication and optical recording is to reduce the mark size. For achieving the minimal mark size, the optical fiber probe with the smallest aperture of 40 nm in diameter was examined. The mark formation processes induced by light pulses of 200 kW/cm^2 and 1.5 W/cm^2 in optical power density are shown in Figure 4. 7 and Figure 4. 8, respectively. (200 kW/cm^2 was the limitation in the experimental set up.) In both cases, two-humped marks were formed on the polymer surface and the humps were lined along the polarization direction (Figure 4. 7 and Figure 4. 8). For the light pulse of 200 kW/cm^2, the smallest mark of 90 nm in diameter was formed by the pulse duration of 10 μs (Figure 4. 7). The mark size was slightly smaller than the smallest mark formed by the aperture of 110 nm in diameter (In Figure 4. 4, the smallest mark was 100 nm in diameter). For the light pulse of 1.5 W/cm^2, the mark of 300 nm in diameter was formed by the pulse duration of 2 s (Figure 4. 8). The mark size was clearly smaller than the mark formed by the aperture of 110 nm in diameter at the same optical power density (In Figure 4. 5, the size of the mark was 400 nm in diameter).

The relationship between the sizes of the aperture and the corresponding mark on the polymer surface are summarized in Figure 4. 9. The mark size changed with the optical power density and the aperture size. The influence of the optical power density was dominant for the mark formation; the light pulse of the higher optical power (more than 10^5 W/cm^2) forms the half-sized mark compared to the lower optical power (less than 10^3 W/cm^2). Also, as decreasing the aperture size, the corresponding mark size was decreased. The smallest mark size was around 90 nm in diameter by using the optical fiber probe with the aperture of 40 nm in diameter.

In the above experiment, the smallest mark sizes and the aperture size did not correspond one-to-one. This result is partly due to the imaging artifacts for topographic imaging.[16] The contour line reported by topography sometimes can be quite different from the true contour line of the mark due to the tip-sample convolution effect. The imaging artifact becomes dominant when the objective size become close to the tip size. Considering the imaging artifacts, the mark size of 90 nm, which is imaged by the aperture of 40 nm in diameter, was reconstituted to around 40 nm in diameter as true size.

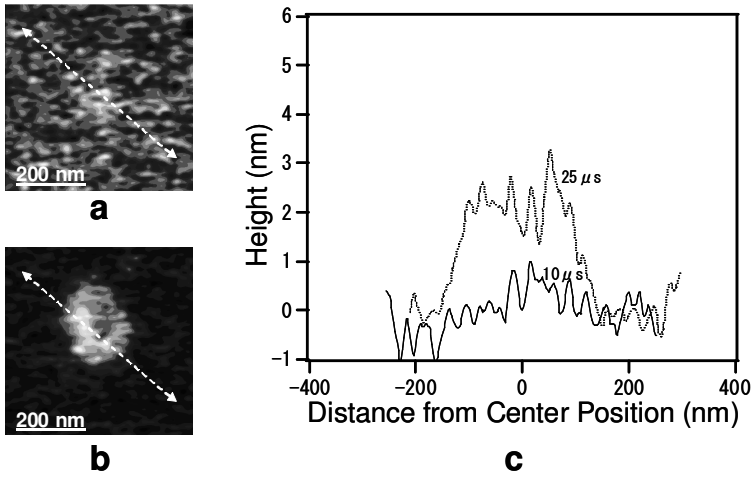

Figure 4. 7. Topographic images of the marks formed on the azobenzene-containing polymer surface by using the optical fiber probe with the aperture of 40 nm in diameter. The estimated optical power density at the aperture was 200 kW/cm^2. **a** and **b**, the mark formed by the light pulses of 10 μs and 25 μs, respectively. Arrows show the polarization direction, which is measured by far field light. **c**, cross sections of the marks formed by the light pulses of 10 μs and 25 μs. The cross sections are along the polarization direction, as shown in **a** and **b** as arrows.

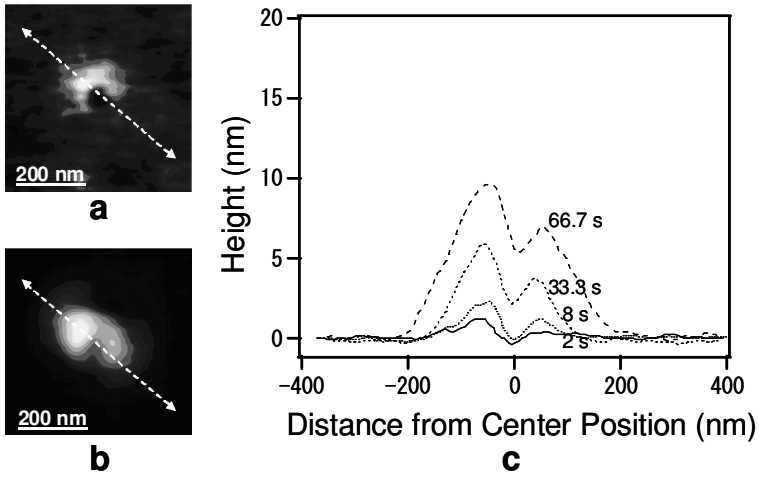

Figure 4. 8. Topographic images of the marks formed on the azobenzene-containing polymer surface by using the optical fiber probe with the aperture of 40 nm in diameter. The estimated optical power density at the aperture was 1.5 W/cm^2. **a** and **b**, the mark formed by the light pulses of 2 s and 66.7 s, respectively. Arrows show the polarization direction, which is measured by far field light. **c**, cross sections of the marks formed by the light pulses of 2 s , 8 s, 33.3 s, and 66.7 s. The cross sections are along the polarization direction, as shown in **a** and **b** as arrows.

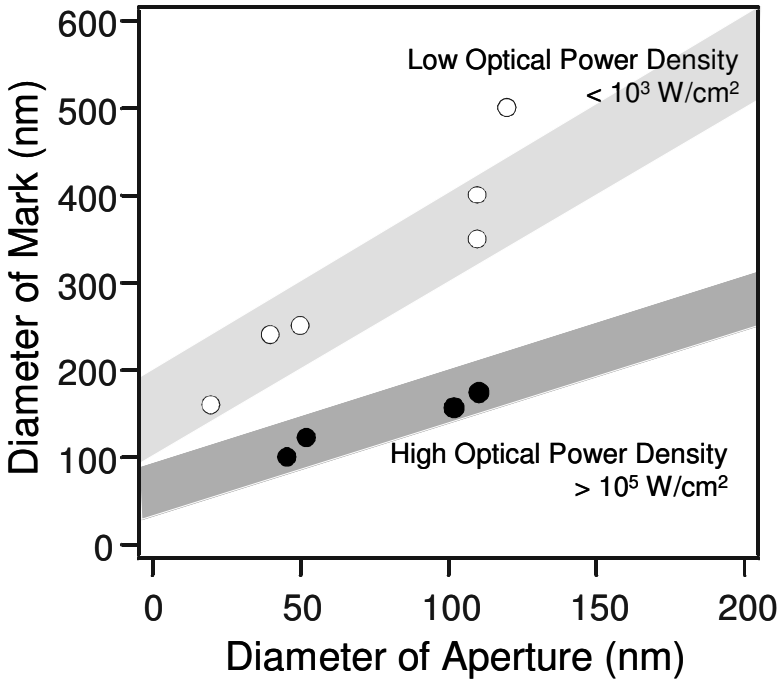

Figure 4. 9. The relationship between the aperture size and the corresponding smallest mark size. Solid and open circles show the mark formed by the light pulse of high optical power density (>10^5 W/cm^2) and low optical power density (< 10^3 W/cm^2).

Influence of the Distance between the Optical Fiber Probe and the Aperture

The intensity of the optical near field at the aperture of the optical fiber probe is believed to decay quickly with a distance (§1.2.2). Hence, an understanding of the influence of the distance between the aperture and the polymer surface on the mark size is important for the analysis of the mark formation mechanism and the utility of nanofabrication and optical recording. The influence was confirmed by changing the aperture-surface distance and the aperture size. Figure 4. 10 and Figure 4. 11 show the results obtained by varying the distance between the polymer surface and the apertures of 40 nm and 100 nm in diameter, respectively. In both apertures, two humped marks were formed. The heights of the formed marks were decreased with increasing the distance between the polymer surface and the aperture. For the aperture of 40 nm in diameter, the mark was not formed at the distance around 100 nm, whereas, for the aperture of 100 nm in diameter, the mark was formed at the distance more than 100 nm. In both cases, the diameters of the marks were almost the same by changing the distance. These results clearly indicate that the marks on the polymer surface were formed by the optical near field of the aperture because the intensity of the optical near field exponentially decays with the distance (chapter 1). Also, the results suggest that the intensity distribution of the aperture of 40 nm in diameter decayed more quickly than the aperture of 100 nm in diameter.

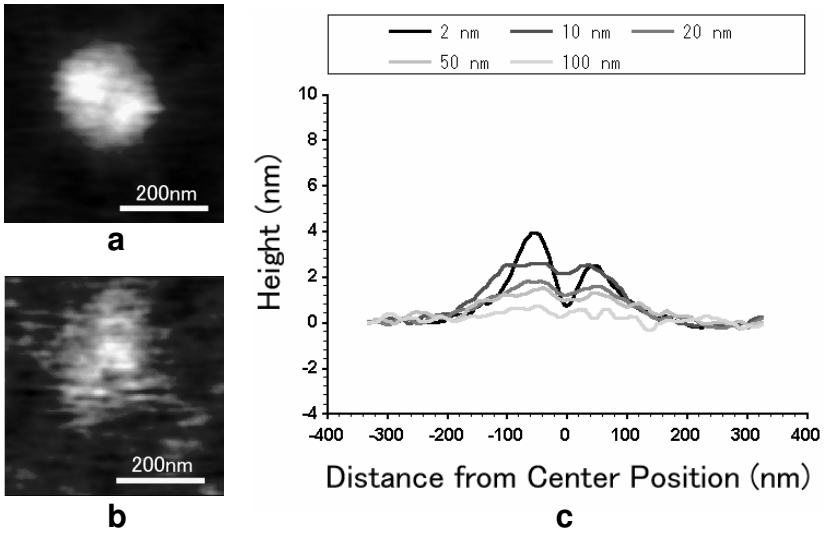

Figure 4. 10. Change in the shape of the azobenzene-containing polymer surface exposed to the optical fiber probe with the aperture of 40 nm in diameter as a function of the distance between the polymer surface and the aperture. The estimated optical power density at the aperture was 1.5 kW/cm^2 and the pulse duration was 8 ms. **a** and **b**, the marks formed at the distances of 10 nm and 100 nm, respectively. **c**, cross sections of the marks at various distances. The cross sections are along the polarization direction.

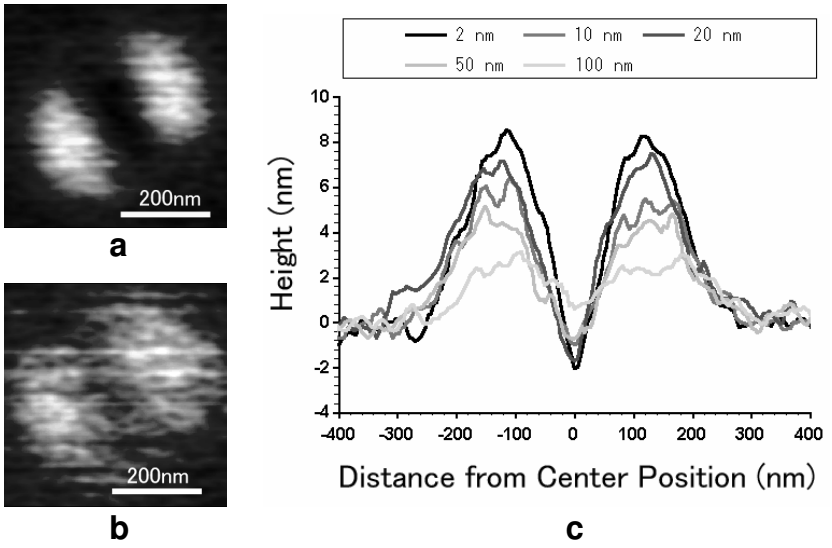

Figure 4. 11. Change in the shape of the azobenzene-containing polymer surface exposed to the optical fiber probe with the aperture of 100 nm in diameter as a function of the distance between the polymer surface and the aperture. The estimated optical power density at the aperture was 1.5 kW/cm^2 and the pulse duration was 8 ms. **a** and **b**, the marks formed at the distances of 10 nm and 100 nm, respectively. **c**, cross sections of the marks at various distances. The cross sections are along the polarization direction.

SNOM Image of the Mark on the Azobenzene-Containing Polymer Surface

By using transmittance-mode SNOM, transmittance optical images of the mark formed on the polymer surface were observed (Figure 4. 12). In these experiments, the topographic and optical images of the same mark were observed at the same scan. The optical images were found to be different from the topographic images. By using cross nicols detection in optical imaging, the humps observed in the topographic image became darker and the center of the mark became bright (Figure 4. 12 a and b). By using open nicols detection, the similar optical image was observed with the slight difference being observed (Figure 4. 12 c and d). The observed difference between the optical images at open and cross nicols suggests that the birefringence was induced during the mark formation.

At the present stage, it is not clear the reason why the contrast in the optical image was generated because the optical image obtained by SNOM sometimes contains an imaging artifact generating from the z-motion of the aperture for maintaining the constant gap between the sample and the aperture.[17] The artifacts will be reduced by using the constant height mode without Z-motion of the aperture.

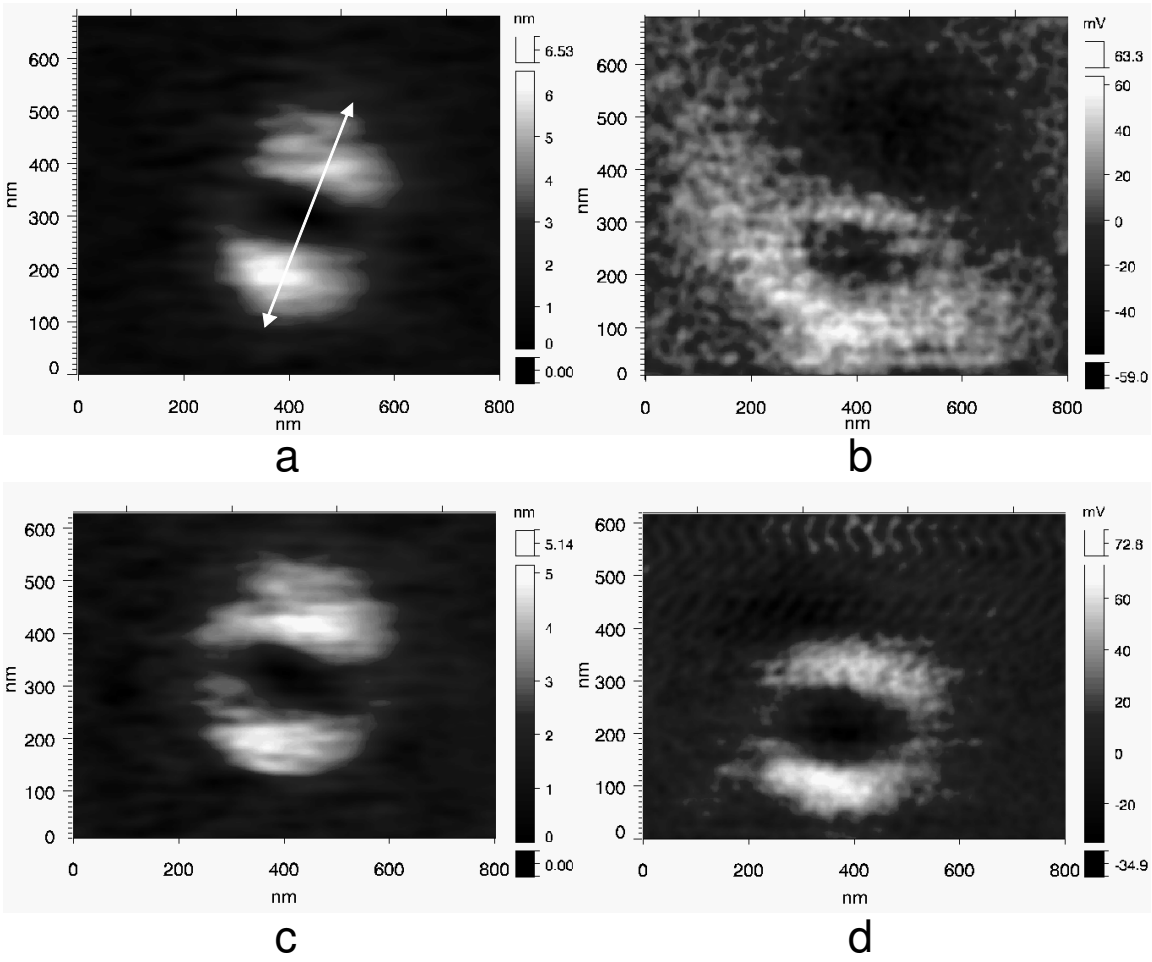

Figure 4. 12. SNOM images of the marks formed on the azobenzene- containing polymer surface by using the optical fiber probe (100 nm in diameter). The directions of the polarization for the mark formation (light of 488 nm in wavelength) and the optical detection (light of 647 nm in wavelength) were the same and were indicated in the figure. **a** and **b,** topographic and optical images at the same scan. For the optical detection, an analyzer was inserted in front of the detector as its polarization direction being perpendicular to the polarization direction at the aperture (cross nicols). **c** and **d.** a topographic and a optical image of the mark same as **a** and **b**. An analyzer was inserted in front of the detector as its polarization direction being parallel to the polarization dierction at aperture (open nicols).

The Mark Formation Mechanism

In the above experiments, when the optical fiber probe was coupled with the low power light pulse, the formed mark showed the anisotropic shape (Figure 4. 5 and Figure 4. 8). In contrast, when the optical fiber probe was coupled with the high power light pulse, the shapes of the mark were circularly symmetric (Figure 4. 3). These results strongly suggest that the mark formation mechanism changes with the optical power.

For the low optical power light pulse, the shape of the formed mark is considered to reflect the electromagnetic field around the aperture of the optical fiber probe. Generally, it is known that the photoinduced surface deformation of the azobenzene-containing polymer is closely related to the polarization of the incident light when the optical power of the incident light is low enough to neglect both the photochemical reactions (e.g., degradation, cross-linkage and bleach) and the evolution of the heat.[18] In chapter 2, the dent structure formed by photoirradiation with the PS particles also shows anisotropic shape reflecting the electromagnetic field around the particles. For the mark formation by the optical fiber probe, the electromagnetic field around the aperture also plays an important role.

Regarding the electromagnetic field around the aperture, Novotny and co-workers have used the multiple multipole method into the field distribution of the optical fiber probes near the sample surface.[19, 20] In their results, large electric field enhancement was observed near the rim of the aperture along the polarization direction. Some other groups reported the similar results.[6,15] These calculations coincide with the surface deformation model based on the near field's gradient force which is proposed in chapter 3. In chapter 3, the gradient force of the optical near field was shown to draws up the azobenzene-containing polymer toward the stronger electric field area. Likewise, in Figure 4. 4, Figure 4. 5, Figure 4. 7 and Figure 4. 8, two humps were formed and aligned along the polarization direction. Comparing the mark shape with the calculated electric field around the aperture, the polymer surface was drawn up towards the stronger field area at the rims of the aperture (Figure 4. 13).

For the high power light pulse, on the other hand, the evolution of the heat is considered to contribute to the mark formation. Thus far, several models such as back pressure due to material ablation[21] and surface tension gradient correlated with the

temperature distribution[22] were proposed for describing the mark formation on the optical recording medium by a direct exposure to laser pulse. In the back pressure model, the ablation process is essential. Concerning the possibility of the ablation process in the experiment, the laser fluence of 1 J/cm^2, corresponding to 20 MW/cm^2 optical power density, is needed for inducing ablation on the polymer surface.[5] Hence it is believed that no ablation occurred in our experiments. In addition, the photochemical reactions such as linkage and degradation might not be caused, because the formed marks can be erased by the direct exposure to light of 488 nm in wavelength. In the surface tension model, the surface tension variation due to the evolution of the heat at the surface causes the mass transportation, and then, the mark with a rim around the depression is formed. In the experiment shown in Figure 4. 3, the mark shape showed the large rim and the mark can be erased by direct exposure to light, suggesting the deformation was the mass transport process. Accordingly, the surface tension variation due to the evolution of the heat at the surface, followed by the absorption of light, should be the origin of the mark formation for the high power light pulse.

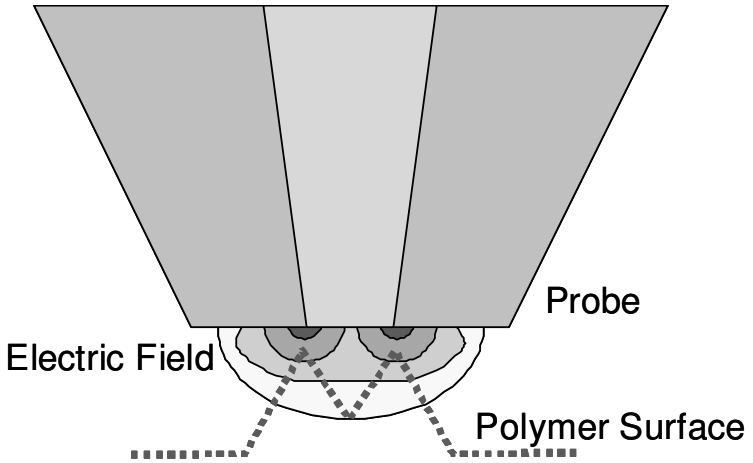

Figure 4. 13. Illustration of electric filed around the aperture of the optical fiber probe and the shape of the formed mark by the low optical power light pulse.

The Feasibility of the Optical Recording System

In the above experiment using the optical fiber probe and the azobenzene-containing polymer, the mark of 150 nm in diameter was formed by the optical near field of 250 kW/cm^2 and 50 ns pulse. The formed mark could be observed by the same optical fiber probe, although imaging artifacts should be included in the image. These results correspond to the recording density of 30 Gbit/Inch^2 and the recording speed of 20 MHz, which can be achieved by laser light of 20 mW. Comparing with the preceding reports in §4.1, it is confirmed that the polymer is sensitive, but slightly lower memory density.

The optical reading of the formed mark is suggested to be difficult because the contrast of the mark in the SNOM image was small and imaging artifacts should be included. Assuming that the contact slider equipped with the small aperture will be used for recording and reading the mark on the polymer surface, and that the flying height of the contact slider will be maintained at about 10 nm to 20 nm[71], the optical contrast might be enhanced because the imaging artifact is reduced.[19]

4. 4. Conclusion

The nanofabrication on the surface of the azobenzene-containing polymer by using the optical fiber probe with the aperture ranging from 40 nm to 100 nm in diameter was demonstrated. The shape of the formed mark on the polymer surface varied with the optical power density, suggesting that the mark generation mechanism changed with the optical power density. At low optical power density ($<10^3$ W/cm^2), two humps were formed along the polarization direction, with the smallest mark size being around 200 nm, which was 4 times larger than the aperture size. Comparing the mark shape and the electric field around the aperture, the mark is considered to be formed by the near field gradient force mechanism. At high optical power density ($>10^5$ W/cm^2), on the other hand, the circular symmetric mark was formed with the smallest mark size being 100 nm in diameter. The mark shape suggests that the surface tension variation due to the evolution of the heat at the surface is the origin of the mark formation. By using the optical near-field of 250 kW/cm^2 and 50 ns pulse, the mark of 150 nm in diameter was formed, corresponding to the recording density of 30 Gbit/Inch^2 and the recording speed of 20 MHz.

References

[1] T. Todorov, L. Nikokova, and N. Tomova, *Appl. Opt*., **23**, 4588 (1984).

[2] Y. Kawata, C. Egami, O. Nakamura, O. Sugihara, N. Okamoto, M. Tsuchimori, and O. Watanabe, *Optics Communications,* **161**, 6 (1999).

[3] T. Ikawa, T. Mitsuoka, M. Hasegawa, M. Tsuchimori, O. Watanabe, Y. Kawata, C. Egami, O. Sugihara, and N. Okamoto, *J. Phys. Chem.*, **104**, 9055 (2000).

[4] T. Ikawa, T. Mitsuoka, M. Hasegawa, M. Tsuchimori, O. Watanabe, and Y. Kawata, *Phys. Rev. B.*, **64**,195408 (2001).

[5] O. Watanabe, T. Ikawa, M. Hasegawa, M. Tsuchimori, and Y. Kawata, *Appl. Phys. Lett.*, **79**, 1366 (2001).

[6] E. Betzig, J.K. Trautman, R. Wolfe, E.M. Gyorgy, and P.L. Finn, *Appl. Phys. Lett.*, **61**, 142 (1992).

[7] B.D. Terris, H.J. Mamin, and D. Rugar, *Appl. Phys. Lett.*, **65**, 388 (1994).

[8] J. Tominaga, T. Nakano, and N. Atoda, *Appl. Phys. Lett,* **73**, 2078 (1998).

[9] S. Hosaka, T. Shintani, M. Miyamoto, A. Hirotsune, M. Hirotsune, M. Terao, M.Yoshida, K. Fujita, and S. Kammer, *Jpn. J. Appl. Phys.*, **35**, 443 (1996).

[10] T. Yatsui, M. Kourogi, K. Tsutsui, M. Ohtsu, and J. Takahashi, *Opt. Lett.*, **25**, 1279 (2000).

[11] T. Tsujioka, Y. Shimizu, and M. Irie, *Jpn. J. Appl. Phys.*, **33**, 4A, 1914 (1994).

[12] S. Davy, and M. Spajer, *Appl. Phys. Lett.*, **69**, 3306 (1996).

[13] B. Vohnsen, and S.I. Bozhevolnyi, *Appl. Opt.*, **38**, 1792 (1999).

[14] T. Fukuda, K. Sumaru, T. Kimura, H. Matsuda, Y. Narita, T. Inoue, and F. Sato, *Jpn. J. Appl. Phys.*, **40**, L900 (2001).

[15] M. Ohtsu, ed., Near-*Field Nano/Atom Optics and Technology*, Springer-Verlag, Tokyo, 1998.

[16] D. Keller, *Surface Science*, **253**, 353 (1991).

[17] C. E. Jordan, S. J. Stranick, L. J. Richter, R. R. Cavanagh, *J. Appl. Phys.* **86**, 2785 (1999)

[18] S. Bian, L. Li., J. Kumar, D.Y. Kim, J. Williams, and S.K. Tripathy, *Appl. Phys. Lett.,* **73**, 1817 (1998).

[19] L. Novotny, D. W. Pohl, and P. Regli, *J. Opt. Soc. Am. A*, **11**, 1768 (1994).

[20] R. C. Dunn, *Chem. Rev.*, **99**, 2891 (1999).

[21] J. J. Wrobel, A.B. Marchant, and D.G. Howe, *Appl. Phys. Lett*., **40**, 928 (1982).

[22] G. M. Blom, *J. Appl. Phys.,* **54**, 6175 (1983).

Part II Immobilization of Nano-Scale Particles on Azobenzene-Containing Polymers by Nanostructure Imprinting

Chapter 5. Molecular-Shape Imprinting and Immobilization of Biomolecules on Azobenzene-Containing Polymers

5.1. Introduction

In chapter 5, the author demonstrates a novel technique for the noncovalent immobilization of nano-scale particles including biologically-derived macromolecules (biomolecules) by using an azobenzene-containing polymer. The principle of this technique is represented in Figure 5. 1; the polymer surface is deformed along contours of nano-scale particles during photoirradiation, effectively immobilizing the particles without any chemical modification. This finding was brought from the previous studies using polystyrene (PS) particles, which was presented in chapter 2 and chapter 3 (Figure 5. 2).[1,2,3,4] In the course of these studies, the PS particles on the surface of the azobenzene-containing polymer were found to be immobilized after photo-irradiation. The particles were effectively sustained on the deformed surface of the polymer as shown in Figure 5. 2 b. In a similar way, biomolecules such as deoxyribonucleic acid (DNA) and proteins were found to be immobilized on the polymer surface only by photoirradiation.

Biomolecules are extremely diverse in their physical sizes, chemical and structural properties. Efficient immobilization of various biomolecules is a key aspect of many applications including microarray technologies,[5,6] cell adhesion[7,8] and biotechnology in general.[9,10,] Functions of the biomolecules are susceptible to physical and chemical surface properties and nanotopography of the substrate, as such interfacial forces effect a nanoscale change in molecular shape and structure.[11, 12, 13] The first problem to be overcome is the tendency for biomolecules to denature on contact with the substrate surfaces. Extensive approaches have been developed, using either covalent attachment or noncovalent affinity binding.[9] The covalent coupling process can achieve stable coupling, but it needs complexity and cost of derivation steps, and limited sites for attachment leads to shorter lifetime. On the other hand, the noncovalent affinity binding process is the simplest approach to the immobilization but it tends not to be stable, and activity of biomolecule is often lost in time-dependent structural changes.[11] Recent study for the noncovalent affinity binding process has been directed toward the selective adsorption of biomolecules using nanopatterned surfaces [14 , 15 , 16] and/or molecularly imprinted

polymers[17,18] so as to hold the 3-dimensional structure of the biomolecules. However, these approaches have met with limited success due to their complicated chemical processes and the often expensive facilities required for nanofabrication. The present technique using the azobenzene-containing polymer offers a promising way for the immobilization of biomolecules, because various biomolecules can be held on the polymer surface, keeping their shapes as they are, in a simple process.

In this chapter, nano-scale particles including both deoxyribonucleic acid (DNA) and proteins are shown to be immobilized on the surface of the azobenzene-containing polymer only by photoirradiation. Atomic force microscopy (AFM) reveals that the polymer surface deforms along the contour of the nano-scale particles and physically holds them upon photo-irradiation. Immunological and enzymatic studies presents that proteins immobilized on the polymer surface retained their original functionality. Based on these studies, the potential of this technique for biological applications is discussed.

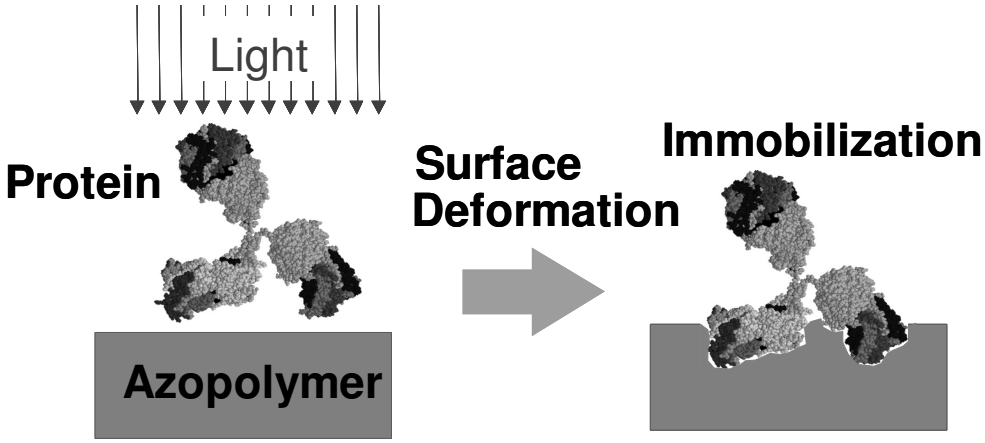

Figure 5. 1. A schematic illustration of molecular-shape imprinting and immobilization on an azobenzene-containing polymer.

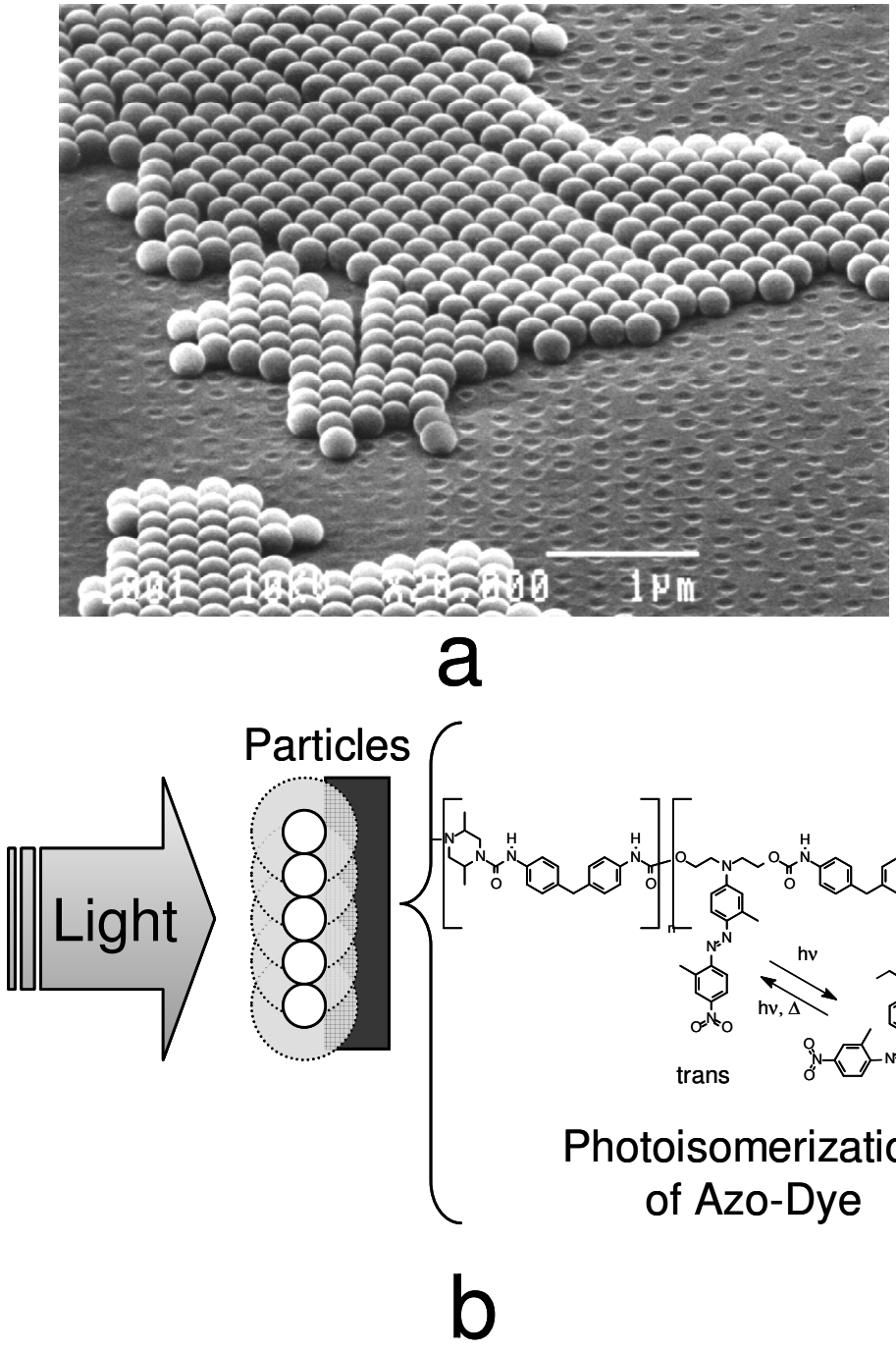

Figure 5. 2. The surface deformation of an azobenzene-containing polymer by small particles. **a**, A SEM image of the polymer surface covered with 250 nm polystyrene particles. **b**, A photoisomerization motion of an azobenzene group.

5.2. Experimental

Materials

Two kinds of azobenzene-containing polymers were used. A urethane-urea copolymer containing pseudostilbene-type azobenzene (disperse red 19 type) was synthesized (§2.2) [1-4] and used for the experiments in Figure 5. 2, , Figure 5. 3 and Figure 5. 4. The polymer had a molecular weight of 170,000 (relative to polystyrene), a glass transition temperature (T_g) of 145ºC and an absorption maximum of 475 nm in wavelength. Contact angles of water and ethylene glycol to the polymer were 83º and 58º, respectively. Changes in the absorption spectrum and the contact angles cannot be detected before and after photoirradiation with light from a 5x10 arrays of blue light emitting diodes (LEDs, Toyoda Gosei, 10 mW/cm^2 in optical power density) for 1 hour. Poly{4'-[[[2-(methacryloyloxy) ethyl]ethyl] amino]-4-cyanoazobenzene-co-methyl methacrylate} (15 mol% azobenzene group) was obtained by free-radical polymerization and used for the experiments in Figure 5. 5, Figure 5. 6 and Figure 5. 7. The polymer had a molecular weight of 25,000, a T_g of 102ºC and an absorption maximum of 447 nm in wavelength. Contact angle of water and ethylene glycol to the polymer were 75º and 53º, respectively. Changes in the absorption spectrum and the contact angles cannot be detected before and after photoirradiation with light from the LEDs. The azobenzene-containing polymer films of 50 nm in thickness were prepared on amino-conjugated glass slides by spin coating from a pyridine solution.

Four kinds of materials were examined for the photo-immobilization on the azobenzene-containing polymer, monodisperse PS particles (1 μm in diameter, 10 wt% in aqueous solutions, Duke Scientific), λ-DNA (48 k b.p., Wako Chemicals), immunoglobulin G (IgG, 150 kDa, Cosmo Bio) and a bacterial protease (Subtilisin Carlsberg, 27.5 kDa, Sigma).

Photo-Immobilization

Photopatterning of PS particles, λ-DNA and IgG were demonstrated. For the photopatterning of PS particles, after forming a monolayer of PS particles with 1 μm in diameter on the azobenzene-containing polymer surface, the specimen was irradiated with a linear-shaped laser beam of 488 nm in wavelength and 10 mW/cm^2 in optical

power density using a cylindrical lens for 5 minutes. The surface was cleaned by sonication for 5 min, and then was observed by a conventional optical microscope.

For the photopatterning of λ-DNA, an aqueous solution of 1 mg/mL λ-DNA (λ-DNA was stained with fluorophore (YoYo-1 iodide, Molecular Probe), in advance) was spotted on the azobenzene-containing polymer surface and covered with a cover glass. The surface was then irradiated with the same linear-shaped laser beam for 5 min. The surface was washed for 5 min in an aqueous solution, and then was observed by a conventional fluorescence microscope.

For the photopatterning of IgG, an aqueous solution of 0.1 mg/mL fluorophore (Cy5)-linked IgG was penetrate into a gap of 50 μm between the azobenzene-containing polymer surface and a photo mask, and then the surface was irradiated with incoherent light from the LEDs for 30 minutes. After washing the surface with an aqueous solution containing a nonionic surfactant (polyoxyethylene sorbitane alkyl ester, Tween 20), the fluorescence was detected using a confocal microscope (Affymetrix 428 array scanner).

AFM Study

Changes in the azobenzene-containing polymer surface topography with λ-DNA and IgG before and after photoirradiation were probed by atomic force microscopy (AFM). Mean roughnesses (R_a) of the bare azobenzene-containing polymer surfaces were around 0.6 nm, being about the same before and after photo-irradiation without those biomolecules.

In case of λ-DNA, an aqueous solution of 1 mg/mL λ-DNA was spin-coated onto the azobenzene-containing polymer surface and then the surface was irradiated with laser light of 488 nm in wavelength and 10 mW/cm^2 in optical power densities for 10 min. The surface was observed by contact-mode AFM (Digital Instruments Nanoscope E) and a silicon nitrite cantilever (the typical tip radius of curvature is 15 nm, Nanoworld).

In case of IgG, 1 μL of a phosphate buffered saline solution (PBS) containing fluorophore (Cy5)-linked IgG was spotted on the azobenzene-containing polymer surface. After evaporating the solution, the surface was irradiated with light from the LEDs for 30 min, and then the surface was washed for 30 min with PBS containing 0.01 wt% Tween20 as a nonionic surfactant. The amount of the immobilized IgG was confirmed by

the fluorescence intensity of the spot. The fluorescence intensity increased linearly with the concentration of IgG in the spotting solution (e.g. Figure 5. 7a) and saturated around 2 μg/mL. Under this condition, the area density of IgG on the spot was about 2.5 ng/mm^2, corresponding to the amount calculated for a close-packed monolayer of IgG. For the AFM experiments, the spotting solution containing 0.5 μg/mL IgG was selected, so as to avoid the formation of the multilayer. The surface image was obtained by tapping-mode AFM (Digital Instruments, Dimension 3100) and a sharp silicon cantilever (the tip radius of curvature is under 5 nm. Nanoworld). The azobenzene-containing polymer surface was then washed with PBS containing 2 wt% of sodium dodecyl sulfate (SDS) to remove IgG. After confirming that the fluorescence from the spot had disappeared, a further AFM image was obtained.

Retention of Proteins on the Azobenzene-Containing Polymer Surface

The retention of fluorophore-linked IgG on the azobenzene-containing polymer surface was investigated. The sample preparation procedure is same as the above AFM study except at the photoirradiation time (0, 15, 30, 60 min). The samples were immersed and kept in PBS at both room temperature and 4 °C. The fluorescence intensity from the spot was measured at regular time intervals by the confocal microscope.

Immunological and Enzymatic Activities of Proteins on the Azobenzene-Containing Polymer Surface

The activities of antibodies and enzymes immobilized on the azobenzene-containing polymer surface were analyzed. To verify the antibody activity, (Cy5)-linked Rabbit IgG (to Mouse IgG) and Goat IgG to Rabbit IgG(H+L) were spotted and photo-immobilized on the azobenzene-containing polymer substrates in the same procedure as the above AFM study. The substrates were kept at both 4 °C and room temperature in a desiccator. Next, the substrates were immersed in PBS containing 1 μg/mL (Cy5)-linked Rabbit IgG and 0.01 wt% Tween20 for 30 min as an immunological binding step, and then were immersed in PBS containing 0.01 wt% Tween20 for 5 minutes as a washing step. After drying the substrates in air, the fluorescence of the spot was detected by the confocal microscope.

To verify the enzyme activity, 50 μL of an aqueous solution of 1 mg/mL subtilisin carlsberg (27.5 kDa, Sigma) was spotted on the azobenzene-containing polymer surface, and the surface was irradiated with a laser beam of 488 nm in wavelength and 80 mW/cm^2 in optical power density for 5 minutes, keeping the solution intact. As a control experiment, the same specimen without the photoirradiation step was prepared. The specimens were immersed in water at room temperature for 5 days. The activity of immobilized subtilisin was examined as the hydrolysis of the artificial substrate (tert-butoxycarbonyl-Gly-Gly-Leu- p-nitroanilide, Mw 465.5, Merck).[19,20] 50 μL of dimethylformamide containing 1 mg/mL the artificial substrate was added to 450 μL of 10 mM Tris-HCl buffer solution. 50 μL of the artificial substrate solution was spotted on the azobenzene-containing polymer surface at the same area where subtilisin had been immobilized, and then the specimen was maintained at 37 °C and 85% relative humidity for 1 hour. The hydrolysis of the artificial substrate was determined spectroscopically by immediately measuring the absorbance of the reactant at the wavelength of 410 nm (ε 8900 $M^{-1}cm^{-1}$).

5.3. Results and Discussion

Photo-Immobilization

The azobenzene-containing polymer is shown to immobilize objects ranging from micrometer-sized particles to macromolecules. Figure 5. 3a shows an optical image of 1 μm PS particles bound to the polymer surface after exposure to a linear-shaped laser beam. Only the particles in the photoirradiated region were successfully immobilized. Figure 5. 3b shows a fluorescent image of λ-DNA immobilized on the polymer surface from an aqueous solution using the same linear laser irradiation scheme. The image contrast suggests that DNA filaments were bundled and the bundled filaments were aligned along with the laser pattern. Figure 5. 3c and 3d demonstrate the photopatterning of fluorophore(Cy5)-linked IgG on the polymer surface. The fluorescence intensity ratio of the exposed area to the masked one was about 10000 to 500 (The intensity of the background was about 100 in Figure 5. 3d). IgG was well photopatterned even though a slight non-specific adsorption was found in this condition.

These experiments utilize three important advantages. Firstly, the azobenzene-containing polymer can capture micron to nanometer-scale macromolecules located only on the photoirradiated area. Second, the polymer can bind macromolecules having a variety of surface properties and sizes, including negatively charged DNA, charged proteins, and hydrophobic polystyrene. Third, the binding of the macromolecules can be performed even in aqueous solutions, so that their form in solution is expected to be preserved by this technique. These characters of the azobenzene-containing polymer make it possible to immobilize of a wide variety of biomolecules on the same substrate by the one step photoirradiation.

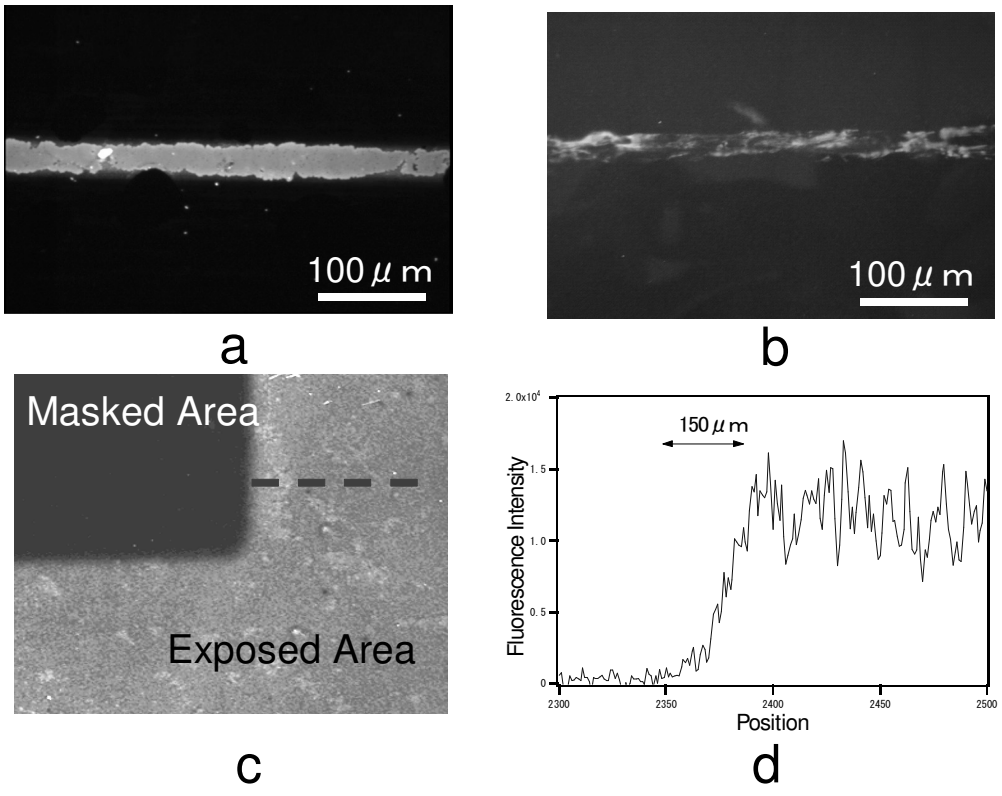

Figure 5. 3. Photopatterning of macromolecules on an azobenzene-containing polymer surface. **a**, A dark-field optical image of the polymer surface. 1 μm polystyrene particles were immobilized by photoirradiation with linear-shaped laser light. **b**, A fluorescence image of the polymer surface. Fluorophore-intercalated DNA was immobilized by the same photoirradiation scheme. **c** and **d**, Surface patterning of IgG on the polymer surface using a photo mask: **c**, the fluorescence image of the patterned area and **d**, the cross-section of the fluorescence intensity (from a dotted line in Figure 5.3c).

Molecular-Shape Imprinting

The surface of the azobenzene-containing polymer is shown to deform around the molecular template during photoirradiation. AFM images of two typical examples, fibrous and globular molecules, are shown in Figure 5. 4 and Figure 5. 5.

The fibrous object in Figure 5. 4a was a bundle of λ-DNA (the diameter of the bundle is about 50 nm), which had been immobilized on the azobenzene-containing polymer surface by spin-casting from the DNA aqueous solutions and subsequent photoirradiation with laser light. By increasing the applied force of the AFM tip (Figure 5. 4b), the fibrous object was wiped away by the tip and it can be seen that the shape of the fibrous object was clearly imprinted as a fibrous valley on the polymer.

The phenomenon also can be seen for the globular molecules IgG in Figure 5. 5. In Figure 5. 5a, the azobenzene-containing polymer surface was covered with a layer of small granulated particles of 10 nm - 30 nm in diameter and around 8 nm in height. (The height was estimated from the defects and the edge of the layer. Red markers in Figure 5. 5a.) The sizes of the particles were nearly equivalent to one subunit of IgG (about 10 nm, Fig. 1), considering the image includes the AFM tip-convolution artifact. The layer was so flat that the IgG monolayer is believed to be formed on the polymer surface. Figure 5. 5b shows an AFM image of the same area after washing the surface with PBS containing 2 wt% SDS to remove the IgG layer. The dents of about 20 nm in diameter and 2 nm in depth were observed on the surface (a typical example is indicated by green markers in Figure 5. 5b, cross-section. Larger dents were also observed (red markers)). In contrast, as shown in Figure 5. 5c, no dents were formed on the polymer surface where no IgG was deposited. Comparing these images and cross sections, the dents formed on the polymer surface in Figure 5. 5b is considered to be mirroring the surface shape of the IgG layer shown in Figure 5. 5a.

These findings lead to the conclusion that the azobenzene-containing polymer surface recognizes each molecular shape and deforms along the contour of the biomolecules upon photoirradiation (Figure 5. 1). The result also suggests that the increase in the contact area between the polymer and the macromolecules after photoirradiation inhibits the desorption from the polymer surface.

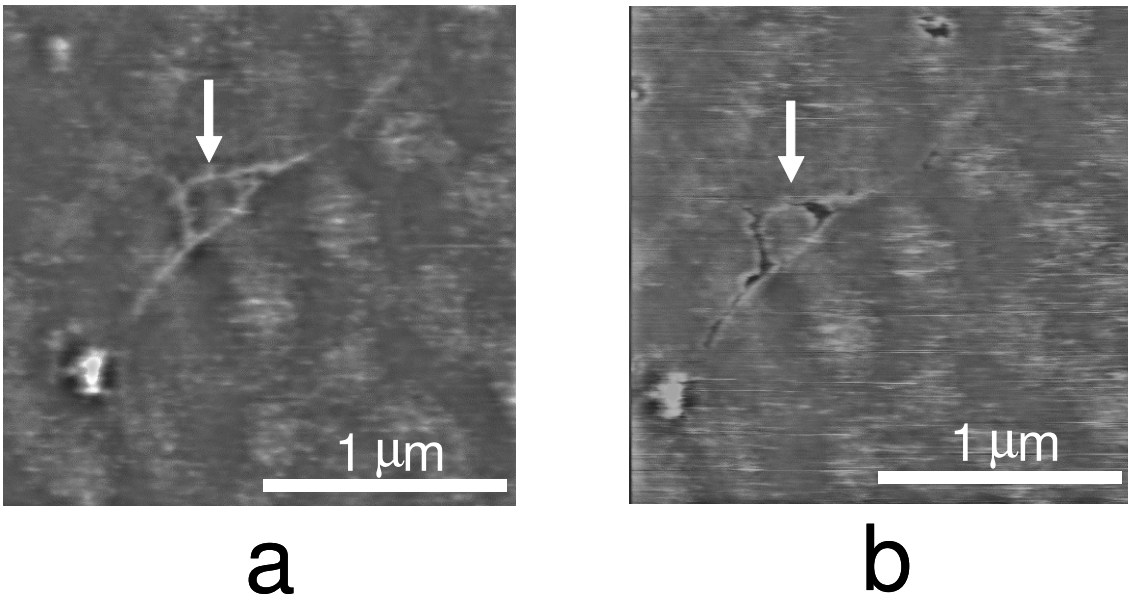

Figure 5. 4. The surface deformation on the azobenzene-containing polymer with DNA. **a** and **b** are contact-mode AFM images of the polymer surface covered with λ-DNA (The image height is from 0 to 20 nm). **a**, First scan of the surface covered with λ-DNA. **b**, the same image taken with a higher contact force after the first scan.

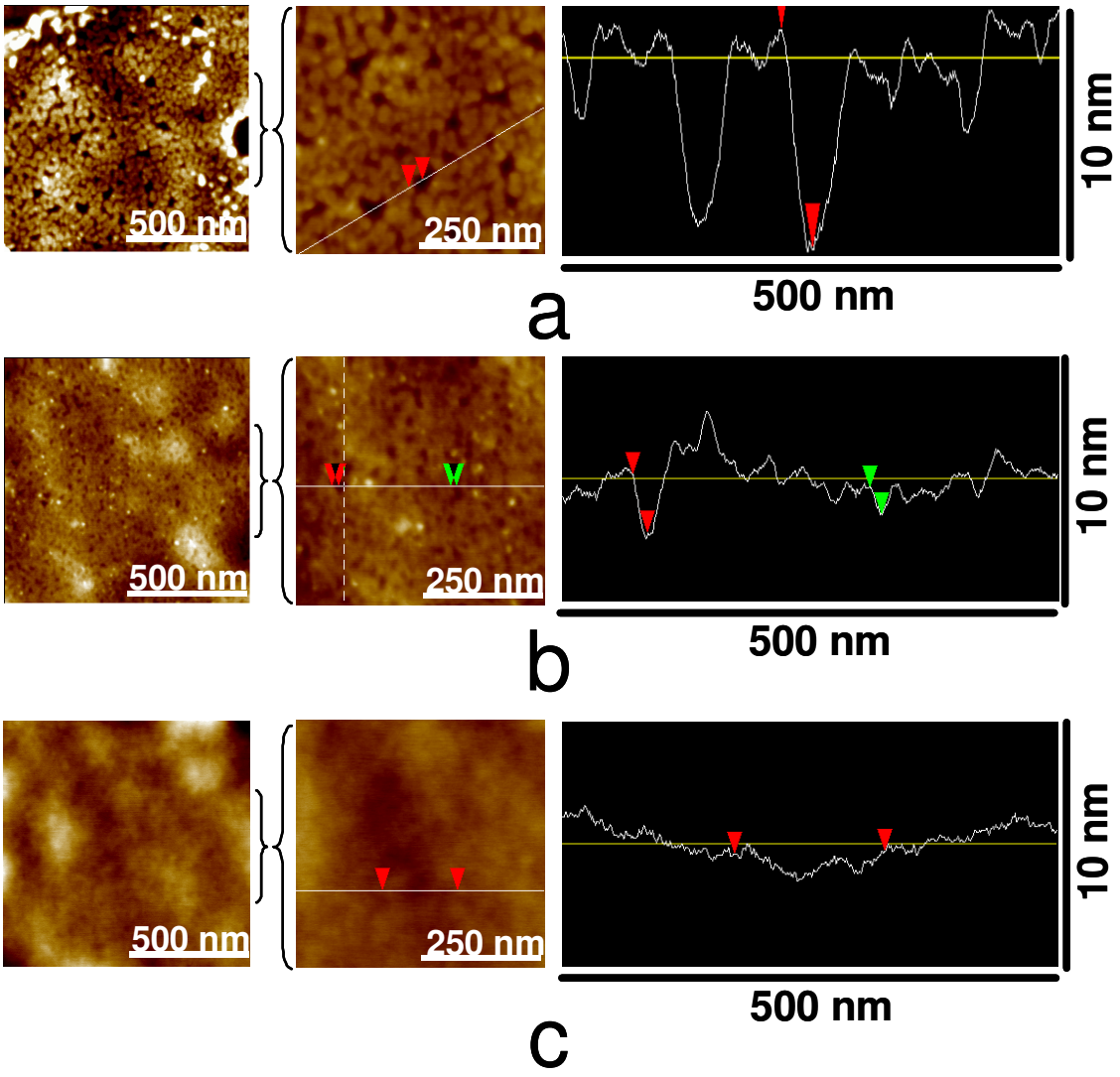

Figure 5. 5. The surface deformation on the azobenzene-containing with IgG. **a**, A tapping-mode AFM image of the polymer surface covered with IgG. **b**, The same image taken after removal of the IgG by washing with PBS containing 2 wt% SDS. **c**, A control showing the bare azobenzene-containing polymer surface after photoirradiation. This image was taken at the outside of the above IgG spot.

Retention of Proteins

Figure 5. 6a shows how the retention of fluorophore (Cy5)-linked IgG on the azobenzene-containing polymer surface changes with the photoirradiation time. The residual amount of IgG increased with the photoirradiation time and saturated over 30 min of photoirradiation. This time-dependent behavior is considered to be analogous to the polymer surface deformation; the deformation is increased with the photoirradiation time but is inclined to saturate (§2.3).[18,19] To investigate this desorption behavior further, the IgG-modified polymer surface which was photoirradiated for 30 min was soaked in PBS at room temperature and 4 ºC (Figure 5. 6b). The IgG molecules immobilized on the polymer surface desorbed very slowly on a time scale of several days, in contrast to a time scale of tens of minutes for the IgG molecules with the shorter photoirradiation time. Note that IgG molecules were removed by just the soak in water. This suggests that the IgG molecules were physically, not chemicly, immobilized on the polymer surface.

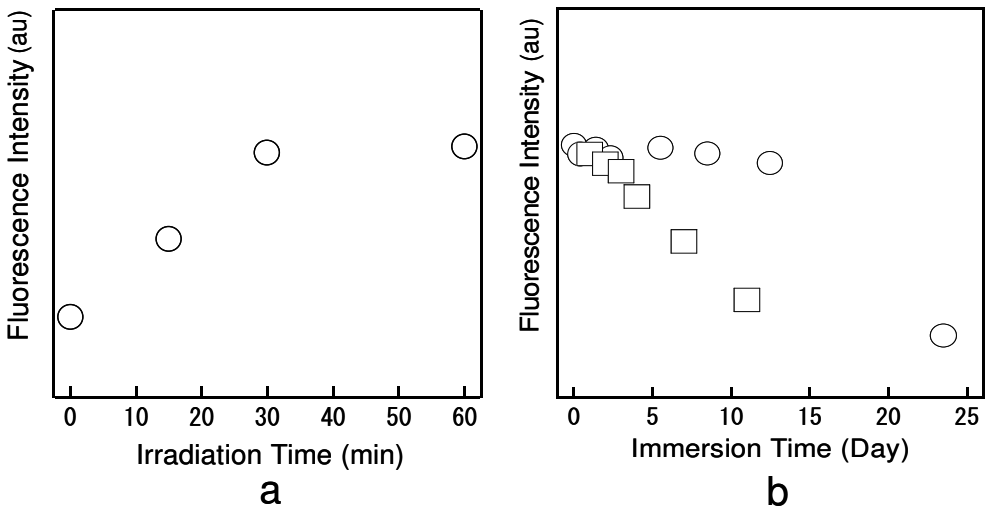

Figure 5. 6. The retention of fluorophore (Cy5)-linked IgG on the azobenzene-containing polymer surface after the photoirradiation. **a**, Photoirradiation time dependence of residual amounts of Cy5-linked IgG on the polymer. **b**, Desorption of IgG from the polymer surface in PBS after 30 min photoirradiation. Circles and squares denote results for 4 °C and room temperature, respectively.

Activity of Immobilized Protein

Activities of proteins, IgG and protease, photo-immobilized on the azobenzene-containing polymers were investigated as follows.

The immunological activity of IgG on the azobenzene-containing polymer is shown in Figure 5. 7. In Figure 5. 7a, two kinds of IgGs were spotted and photo-immobilized on the azobenzene-containing polymer. On the lines of the spots A and B, fluorescent IgG (Cy5-linked Rabbit IgG) was immobilized for a standard calibration curve. On the lines of the spots C and D, non-fluorescent IgG (Goat polyclonal antibody to Rabbit IgG(H+L)) was immobilized on the polymer surface. After the immobilization of IgGs, the polymer substrate was immersed in the aqueous solution of Cy5-linked Rabbit IgG, which was the same one on the spots A and B. Thus, the fluorescence intensities of the spots C and D in Figure 5. 7a indicated the number of Cy5-linked Rabbit IgG captured by non-fluorescent IgG immobilized on the polymer surface. The fluorescence intensities of the spots A, B, C and D were linearly increased with the concentration of the spotting solution. Variation of the fluorescence intensity of the same IgG spot (A and B, C and D) was typically less than 10%. This indicated that IgGs were immobilized evenly on the polymer surface. The fluorescence intensity of the lines of the spots C and D were about 40 % of the intensity of the spots A and B, suggesting that 40% of the immobilized IgG was capable of capturing the antigens (Cy5-linked IgG) in solutions. Considering the steric hindrance between the IgG molecules, the activity of the immobilized IgG was very high. In the same way dozens of antibodies has been confirmed to continue to exhibit reactivity to specific antigens after immobilization on azobenzene-containing polymer.

Next, the temporal stability of the spotted IgG on the azobenzene-containing polymer was examined. The same substrates shown in above were preserved at 4 ℃ and room temperature on dry condition. At a given point in time, the substrates were reacted to antigenic IgG. The immobilized IgG had been kept functioning very well for at least 6 months by the storage at 4 ℃ (Figure 5. 7b).

Furthermore, an activity of a bacterial protease (subtilisin, 35kDa) immobilized on the azobenzene-containing polymer surface was examined.[19, 20] The immobilized subtilisin showed the activity of cleaving a certain peptide bond of an artificial substrate (Boc-Gly-Gly-Leu-p-nitroanilide) in the aqueous solution. The conversion ratio is about

10% for the subtilisin-immobilized sample, whereas about 1% for the control (without photoirradiation step) after 1 hour reaction. The result shows that the polymer is capable of retaining functions of enzymes.

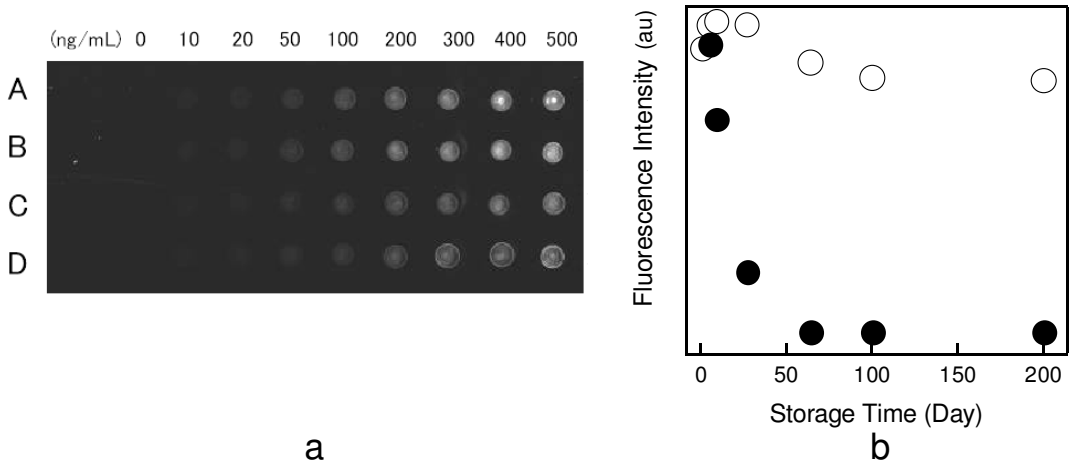

Figure 5. 7. The immunological activity of IgG immobilized on the azobenzene-containing polymer surface. **a**, A fluorescence image of the IgG spots (Cy5-linked Rabbit IgG was immobilized on A and B as controls, and Goat IgG to Rabbit IgG(H+L) was on C and D. The spot C and D had been reacted to Cy5-linked Rabbit IgG in the aqueous solution. **b**, The temporal stability of the IgG activity. Open and solid circles denote results for storage at 4 °C and at room temperature on dry condition, respectively.

Mechanism of Deformation and Immobilization

In what follows, the mechanism of the immobilization of the nano-scale particles on the azobenzene-containing polymer is discussed in some detail.

First of all, the immobilization is believed to be a noncovalent process, not to be a covalent binding process based on the retention experiment in Figure 5. 6. In the experiment, immobilized proteins were desorbed from the polymer surface by just the soak in water although the desorption rate was very slow. In addition, the photo-bleach of the azobenzene groups could not be detected before and after photo-irradiation under these experimental conditions (see experimental section). These results indicate that the macromolecules are physically, not chemically, immobilized on the polymer surface.

From this point, the immobilization can be attributed to the increasing in contact area between the particles and the polymer surfaces during the photo-irradiation. The SEM and AFM studies using the PS particles show that the polymer surface just under the particles deforms along the shape of the particles (Chapter 2, Chapter 3 and Figure 5. 1). The AFM studies using DNA and IgG also reveal that the polymer surface deforms along with the shapes of the biomolecules during the photo-irradiation (Figure 5. 4 and Figure 5. 5.). These studies strongly suggest that the contact area between the particles and the polymer surface are increased during photo-irradiation. The increase in contact area can induce an increase in weak physical interactions (e.g., Van der Waals forces, hydrophobic interactions and hydrogen bonding), which immobilize the particles on the polymer surface.

Ramsden suggested that the desorption rate of proteins on many surfaces decreases exponentially with increasing area of protein–surface contact.[11] Since the adsorption of proteins takes place via multiple weak bonds, the number of which will be roughly proportional to the contact area. If each bond has an energy of approximately kT and desorption requires all bonds to be broken simultaneously, the probability of desorption is roughly given by $\sim e^{-N}$, where N is the number of bonds. As an idea of scale, doubling the contact area between the surface and a protein that would otherwise desorb in 10 min increases the nominal time to desorption to 24 h. This time scale is in accord with the above retention experiments showing that the desorption rate of IgG changes from tens of minutes to several days by the 30 min photoirradiation (Figure 5. 6).

Based on the above considerations, the author concludes that the principal factor responsible for the photo-immobilization of the particles on the azobenzene-containing polymer is an increase in weak physical interactions due to the increase in the contact areas between the polymer and the particles. At the first step of the immobilization behavior, the photo-induced isomerization motion of the azobenzene group plasticize the polymer matrix, allowing it to deform.[21, 22] Even for an azobenzene-containing polymer with a glass transition temperature exceeding 100 ºC, this process occurs without the need to increase the temperature.[23] Because this isomerization only takes place during photoirradiation, the deformed surface shape is retained after irradiation ceases. In the photo-plasticized condition, the surface deformation with the particles has been suggested to be driven by the electric field distribution (chapter 2 and chapter 3)[21,24] and interfacial forces (e.g. Van der Waals forces, hydrophobic interactions and hydrogen bonds). After photoirradiation, each particle is physically held on the polymer surface because of the enlargement of the contact areas.

The functions of the particles including biomolecules could be protected on the azobenzene-containing polymer surface because of its deformation behavior. In general, soluble proteins, even those with low affinity for hydrophobic surfaces, lose their functionality on such surfaces, [10,11] as residence on the surface for a length of time can cause the time-dependent structural changes to bring their hydrophobic interior into contact with the surface. Changes in conformation can occur immediately upon adsorption, but time-dependent conformational changes are also evident.[11] Once the latter transition has taken place, the protein is firmly adsorbed and denatured. Nevertheless, the azobenzene-containing polymer is capable of keeping the functions of proteins such as antibodies and enzymes intact for a long time, even though the polymer has a hydrophobic surface (about 80º contact angle with water). This suggests that the deformed polymer surface can protect the time-dependent conformational change of the proteins.

In addition, the enlargement of the contact area is thought to occur by optimization of the orientation of azobenzene groups against the ionic charge and dipole moment of the bound molecules under the photo-plasticized conditions, as the azobenzene group has a large dipole moment (8.7 D for disperse red 1 type).[25] The reorientation of the

azobenzene groups would enhance binding between the polymer and the macromolecules.[26]

Advantage and Disadvantage of This Technique

This technique provides distinct advantages over conventional methodologies, the most important being that the immobilization of biomolecules does not involve chemical reactions. In the conventional chemical process, three steps are required for immobilization; activation, binding and deactivation. These complicated steps each have the potential to denature the biomolecules. Furthermore, protein stabilization agents such as sodium azide inhibit many chemical reactions.[5] In contrast, the azobenzene-containing polymer process eliminates the possibility of chemical denaturation.

Another important point is that blocking processes are unnecessary for biochip applications in some cases. In general, even in physical immobilization procedures using porous materials,[5] a blocking process is essential to avoid nonspecific adsorption of the biomolecules. This process sometimes reduces the detection sensitivity as a result of non-ideal reactions. In our technique, the level of nonspecific adsorption onto the azobenzene-containing polymer surface is very low when using working solutions with trace levels of a nonionic surfactant (0.01 wt% of polyoxyethylene sorbitane alkyl ester, see Experimental Section). After the optimization of the working solution conditions, the antispecific adsorption of the antibody on the polymer surface can be achieved to less than 1 pg/mm^2 (1 ng/mL), without the application of any blocking processes (Figure 5. 7a). From these advantages, our technique can drastically simplify the fabrication process of the protein chip.

It should be noted that the potential disadvantages of this method. First one is the hydrophobicity of the azobenzene-containing polymer surface. If the active site of the protein is located on the hydrophobic part, the activity of the immobilized protein will fall off because of the hydrophobic interaction. Further investigation is under way for clarifying the surface behavior of the polymer and proteins. Second is the slow deformation of the polymer surface. At present, it needs 5 minutes to 30 minutes for the photo-immobilization step. If a protein loses its functions immediately after contacting with the polymer surface, this method cannot apply. Third is that the azo-dyes quench

fluorescence from fluorophores that fluoresce in the wavelength ranging from 400 nm to 550 nm (coinciding with the absorption band of azobenzene). Although this potentially limits applications to fluorescence detection, it has been confirmed that fluorescence from Cy3 and Cy5 (as used for DNA chip and protein chip applications) [1,2] is not quenched on the azobenzene-containing polymer surface, allowing two-wavelength detection. Therefore, this disadvantage appears trivial with respect to most practical applications.

5.4. Conclusion

The potential of this technique lies in its versatility and simplicity, with expected applications in biomolecule immobilization and macromolecular-scale fabrication. The photo-deformable surface of the azobenzene-containing polymer warrants further investigation for protein chip applications, as the polymer can hold various proteins without causing denaturation by a one step photoirradiation. The technique also provides a new concept of molecular imprinting. The photophysically induced change in the surface shape and reorientation of the azo-dyes make it possible to imprint both the topographic features and the surface functional groups of the template proteins without chemical processes. The introduction of appropriate functional groups, those that allow for hydrogen bonding to azobenzene groups and/or the polymer chain, is also expected to create specific protein recognition sites. Thus, the azobenzene-containing polymer approach also has potential applications in protein chips requiring artificial scaffolds for specific protein adsorption sites.

References

[1] Y. Kawata, O. Egami, O. Nakamura, N. Sugihara, M. Okamoto, M. Tsuchimori, O. Watanabe, *Opt. Commun.* **161**, 6 (1999).

[2] T. Ikawa, T. Mitsuoka, M. Hasegawa, M. Tsuchimori, O. Watanabe, Y. Kawata, C. Egami, O. Sugihara, N. Okamoto, *J. Phys. Chem., B*. **104**, 9055 (2000).

[3] T. Ikawa, T. Mitsuoka, M. Hasegawa, M. Tsuchimori, O. Watanabe, Y. Kawata, *Phys. Rev. B,* **64**, 195408 (2001).

[4] M. Hasegawa, T. Ikawa, M. Tsuchimori, O. Watanabe, Y. Kawata, *Macromolecules*, **34**, 7471 (2001).

[5] *Protein Microarray Technology,* D. Kambhampati, Ed. Wiley-VCH, Weinheim, 2003.

[6] *Protein Microarray,* M. Schena, Ed., Jones and Bartlett Publishers, Sudbury, 2004.

[7] S. P. Palecek, J. C. Loftus, M. H. Ginsberg, D. A. Lauffenburger, A. F. Horwitz, *Nature,* **385**, 537 (1997).

[8] G. L. Griffith, G. Naughton, *Science,* **295**, 1009 (2002).

[9] A. G. Mayers, *Biomolecular Sensors*; E. Gizeli, R. C. Lowe, Eds, Taylor and Francis, London, 2002

[10] G. M. Whitesides, E. Ostuni, S. Takayama, X. Jiang, D. E. Ingber, *Annu. Rev. Biomed. Eng.* **3**, 335 (2001).

[11] J. J. Ramsden, *Quarterly Reviews of Biophysics*, **27**, 41, (1993).

[12] M. Wahlgren, T. Arnebrant, *TIBTECH,* **9**, 201 (1991).

[13] E. Ostuni, R. G. Chapman, R. E. Holmlin, S. Takayama, Whitesides, G. M. *Langmuir*, **17**, 5605 (2001)**.**

[14] A. Curtis, C. Wilkinson, *Trends in biotechnology,* **19**, 97 (2001).

[15] F. Cunin, T. A. Schmedake, J. R. Link, Y. Y. Li, J. Koh, S. N. Bhatia, M. J. Sailor, *Nature Materials,* **1**, 39 (2002).

[16] H. Shi, W-B. Tsai, M. D. Garrison, S. Ferrari, B. D. Ratner, *Nature,* **398**, 593 (1999).

[17] K. Haupt, *Chem. Comm.* 171 (2003).

[18] C. Alexander, L. Davidson, W. Hayes, *Tetrahedron* **59**, 2025 (2003).

[19] H. Takahashi, B. Li, T. Sasaki, C. Miyazaki, T. Kajino, S. Inagaki, *Microporous and Mesoporous Materials,* **44**, 755 (2001).

[20] L. A. Lyubinskaya, S. V. Belyaev, A. YA. Strongin, L. F. Matyash, E. D. Levin, V. M. Stepanov, *Anal. biochem.* **62**, 371 (1974).

[21] P. Karageorgiev, D. Neher, B. Schulz, B. Stiller, U. Pietsch, M. Giersig, L. Brehmer, *Nature Materials,* **4**, 699 (2005).

[22] A. Natansohn, P. Rochon, *Chem. Rev.* **102**, 4139 (2002).

[23] O. Watanabe, M. Narita, T. Ikawa, and M. Tsuchimori, *Polymer,* **47**, 4742 (2006).

[24] C. Hubert, A. Rumyantseva, G. Lerondel, J. Grand, S. Kostcheev, L. Billot, A. Vial, R. Bachelot, P. Royer, S. Chang., K. S. Gray, P.W. Gary, G. C. Schatz, *Nanoletter*, **5**, 615, (2005).

[25] J. C. Hooker, W. R. Burghardt, J. M. Torkelson, *J. Chem. Phys.,***111**, 2779 (1999).

[26] M. Narita, F. Hoshino, M. Mouri, M. Tsuchimori, T. Ikawa, and O. Watanabe, *Macromolecules*, **40**, 623 (2007).

Chapter 6. Molecular Scale Imaging of F-actin Assemblies Immobilized on an Azobenzene-Containing Polymer

6.1. Introduction

In chapter 6, the author presents a new method effectively used to image supramolecular assemblies of biologically-derived macromolecules (biomolecules) with molecular resolution. The method is based both on atomic force microscopy (AFM) and the immobilization technique of the biomolecules by using an azobenzene-containing polymer as shown in chapter 5.[1] Although AFM has become an established technique for imaging the biomolecules,[2,3,4] imaging of the supramolecular assemblies in native environments presents special challenges due to the concentration dependent nature of the phase behaviour. The structures of the supramolecular assemblies change with the concentrations of salts and the biomolecules, therefore, it is difficult to prepare the supramolecular assemblies on the flat surface for AFM (e.g. mica surface provides atomically flat surface, but the surface repels most of the biomolecules because of its negative charge).[2, 5] The technique based on the azobenzene-containing polymer is well suited for imaging biomolecules especially for AFM, providing a non-reactive, non-ionic, and flat surface (the surface roughness can be < 0.3 nm) on which the complex supramolecular assemblies can be immobilized with little conformational change in the native aqueous environment. The immobilization process dramatically reduces the thermal motion of biomolecules, leading to higher imaging resolution allowing individual biomolecules to be resolved.

In this chapter, the author presents a structural study of supramolecular assemblies of cytoskeletal filamentous (F-) actin in the presence of divalent cation. F-actin, a double-stranded helical filament made of the protein G-actin, can be considered as a semi-flexible and highly charged polyelectrolyte, with diameter D_A ~ 80Å, persistence length ξ_A ~ 10 μm and anionic liner charge density λ_A~ $-e$/2.5 Å.[6,7,8] In vitro, F-actin in the presence of divalent cations assembles into gel-like networks and bundles that resemble their cellular counterparts formed with linker proteins. The F-actin/divalent cation aggregation has been used as a good model system, both experimentally and theoretically, for studying biological polyelectrolyte association.[9,10,11,12,13,14,15,16] Recent

experiments using high resolution small-angle X-ray scattering (SAXS) showed that with high concentration of divalent cations, F-actin forms bundles consisting of filaments that are closely packed in a distorted hexagonal arrangement.[9, 10] Within a small range in the low cation concentration regime, a unique layered structure consisting of stacks of nematic F-actin rafts was observed.[9] The detailed structural phase behaviour of the F-actin supramolecular assembly challenges present theoretical model in many aspects. [14-16] Clearly, in addition to the average structures revealed by XRD, to have a detailed view of the individual structural elements (filaments, bundles and networks) at the molecular level would provide much insight into the interactions that drive the self-assembly process of biological polyelectrolytes. Here, the imaging technique based on the azobenzene-containing polymer was used to investigate the phase behaviour of F-actin aggregates as a function of concentration of the divalent cation Mg^{2+}. The data provided direct experimental evidence of a coil-on-coil (braided) structure of F-actin bundles formed at high Mg^{2+} concentrations. At intermediate Mg^{2+} concentrations, the data showed the first images of the two dimensional nematic rafts discovered by recent x-ray studies[9] and theoretical treatments. [15]

6. 2. Experimental

F-actin was polymerized from lyophilized monomeric Globular (G-) actin (2mg/ml) from rabbit skeletal muscle. [9, 10] F-actin length was controlled by the addition of an appropriate amount of 1 mg/mL gelsolin.[9]

The azobenzene-containing polymer, poly{4'-[[[2-(methacryloyloxy) ethyl]ethyl] amino]-4-cyanoazobenzene-co-methyl methacrylate} (15 mol% azobenzene moiety, molecular weight 25,000) was obtained by free-radical polymerization (§5.2).[1]

The photo-immobilization process used to prepare the F-actin/Mg^{2+} samples is shown in Figure 6. 1 (a). F-actin and magnesium chloride solutions were spotted (each spot contains 1 μL of $MgCl_2$ and 1 μL of F-actin) and mixed on the surface of a spin-coated azobenzene-containing polymer film on a glass substrate. Each sample (substrate) contained an array of spots (typically 6-8) with different concentrations of F-actin and Mg^{2+}. The film was then sealed inside a humidity chamber to prevent evaporation and irradiated for 60 minutes with light (470 nm) from a 6x10 array of blue light emitting

diodes (LED) with an optical power density of 10 mW/cm^2. After washing the surface to remove excess sample, the substrate was probed by using a Digital Instruments Dimension 30000 scanning probe microscope in tapping-mode with a standard silicon cantilever (tip radius of curvature ~ 20 nm).

During photo-irradiation, the photo-isomerization motion of the azobenzene group and the resultant photo-plasticization of the polymer matrix lead to a deformation of the polymer surface along the contour of surface biomolecules and thus immobilizes them (chapter 5).[1, 17] After removing F-actin from the polymer surface by washing with 2 wt% sodium dodecyl sulfonate, the imprinted shape of the filaments could be observed on the polymer surface (Figure 6. 1 (b)).

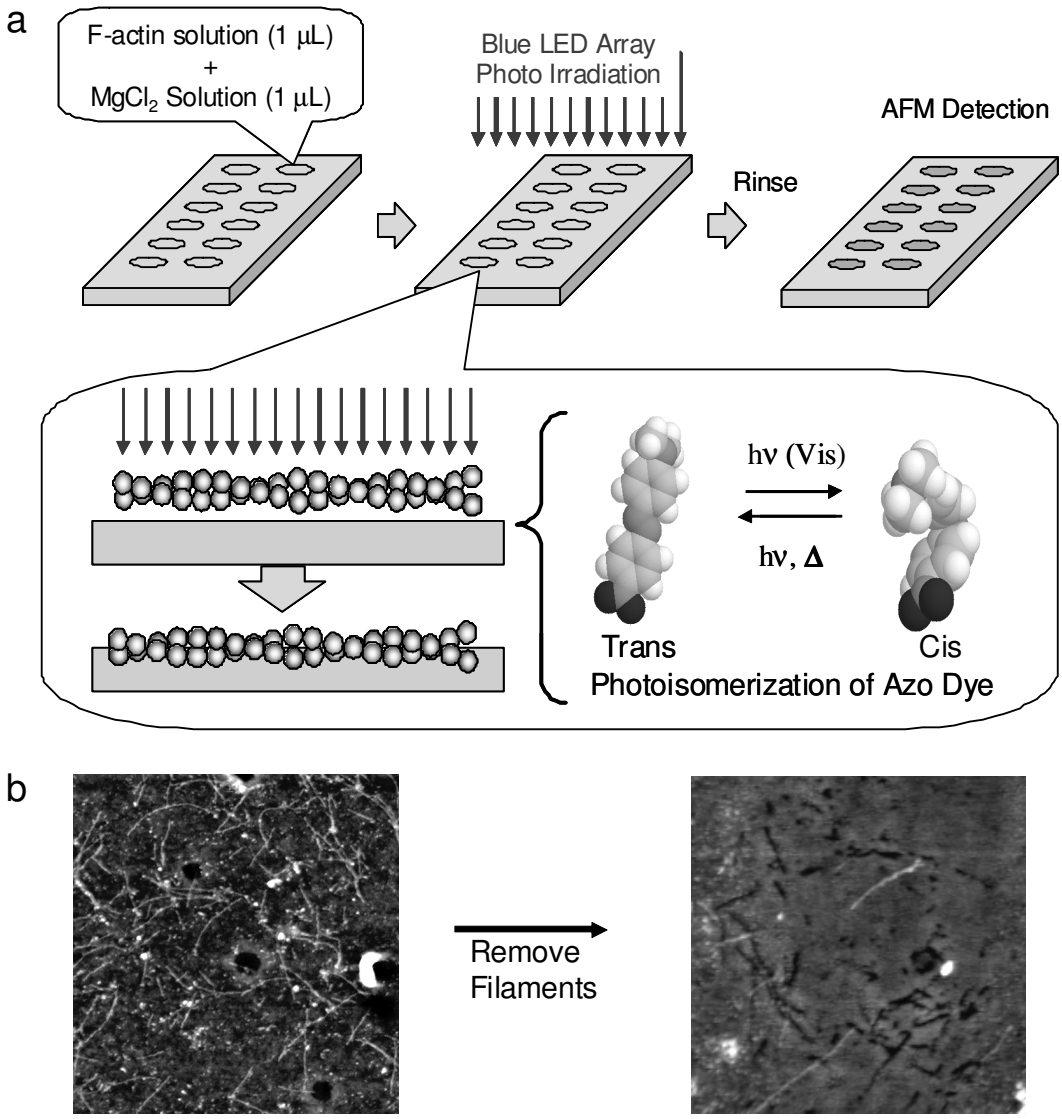

Figure 6. 1. Photo-immobilization of F-actin/Mg^{2+} samples on an azobenzene-containing polymer surface for AFM studies. **a**, a schematic of the photo-immobilization process. Light irradiation induces the azobenzene-containing polymer surface to deform along F-actin due to the photoisomerization motion of the azo-dye. **b**, the polymer surface before and after removing F-actin. Filament-like grooves were formed on the polymer surface after photo-irradiation.

6.3. Results and Discussions

An AFM image and an axial height trace of a single F-actin filament immobilized on the azobenzene-containing polymer surface is shown in Figure 6. 2. The height trace showed periodic variation with a typical repeating distance of 35 nm matching the pitch of the F-actin. The observed pitch varied from 30 nm to 40 nm, which is consistent with previous electron microscopy observations that F-actin is a helix with a random variable twist.[7, 8, 18] The observed height (3 nm – 4 nm from valley to peak) of the filament was about half of the actual F-actin diameter (6-8 nm), suggesting that the filament was about halfway embedded into the azobenzene-containing polymer film after photo-immobilization. The typical observed width of a single filament measured perpendicular to the filament was around 20 nm, about 3 times greater than the actual diameter of F-actin, which could be attributed to a tip-sample convolution effect.[19] Even though it is difficult to remove this tip-sample convolution effect, it is not difficult to differentiate between single filaments and bundles based on their apparent diameter.

The multiple-spot geometry allowed us to investigate F-actin assemblies as a function of increasing cation concentration on a single sample with relative ease. Figure 6. 3 (a-c) demonstrates the progressive association of long actin filaments (up to ~10 μm in length, no gelsolin) with increasing Mg^{2+} concentration (0 mM, 10 mM, 80 mM, respectively) on the azobenzene-containing polymer surface. The F-actin solution with 0 mM Mg^{2+} exhibited an uncondensed isotropic phase (Figure 6. 3 (a)), with filaments maintaining large distances and intersecting angles (~90 degrees) between them to minimize electrostatic repulsion.[12,20] With 10 mM Mg^{2+} (Figure 6. 3 (b)), the distances between filaments became smaller and the filaments formed a network structure with smaller intersecting angles between filaments. The network consisted of predominantly single filaments of F-actin. At 80 mM Mg^{2+} (Figure 6. 3 (c)), however, a different network structure composed of mostly thick filaments (F-actin bundles), was observed. The single filaments and bundles were entangled and oriented randomly in the network, suggesting little excluded volume interaction which drives liquid crystalline ordering in the more concentrated solution. Interestingly, the bundles observed in the networks appeared to be fairly uniform in diameter and large bundles were rarely seen under this condition. This suggests that there might be a growth limit of the bundle size, which has been predicted

theoretically.[21] Overall, the phase behaviour observed in the AFM images is consistent with the previous results obtained using x-ray diffraction and optical microscopy.[9] However, the high resolution data allowed us to examine the structures at a single filament or bundle level, which led to observations relevant to several important unanswered questions about F-actin assemblies.

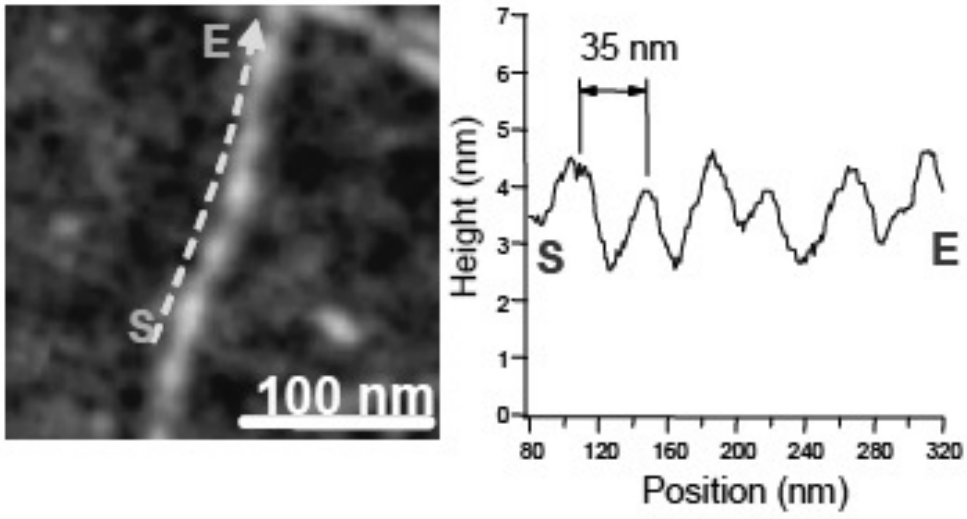

Figure 6. 2. An AFM image of a single F-actin filament and a height trace along the single filament showing periodic variations corresponding to G-actin subunits.

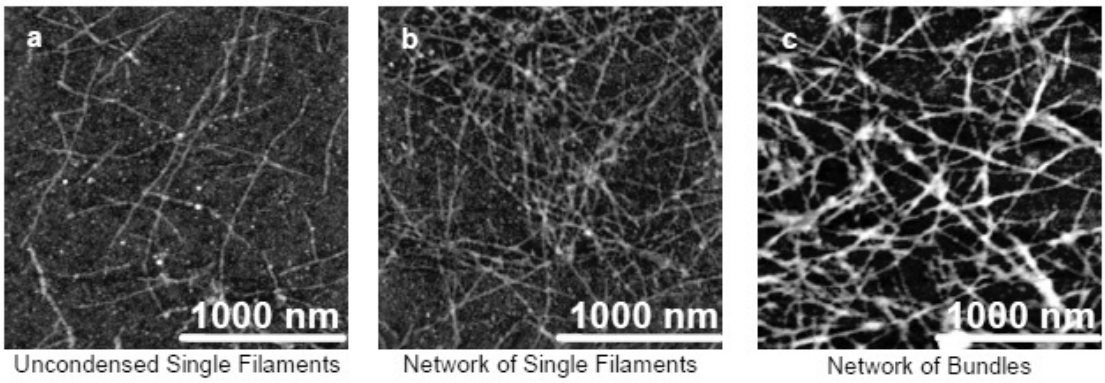

Figure 6. 3. AFM images showing the progressive association of long (no gelsolin) actin filaments as a function of Mg^{2+} concentration. **a**, isotropic phase of F-actin (0 mM Mg^{2+}). **b**, network of F-actin (10 mM Mg^{2+}). **c**, network of F-actin bundles (80 mM Mg^{2+}). The phase map was obtained from one azo-polymer sample containing multiple spots of F-actin/ Mg^{2+} mixed at different ratios.

There has been much discussion about the structure of bundles that are formed by charged biopolymers at high counterion concentrations. One of the intriguing possibilities is whether the F-actin could form helical coil within a bundle.[4] Analogous structures have been theoretically predicted,[22, 23] but never experimentally verified. Using the current technique, we have found direct evidence of the coil-on-coil (braided) bundle structure at higher cation concentrations (>20 mM Mg^{2+}). In Figure 6. 4 (a, b), two examples of the braided bundles formed with short F-actin (average length = 680 nm controlled with gelsolin) and 80 mM Mg^{2+} are shown. Under this condition, co-existence of both single filaments and bundles were observed, which can be easily differentiated in the magnified images by their apparent diameter. Following the trace lines, it can be seen that the bundles unraveled at their ends into three or more single filaments. The braided configuration of the bundle is especially obvious in Figure 6. 4 (b). The braided structure was found to exist in a wide range of Mg^{2+} concentrations (5 mM to 160 mM), from the uncondensed phase to the bundled phase. In comparison, such spiral structures were not readily discernible in the bundles that were formed by longer filaments (Figure 6. 3 (c)). One could argue that the longer filaments are more prone to kinetic hindrance to forming braided structures due to increased difficulty in rotational movements.

AFM images of F-actin at lower Mg^{2+} concentrations offered some clues as to how the helical bundles may be formed. Figure 6. 4 (c-d) show several distinct F-actin junctions (points where single filaments are joined or crossed) observed at 5 mM Mg^{2+} concentration. In Figure 6. 4 (c), three filaments formed a knot structure of about 100 nm in length, and the knot unraveled at both ends into three single filaments with fairly large angular separation. Also, entangled points formed by two filaments were observed in Figure 6. 4 (d). In the same image, two other types of joints could be seen: an X overlap in which the two filaments simply crossed each other and a T junction where the end of one filament was seemingly attached to another filament at a near 90 degree angle. All these junctions can be considered as precursor sites of the more extensive helical bundle structure shown in Figure 6. 4 (a-b) at higher Mg^{2+} concentrations.

The braided bundle structure may have been present in previous images of F-actin bundles obtained using electron microscopy, AFM, and confocal optical microscopy, but was not recognized as such. For example, high resolution cryo-AFM images of F-actin

clearly showed the existence of braided bundles.[4] Synchrotron x-ray diffraction data showed that the close packing pattern of the bundle deviates from an exact hexagonal arrangement (q_{10}=0.089Å^{-1} and q_{11} = 0.139 Å^{-1}, respectively), which may be partially attributed to the braided arrangement of some F-actin inside the bundle.[9, 10] The observed axial repeat distance of the braided bundles was around 100 nm (Figure 6. 4 (b,c)), comparable to the pitch of a single F-actin twisted structure. This strongly suggests that the F-actin filament follows the topology of the twist of F-actin in order to achieve tighter packing.

It is important to note that the existence of braided F-actin bundles does not necessarily contradict the earlier conclusion of hexagonal packing of filaments inside the bundles. Because of the limited statistical sampling of AFM imaging and the large F-actin length distribution, it is likely that the actual samples contain both structures, with hexagonal bundles being the prevalent structure giving rise to the x-ray diffraction peaks.

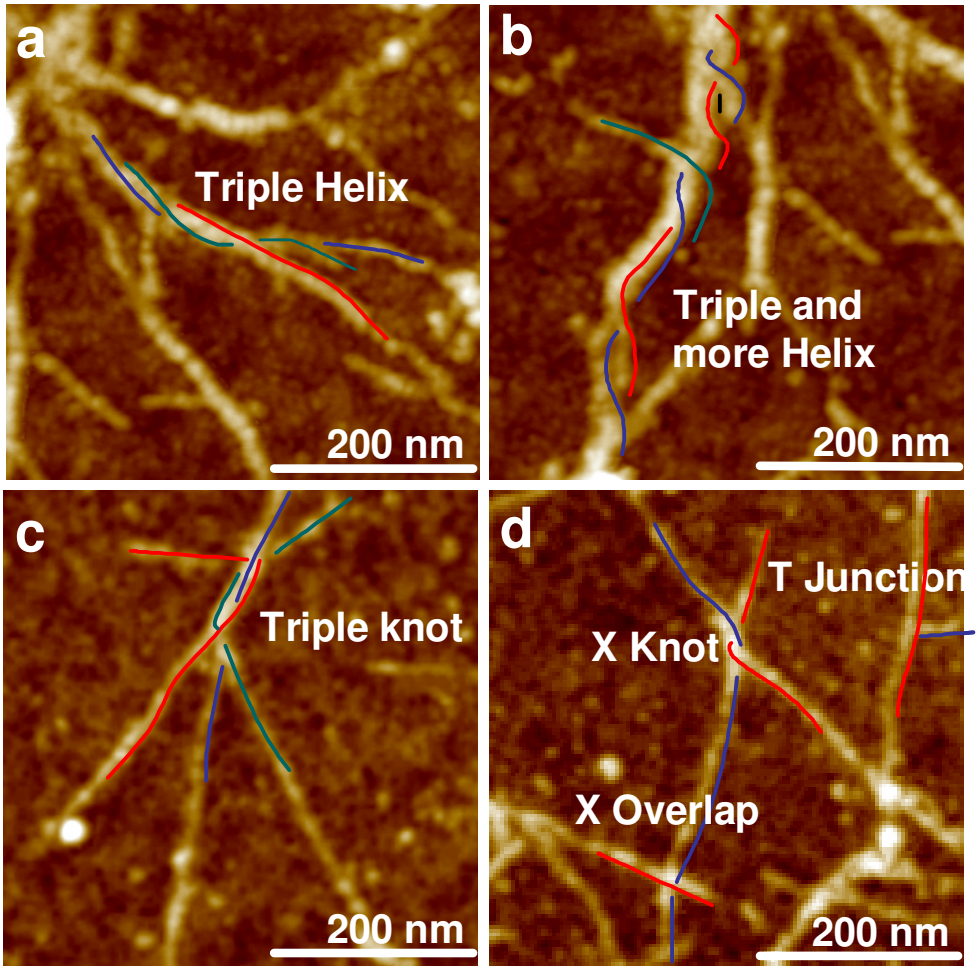

Figure 6. 4. Braided structures of short F-actin (average length 680 nm) bundles and precursor junctions. **a** and **b**, braided bundles at high concentration of Mg^{2+} (80 mM). The bundle in image **a** consisted of three filaments and the bundle in (**b**) consisted possibly of more than three filaments. **c** and **d**, junction-type precursor structures formed in the uncondensed phase of F-actin with 5 mM Mg^{2+}. All the images are 0-10 nm in height.

The structures formed in the intermediate range of concentration are of particular interests, as previous x-ray studies revealed in this regime an unique phase composed of lamellar stacks of crossed rafts (L_{XR} phase).[9] Such a structure, formed with 20 mM of Mg^{2+}, is shown in Figure 6. 5 (a). The filaments formed a 2D nematic-like rafts with a lateral repeat distance of about 12 nm, slightly larger than the F-actin diameter. The rafts were stacked at a large angle from each other, as was deduced from x-ray data, which showed a series of strong (00L) harmonic peaks due to stacking. The raft-like structures were observed in a wide range of Mg^{2+} concentration (5-40 mM) with short F-actin and were much less dominant with longer filaments. This is consistent with the phase diagram compiled with x-ray data.[9] Similar structure has been observed in the system consisting of microtubules and divalent cations,[24] suggesting a certain degree of universality of phase behaviour of rod-like biological filaments with divalent cations.

The 2D nemtic-like rafts were found to coexist with aggregated perpendicular filaments at slightly lower Mg^{2+} concentrations (5-10 mM), as shown in Figure 6. 5 (b), which is consistent with recent molecular dynamic simulation predictions that isolated stiff polyelectrolyte filaments in general evolve from aggregated perpendicular filaments to aggregated parallel rods.[16] The theoretical treatment also describes that the aggregated perpendicular filaments can form two-dimensional rafts.[15] This image clearly shows the coexistence of the parallel filaments and the perpendicular one.

Based on the above AFM images, the phase diagram of the supramolecular assembly of F-actin is summarized in Figure 6. 6. The structures of the assemblies change with concentration of Mg^{2+} and length of the filamets, which is consistent with the previous X-ray study [9] and the theoretical predictions.[15, 16] The AFM study clearly shows the first-time-seen images of the following structures: (1) the cross stacking of the 2D nematic-like rafts of short F-actin at intermediate concentration of Mg^{2+} (5 - 10 mM) and (2) the braided bundle structure at high concentration of Mg^{2+} (more than 20 mM).

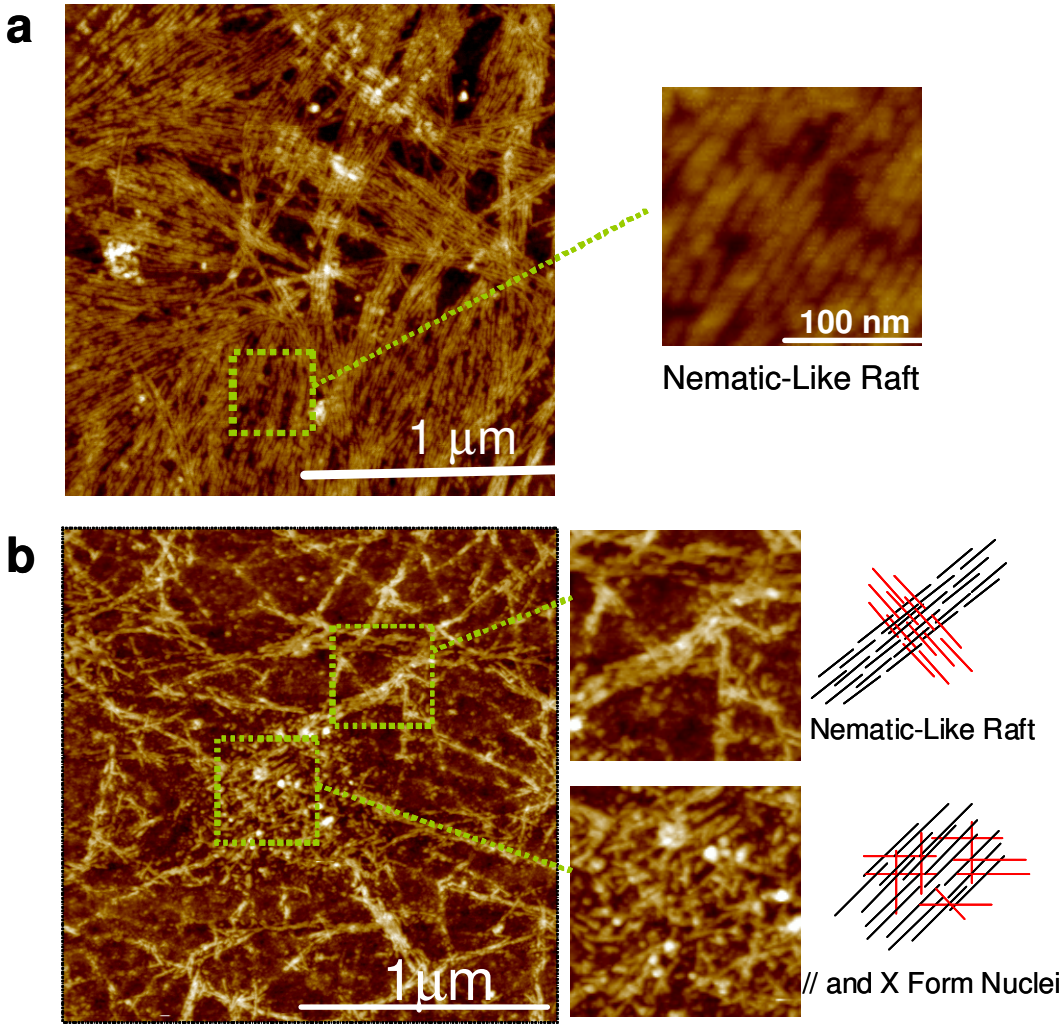

Figure 6. 5. AFM images of intermediate phases of short F-actin (average length 170 nm) Mg^{2+}. **a**, A phase consists of the nematic-like rafts with 20 mM Mg^{2+}. In part, the rafts were stacked. **b**, A phase consists of both the nematic-like rafts and the perpendicular aggregates with 10 mM Mg^{2+}.

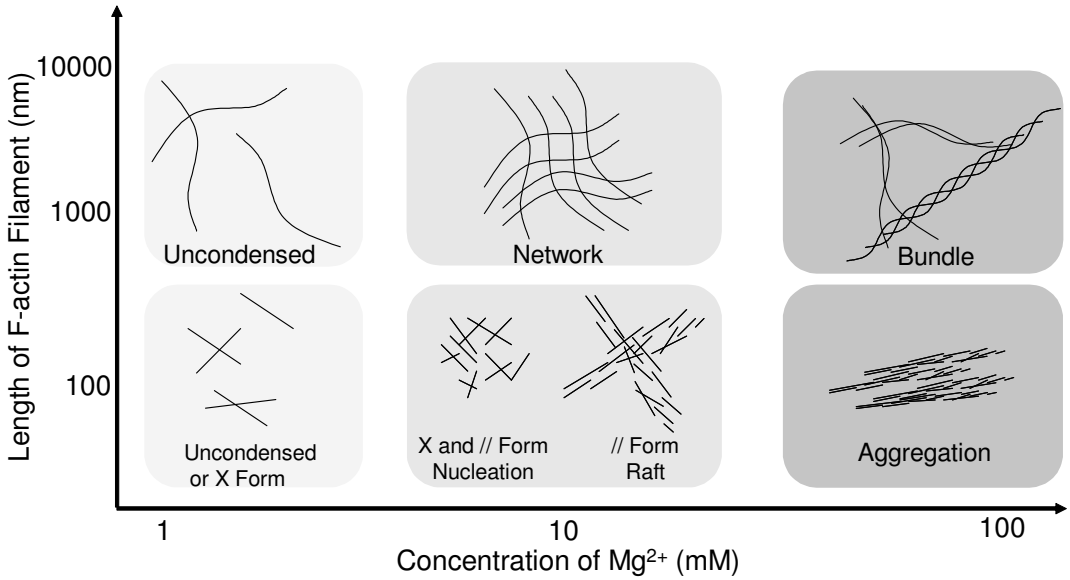

Figure 6. 6. A phase diagram of the supramolecular assembly of F-actin as a function of Mg^{2+} concentration.

6. 4. Conclusion

A new protein immobilization technique was developed for molecular scale imaging by AFM of F-actin supramolecular structures formed in the presence of Mg^{2+}. The technique allowed combinatorial investigations of the phase behaviour of the F-actin/ Mg^{2+} system and revealed new structural details relevant to the understanding of cation-induced biopolymer aggregates. The author found, in particular, a predominantly three-filament helical coil-on-coil structure in the F-actin bundles at higher divalent cation concentrations. The existence of the layered, raft-like F-actin structure at intermediate cation concentration, first revealed by x-ray diffraction, is confirmed unambiguously.

References

[1] T. Ikawa, F. Hoshino, T. Matsuyama, H. Takahashi, and O. Watanabe, *Langmuir* **22**, 2747 (2006).

[2] H.G. Hansma, *Annu. Rev. Phys. Chem.* **52**, 71 (2001).

[3] T. Lehto, M. Miaczynska, M. Zerial, D.J. Müller, and F. Severin, *FEBS Lett*. **551**, 25 (2003).

[4] Z. Shao, D. Shi, and A.V. Somlyo, *Biophys. J.* **78**, 950 (2000).

[5] O. J. Rojas, M. Erinstsson, R. D. Neuman, and P. M. Claesson, *Langmuir*, **18**, 1604 (2002)

[6] U. Aebi, R. Millonig, H. Salvo, and A. Engel, *Ann. N. Y. Acad, Sci.* **483**, 100 (1986).

[7] E.H. Egelman, *Curr. Bio.* **14**, R959 (2004).

[8] B. Alberts et al., *Molecular biology of the cell* (Garland Science, New York, 2002), 4th ed.

[9] G.C.L. Wong, A. Lin, J.X. Tang, Y. Li, P.A. Janmey, and C.R. Safinya, *Phys. Rev. Lett.* **91**, 018103 (2003).

[10] T.E. Angelini, H. Liang, W. Wriggers, and G.C.L. Wong, *Proc. Natl. Acad. Sci.* USA **100**, 8634 (2003).

[11] K. Yamamoto, M. Yanagida, M. Kawamura, K. Maruyama, and H. Noda, *J. Mol. Biol.*

91, 463 (1975).

[12] H. Strzelecka-Golaszewska, E. Prochniewicz, and W. Drabikowski, *Eur. J. Biochem.* **88**, 219 (1978).

[13] J.X. Tang, and P.A. Janmey, *J. Biol. Chem.* **271**, 8556 (1996).

[14] B.-Y. Ha, and A.J. Liu, *Phys. Rev. Lett.* **79**, 1289 (1997).

[15] I. Borukhov, and R.F. Bruinsma, *Phys. Rev. Lett.* **87**, 158101 (2001).

[16] K-C. Lee, I. Borukhov, W.M. Gelbart, A.J. Liu, and M.J. Stevens, *Phys. Rev. Lett.* **93**, 128101 (2004).

[17] A. Natansohn, and P. Rochon, *Chem. Rev.* **102**, 4139 (2002)

[18] E.H. Egelman, N. Francis, and D.J. DeRosier, *Nature,* **298**, 131 (1982).

[19] P. Markiewicz, and C. Goh, *J. Vac. Sci. Technol.* B **13**, 1115 (1995).

[20] S.L. Brenner, and V.A. Parsegian, *Biophys. J.* **14**, 327 (1974).

[21] B.-Y. Ha, and A.J. Liu, *Europhys. Lett.*, **46**, 624 (1999).

[22] Y. Snir, and R.D. Kamien, *Science,* **307**, 1067 (2005).

[23] R.D. Kamien, and D.R. Nelson, *Phys. Rev. Lett.*, 74, 2499 (1995).

[24] D.J. Needleman, M.A. Ojeda-Lopez, U. Raviv, H.P. Miller, L. Wilson, and C.R. Safinya, *Proc. Natl. Acad. Sci.* **101**, 16099 (2004).

Summary

This thesis described the nanoscale photofabrication on the surface of azobenzene-containing polymers and its utilization for an optical recording and biological applications. In chapter 1, the background and the motivation of this thesis were introduced; the principles of the dynamics of azobenzene-containing polymers, optical near field, atomic force microscopy and scanning near-field optical microscopy were presented.

The following chapters divided into two parts. In Part I, two kinds of photofabrication methods of the nanostructure on the surface of the azobenzene-containing polymer by using optical near field were described from chapter 2 to chapter 4. In Part II, a novel and simple concept for photo-immobilization of small particles based on the nanoscale surface deformation on the azobenzene-containing polymers, and its application for biological imaging technique were presented in chapter 5 and chapter 6.

In chapter 2, the formation of a hexagonally arrayed indented nanostructure on the surface of azobenzene-containing polyurethane films by the optical near field generated around dielectric spherical particles were demonstrated. The size effect of the polystyrene particles ranging from 98 nm to 990 nm in diameters and the influence of polarization of light were examined. The indentation shapes were dependent on the size of particles and the polarization of the incident light, which strongly suggested that the indentations were induced by the electromagnetic field around the particles.

In chapter 3, the surface deformation mechanism of the azobenzene-containing polyurethane by the optical near field generated around the PS particles were examined. The deformation pattern on the film surface was compared with the calculated intensity distribution around the particles, and the polymer migration on the film surface was analyzed by tapping mode atomic force microscopy. These analyses concluded that the near-field gradient force induced the surface deformation.

In chapter 4, photofabrication on the surface of the azobenzene-containing polymer film by the scanning near-field optical microscope equipped with the optical fiber probes with the subwavelength-sized aperture. The formation of the 150 nm diameter pit structure was achieved by the optical fiber probe coupled with a 50 ns pulse of 10 mW and 488 nm wavelength coherent light.

In chapter 5, a detailed description of the photo-immobilization method for nano-scale particles including biologically derived macromolecules was shown. In short, the surface of an azobenzene-containing polymer deforms along the contour of the small particles and physically holds them upon photo-irradiation. Various proteins were held on the azopolymer surface in a simple process, retaining their original functionality. The favorable prospects for biological applications such as immunological detection and enzyme reaction were shown.

In chapter 6, the direct imaging of hierarchical assemblies of biologically derived macromolecules, filamentous (F-) actin, were shown based on the photo-immobilization on the azobenzene-containing polymer surface. The imaging technique was used to investigate the phase behavior of F-actin assemblies as a function of concentration of the divalent cation Mg^{2+}. The data provided direct experimental evidence of a coil-on-coil (braided) bundle structure at high Mg^{2+} concentrations and a two-dimensional nematic raft structure at medium Mg^{2+} concentrations. This new technique was expected to be broadly applicable to the direct imaging of the large class of biological filamentous systems.

List of Publications

Chapter 2

Transcription of Near-Field Induced by Photo-Irradiation on a Film of Azo-Containing Urethane-Urea Copolymer
Osamu Watanabe, Taiji Ikawa, Makoto Hasegawa, Masaaki Tsuchimori, Yoshimasa Kawata, Chikara Egami, Okihiro Sugihara, and Naomichi Okamoto
Molecular Crystals and Liquid Crystals, **345**, 305-310 (2000)

Topographical Nanostructure Patterning on the Surface of a Thin Film of Polyurethane Containing Azobenzene Moiety Using the Optical Near Field around Polystyrene Spheres
Makoto Hasegawa, Taiji Ikawa, Masaaki Tsuchimori, Osamu Watanabe, and Yoshimasa Kawata
Macromolecules, **34**, 7471-7476 (2001)

Surface Deformation on Azobenzene Polymer Film Induced by Optical Near-Field around Polystyrene Microspheres
Taiji Ikawa, Makoto Hasegawa, Masaaki Tsuchimori, Osamu Watanabe, Yoshimasa Kawata, Chikara Egami, Okihiro Sugihara, and Naomichi Okamoto
Synthetic Metals, 124, 159-161 (2001)

Chapter 3

Optical Near Field Induced Change in Viscoelasticity on an Azobenzene-Containing Polymer Surface
Taiji Ikawa, Takuya Mitsuoka, Makoto Hasegawa, Masaaki Tsuchimori, Osamu Watanabe, Yoshimasa Kawata, Chikara Egami, Okihiro Sugihara, and Naomichi Okamoto
The Journal of Physical Chemistry B, **104**, 9055-9058 (2000)

Azobenzene Polymer Surface Deformation Due to the Gradient Force of the Optical Near Field of Monodispersed Polystyrene Spheres
Taiji Ikawa, Takuya Mitsuoka, Makoto Hasegawa, Masaaki Tsuchimori, Osamu Watanabe, and Yoshimasa Kawata
Physical Review B, **64**, 195408 (2001)

Chapter 4

Nano-Fabrication of Azopolymer by Scanning Near-Field Optical Microscope
Wataru Mori, Masahiro Tawada, Hiroshi Shimoyama, Taiji Ikawa, Masaaki Tsuchimori, and Osamu Watanabe
Electronics and Communications in Japan, Part 2, **87**, 55-61 (2004)

Near Field Optical Recording on Azopolymer Using a Sub-Microsecond Pulse
Taiji Ikawa, Chang-Dae Keum, Hideki Takagi, Masaaki Tsuchimori, Osamu Watanabe, Wataru Mori, Masaya Harada, Masahiro Tawada, and Hiroshi Shimoyama
IEICE Transactions on Electronics, **E85-C**, 1287-1290 (2002)

Chapter 5

Molecular-Shape Imprinting and Immobilization of Biomolecules on a Polymer Containing Azo Dye
Taiji Ikawa, Fumihiko Hoshino, Takashi Matsuyama, Haruo Takahashi, and Osamu Watanabe
Langmuir, **22**, 2747-2753 (2006)

Chapter 6

Molecular Scale Imaging of F-actin Assemblies Immobilized on a Polymer Cotaining Azo Dye
Taiji Ikawa, Fumihiko Hoshino, Osamu Watanabe, Youli Li, Philip Pincus, Cyrus R. Safinya
Physical Review Letters, **98**, 018101 (2007)

Other publications not described in this thesis

Nanostructure Patterning on an Azobenezene-Containing Polymer Surface

Topographical Change of Azopolymer Surface Induced by Optical Near-Field around Photo-Irradiated Nanoparticles.,
Osamu Watanabe, Taiji Ikawa, Makoto Hasegawa, Masaaki Tsuchimori, Yoshimasa Kawata, Chikara Egami, Okihiro Sugihara, and Naomichi Okamoto
IEICE Transactions on Electronics, **E83-C**, 1125-1127 (2000)

Nanofabrication Induced by Near-Field Exposure from a Nanosecond Laser Pulse
Osamu Watanabe, Taiji Ikawa, Makoto Hasegawa, Masaaki Tsuchimori, and Yoshimasa Kawata
Applied Physics Letters, **79**, 1366-1368 (2001)

Photochemically Induced Birefringence in Polyurethans Containing Donor-Acceptor Azobenzenes as Photoresponsive Moieties
Makoto Hasegawa, Taiji Ikawa, Masaaki Tsuchimori, and Osamu Watanabe
Journal of Applied Polymer Science, **86**, 17-22 (2002)

Photodeformation Behavior of Photodynamic Polymers Bearing Azobenzene Moieties in Their Main and/or Side Chain
Chang-Dae Keum, Taiji Ikawa, Masaaki Tsuchimori, and Osamu Watanabe
Macromolecules, **36**, 4916-4923 (2003)

Area-Selective Photo-Immobilization of a Two-Dimensional Array of Colloidal Spheres on a Photo-Deformed Template Formed in Photo Responsive Azopolymer Film
Osamu Watanabe, Taiji Ikawa, Takahiro Kato, Masahiro Tawata, and Hiroshi Shimoyama
Applied Physics Letters, **88**, 204107 (2006)

Photo-Induced Deformation Behavior Depending on the Glass Transition Temperature on the Surface of the Urethane Copolymers Containing a Push-Pull Type Azobenzene Moiety
Osamu Watanabe, Mamiko Narita, Taiji Ikawa and Masaaki Tsuchimori
Polymer, **47**, 4742-4749 (2006)

Photoinduced Immobilization of Biomolecules on the Surface of Azopolymer Films and Its Dependence on the Concentration and Type of the Azobenzene Moiety
Mamiko Narita, Fumihiko Hoshino, Makoto Mouri, Masaaki Tsuchimori, Taiji Ikawa and Osamu Watanabe
Macromolecules, **40**, 623-629 (2007)

Stress Monitoring of Organic Materials by Time-Resolved Fluorescence Measurement

Fluorescence from Poly(N-vinylcarbazole) in Uniaxially Stretched Polymer Films
Taiji Ikawa, Tohru Shiga, and Akane Okada
Journal of Applied Polymer Science, **67**, 259 (1997).

Stress Monitoring in Thin Polymer Coatings Using Time Resolved Fluorescence
Tohru Shiga, Takeshi Narita, Taiji Ikawa, Akane Okada
Polymer Engineering Science, **38**, 693 (1998).

Fluorescence from Soluble Polythiophenes in Uniaxially Stretched Polymers,
Tohru Shiga, T. Ikawa and Akane Okada
Journal of Applied Polymer Science, **67**, 259 (1998).

Measurement of Residual Stresses in Injection-Molded Polymer Parts by Time-Resolved Fluorescence,
Taiji Ikawa, Tohru Shiga, and Akane Okada
Journal of Applied Polymer Science, **83**, 2600 (2002)

Measurement of internal stress in polymeric coatings using time resolved fluorescence
Taiji Ikawa, and Tohru Shiga
Adhesion Aspects of Polymer Coatings, Vol. 2, pp. 151-163, Ed. K.L. Mittal, (VSP BV, Netherlands, 2003).

Excimer, Exciplex and Dimer Radical Cation Formation in a Pyrene-Containing Polymer Systems

Dimer Radical Cation Formation in Poly(vinyl pyrenes) studied by Puls Radiolysis.
Akira Tsuchida, Taiji Ikawa, Masahide Yamamoto, Akito Ishida and Setsuo Takmuku
The Journal of Physical Chemistry, **99**, 14793 (1995)

Intramolecular Pyrene Excimer Formation of 1,3-Dipyrenyl propanes with Full and Partial Ring Overlaps
Akira Tsuchida, Taiji Ikawa**,** Takashi Tomie and Masahide Yamamoto
The Journal of Phyical Chemistry, **99**, 8196 (1995)

Intrapolymer Excimer formation solely with the full-overlap conformation in poly(2-vinylpyrene)
Akira Tsuchida, Taiji Ikawa, and Masahide Yamamoto
Polymer, **36**, 3103 (1995)

Acknowledgment

The studies in this thesis were carried out at Toyota Central Research & Development Laboratories, Inc. from 1999 to 2004 under the guidance of Dr. Osamu Watanabe, and Materials Research Laboratory, University of California at Santa Barbara from 2004 to 2005 under the guidance of Professor Cyrus Safinya. I express my sincere gratitude to Dr. Osamu Watanabe for valuable discussions, supports, and continuous encouragement throughout this work. I would like to thank Professor Cyrus Safinya for kind guidance and thoughtful advice especially on the study of biological molecular assemblies.

I would like to thank Professor Shinzaburo Ito, for introducing me to polymer chemistry and photochemistry, and for supervising this thesis and providing critical comments and valuable discussions. I would also like to thank Professor Hiroo Iwata and Professor Toshiji Kanaya for co-supervising this thesis.

I would like to thank Dr. Makoto Hasegawa, Mr. Fumihiko Hoshino and Mr. Masaaki Tsuchimori for their active discussions and advice and supports.

I would like to thank Mr. Takuya Mitsuoka for his support on the AFM experiments.

I would like to thank Dr. Takashi Matsuyama for his assistance and discussion on the biochip fabrications.

I would like to thank Professor Yoshimasa Kawata and Dr. Wataru Inami for the calculation of the electromagnetic field around the polystyrene particles.

Thanks are also due to Professor Chikara Egami, Professor Okihiro Sugihara, and Professor Naomichi Okamoto for their cooperation.

I am really indebted to Dr. Youli Li for his support and advice in various situations. With his help I could start the life in Santa Barbara.

Thanks are also due to all members of Safinya laboratories: especially Dr. Linda S. Hirst, Dr. Kai Ewert, Dr. Myung Chul Choi and Professor Philip Pincus for their kind support on the experiments and the life in UC Santa Barbara.

I wish to thank gratefully Mr. Wataru Mori, Mr. Masaya Harada, Mr. Takeshi Yamada, Mr. Yuji Kato, Mr. Takahiro Kato, Professor Masahiro Tawada and Professor Hiroshi Shimoyama for the SNOM measurements and active collaborations.

I acknowledge the active collaboration and discussion with Dr. Chang-Dae Keum, Dr.

Mamiko Narita, Dr. Hideki Takagi, Mr. Makoto Mouri, Mr. Kazumasa Kawamoto and Dr. Haruo Takahashi.

I wish to thank Dr. Tohru Shiga and Dr. Akane Okada for their helpful advice and supports.

I am deeply grateful to Professor Masahide Yamamoto and Professor Akira Tsuchida for introducing me to polymer chemistry and photochemistry. I obtained much knowledge and inspiration from them.

Thanks are also due to the previous and present colleagues of Yamamoto and Ito Laboratories: especially, Mr. Kenji Kawano, Mr. Sadahito Misumi, Dr. Masaya Mitsuishi and Mr. Tsuyoshi Sasaki for their encouragement and support.

Finally, I heartily express my appreciation to my wife and my daughter, Saori and Ayana Ikawa, and to my parents, Kanji and Etsuko Ikawa, for their support and encouragement.

March, 2008

Taiji Ikawa